



Jussi Antero Lahti, MSc

**CLUPAK PROCESS AND ITS  
SIGNIFICANCE FOR THE PROPERTIES  
OF EXTENSIBLE KRAFT PAPER**

**DOCTORAL THESIS**

to achieve the university degree of

Doktor der technischen Wissenschaften

submitted to

**Graz University of Technology**

Supervisor

Univ.-Prof. Dipl.-Ing. Dr.techn. Wolfgang Bauer

Institute for Paper-, Pulp- and Fibre Technology

Second Supervisor

Ao.Univ.-Prof. Mag. Dr.rer.nat. Robert Schennach

Graz, July 2015

## **AFFIDAVIT**

I declare that I have authored this thesis independently, that I have not used other than the declared sources/resources, and that I have explicitly indicated all material which has been quoted either literally or by content from the sources used. The text document uploaded to TUGRAZonline is identical to the present doctoral thesis.

---

Date

---

Signature

# Abstract

Industrial bags made from extensible kraft paper are used in storing and transporting a wide variety of powdered goods. In order to withstand stresses without breaking, the extensible kraft paper needs to absorb a high amount of energy in machine direction (MD) and cross machine direction (CD). The tensile energy absorption is increased by increasing the stretch of the paper. In CD this is done through the combination of high consistency refining and free shrinkage. An extensible unit is in turn utilized in MD to increase the stretch through MD compaction.

This thesis focused on the production of extensible kraft paper with a Clupak extensible unit. The aim was to gain an extensive understanding of the Clupak process as well as the properties of extensible kraft paper to create a foundation for the further technological development. The operation of the Clupak process is based on the recoiling of a stretched rubber surface in a nip consisting of a heated cylinder and a nip bar. The moist paper web compacts in MD with the shrinking rubber surface while simultaneously sliding on the cylinder surface. Consequently, a microcreping effect is induced through curling of the fibers. For broadening the knowledge base further, the following three research perspectives were taken: (1) relation between microcreped structure and stress-strain curve, (2) effect of microcrepes on time-dependent mechanical properties and (3) effect of microcrepes on distribution of tensile damage.

The laboratory and industrial scale studies revealed that the higher solids content of paper during MD compaction leads to a more pronounced microcreped structure. Consequently, the stress-strain curve of extensible kraft paper becomes more sigmoidally shaped with higher strain and lower tensile stiffness whereas tensile index remains approximately constant. The dynamic mechanical and creep analyses illustrated in turn the more ductile/viscous nature of extensible kraft paper in comparison to kraft paper without microcreped structure. Finally, the infrared thermographic analysis of kraft and extensible kraft paper during tensile testing showed that the tensile damage is more evenly distributed within the extensible kraft paper. Altogether, the studies created a versatile base for the further technological development.

Keywords: Clupak, extensible kraft paper, microcreping, stress-strain curve, dynamic mechanical analysis, creep, infrared thermography, tensile damage distribution

# Kurzfassung

Industriesäcke hergestellt aus dehnfähigem Kraftpapier werden für den Transport einer Vielzahl von pulverförmigen Gütern genutzt. Um Spannungsspitze ohne Bruch zu überstehen, muss das dehnfähige Kraftpapier hohe Energien in Maschinenrichtung (MD) und Querrichtung (CD) absorbieren. Die Zugbrucharbeit wird umso größer, je höher die Dehnfähigkeit des Papiers ist. Um die Dehnfähigkeit in CD zu erhöhen, werden die eingesetzten Zellstoffe in einem Hochkonsistenz-Refiner gemahlen und ein hoher Grad an freier Schrumpfung in der Papiererzeugung zugelassen. In Papiermaschinen zur Herstellung von Kraftsackpapier wird häufig auch eine sogenannte Clupak-Einheit eingesetzt, um die Dehnfähigkeit des Papiers durch eine Mikrokreppung in MD zu erhöhen.

Diese Arbeit fokussiert sich auf die Produktion eines dehnfähigen Papiers mittels einer Clupak Einheit. Das Ziel war, ein tieferes Verständnis über die Vorgänge im Clupak-Prozess und über die Eigenschaften der damit produzierten Papiere zu erhalten, um auf dieser Basis eine Weiterentwicklung des Prozesses voranzutreiben. Der Clupak-Prozess basiert auf der Entspannung eines vorgespannten Gummituchs im Nip zwischen einem beheizten Zylinders und einem Gegendruckstab. Durch das Zusammenziehen des Gummituchs wird die noch feuchte Papierbahn in CD gestaut während sie über die Zylinderoberfläche gleitet, was zu Mikrokreppungen der Fasern in MD führt. Diese Mikrokreppungen bleiben in der weiteren Trocknung erhalten und bewirken eine Erhöhung der Dehnfähigkeit und Zugbrucharbeit des Papiers bei gleichzeitiger Reduzierung der maximalen Bruchkraft.

Um den Wissenshorizont zu erweitern, wurden folgende drei Forschungsfragen adressiert:

- Zusammenhang zwischen Mikrokreppung und Spannungs-Dehnungskurven
- Effekt der Mikrokreppung auf zeitabhängige mechanische Eigenschaften (Viskoelastizität)
- Zusammenhang zwischen Mikrokreppung und lokalem Versagen des Papiers unter Last

Labor- und Industrierversuchen zeigten, dass eine niedrigere Papierfeuchte in der Clupak-Einrichtung ausgeprägtere Mikrokreppungen erzeugt. Die resultierenden

Spannungs-Dehnungskurven des dehnfähigen Kraftpapieres werden S-förmiger bei höherer Dehnung und geringerer Zugsteifigkeit, während die Bruchkraft in etwa konstant bleibt. Die dynamisch-mechanische Analyse zeigte ein höheres duktilen Verhalten des dehnfähigen Kraftpapieres im Vergleich zu gewöhnlichem Kraftpapier. Eine Untersuchung der Papiere mittels lokaler Infrarot-Thermografie während des Zugversuchs ergab, dass dehnfähige Kraftpapiere weniger lokalisierte Spannungsspitzen aufweisen als herkömmliche Kraftpapiere.

Schlagwörter: Clupak, dehnfähiges Kraftpapier, Mikrokreppung, Spannungs-Dehnungs Kurve, dynamisch-mechanische Analyse, Kriechen, Infrarot-Thermografie, Zugbrucharbeit

# Acknowledgements

First of all, I wish to express my gratitude to Prof. Dr. Robert Schennach and DI Leo Arpa for giving me the opportunity to carry out this PhD thesis in Austria. In this context, I would also like to thank my Master's thesis instructor Prof. Dr. Eero Kontturi for the recommendation.

I wish to thank my supervisors Prof. Dr. Wolfgang Bauer and Prof. Dr. Robert Schennach for all the help and valuable discussions. I acknowledge Dr. Ulrich Hirn for the help in analyzing the correlation between local structure and tensile damage and Dr. Adriana Gregorova for analyzing the time-dependent mechanical properties of kraft and extensible kraft paper.

I conducted a major part of this thesis in Mondi's R&D Innovation Centre at Frantschach. Therefore, I would like to use this opportunity to thank all my colleagues working there for the positive, supportive and inspiring atmosphere. I would especially like to thank DI Leo Arpa and Dr. Franz Schmied for all the help and valuable discussions. I'm also very grateful to Mondi Frantschach's mechanical workshop for building the MD compaction apparatus. Furthermore, I acknowledge Mondi sack kraft paper for the possibility to conduct mill scale trials, and especially DI Jürgen Paulitsch for the help in data analysis.

I acknowledge Innventia for the expertise in IR thermography and local air permeance measurement.

I also wish to thank Mag. Esther Schennach and Mag. Marianne Wolschak for all the administrative support.

I gratefully acknowledge financial support from Mondi, Austrian Federal Ministry of Economy, Family and Youth as well as Austrian National Foundation for Research, Technology and Development.

Finally, I would like to express my deepest gratitude to my late grandfather DI Aimo Lahti for encouraging me to study natural sciences and engineering.

Jussi Antero Lahti  
Graz, July 8, 2015

# Contents

<b>1</b>	<b>Introduction</b>	<b>1</b>
1.1	Sack kraft paper . . . . .	1
1.2	Objective . . . . .	3
1.3	Outline . . . . .	4
<b>2</b>	<b>Background</b>	<b>6</b>
2.1	Structure and mechanical properties of paper . . . . .	6
2.1.1	Structure . . . . .	6
2.1.2	Stress versus strain curve . . . . .	7
2.1.3	Viscoelastic-plastic behavior . . . . .	9
2.1.4	Creep, creep recovery and stress relaxation . . . . .	13
2.2	Clupak process and extensible kraft paper . . . . .	15
2.2.1	Introduction . . . . .	15
2.2.2	Clupak extensible unit and its compaction mechanism . . . . .	16
2.2.3	Structure and mechanical properties of extensible kraft paper . . . . .	17
2.3	Link between structural and mechanical properties . . . . .	20
2.3.1	Effect of structural non-uniformity on deformation . . . . .	20
2.3.2	Effect of sample size on deformation . . . . .	23
2.3.3	Deformation studies with infrared thermography . . . . .	24
2.4	Conclusions . . . . .	28
<b>3</b>	<b>Materials and methods</b>	<b>31</b>
3.1	Laboratory scale study of extensible kraft paper . . . . .	31
3.1.1	Sample preparation . . . . .	31
3.1.2	Sample analysis . . . . .	34
3.2	Industrial scale study of extensible kraft paper . . . . .	35
3.2.1	Sample preparation . . . . .	35
3.2.2	Sample analysis . . . . .	35
3.3	Analysis of viscoelasticity, creep and creep recovery . . . . .	37
3.3.1	Analysis of viscoelasticity . . . . .	37
3.3.2	Analysis of creep and creep recovery . . . . .	37

3.4	Linking structural and mechanical properties . . . . .	40
3.4.1	Measurement procedure . . . . .	40
3.4.2	Data processing . . . . .	44
3.4.3	Registration and correlation analysis . . . . .	45
<b>4</b>	<b>Results and Discussion</b>	<b>47</b>
4.1	Laboratory scale trial . . . . .	47
4.1.1	Effect of MD compaction on the dimensions of paper sheets . . .	47
4.1.2	MD mechanical properties of paper sheets . . . . .	50
4.1.3	Evaluation of the laboratory scale method . . . . .	54
4.2	Industrial scale trial . . . . .	54
4.2.1	Structural properties . . . . .	54
4.2.2	MD mechanical properties . . . . .	58
4.2.3	CD mechanical properties . . . . .	61
4.2.4	Geometric mechanical properties . . . . .	63
4.3	Viscoelastic, creep and creep recovery behavior . . . . .	65
4.3.1	Viscoelasticity . . . . .	65
4.3.2	Creep and creep recovery . . . . .	67
4.3.3	Challenges for practical mechanical performance . . . . .	72
4.4	Linking local structure and tensile damage . . . . .	74
4.4.1	Kraft paper . . . . .	74
4.4.2	Extensible kraft paper . . . . .	80
4.5	Conclusions . . . . .	86
<b>5</b>	<b>Conclusions and Outlook</b>	<b>89</b>
	<b>Bibliography</b>	<b>92</b>

# List of Figures

1.1	End-use applications of industrial bags made of sack kraft paper. . . . .	1
1.2	Regional distribution of demand for sack kraft paper. . . . .	3
1.3	Dropping of industrial bags made of extensible kraft paper. . . . .	3
2.1	Paper structure and stress vs. strain curve. . . . .	7
2.2	Effect of strain rate, temperature and RH on stress vs. strain curve. . . . .	10
2.3	Principle of DMA and determination of viscoelastic properties. . . . .	11
2.4	Effect of temperature on viscoelasticity under dry atmosphere. . . . .	12
2.5	Effect of applied stress and RH on creep behavior. . . . .	15
2.6	Principle of Clupak extensible unit. . . . .	16
2.7	Surfaces and cross section of kraft and extensible kraft papers. . . . .	18
2.8	Stress vs. strain for kraft and extensible kraft paper. . . . .	19
2.9	Cross section of extensible kraft paper before and after straining. . . . .	19
2.10	Local strain behavior of paperboard strip. . . . .	22
2.11	Local vs. global strain for copy papers. . . . .	23
2.12	Size dependence of local and global strain for paperboard. . . . .	24
2.13	Cyclic stress vs. strain curve and thermodynamic behavior. . . . .	25
2.14	Temperature map, formation map and breaking load/strain. . . . .	27
2.15	Formation map, strain map and rupture line. . . . .	28
3.1	Process steps for preparing extensible paper in laboratory. . . . .	32
3.2	Photographs of MD compaction apparatus. . . . .	33
3.3	Principle of MD compaction apparatus. . . . .	34
3.4	Programs for studying creep-recovery behavior. . . . .	39
3.5	Determined property maps for kraft and extensible kraft paper. . . . .	41
3.6	Measurement principle of local air permeance of paper. . . . .	42
3.7	IR image of paper strip before tensile test. . . . .	44
3.8	Principle of image registration. . . . .	46
4.1	MD strain vs. solids content during MD compaction. . . . .	49
4.2	CD strain vs. solids content during MD compaction. . . . .	49
4.3	Plastic Poisson's ratio vs. solids content during MD compaction. . . . .	50

4.4	Stress vs. strain for sheets produced with rubber recoiling of 7%. . . . .	51
4.5	Stress vs. strain for sheets produced with rubber recoiling of 14%. . . . .	51
4.6	Effect of solids content during MD compaction on structure. . . . .	53
4.7	Air permeance and roughness for extensible kraft papers. . . . .	56
4.8	Basis weight and formation for extensible kraft papers. . . . .	57
4.9	MD mechanical properties for extensible kraft papers. . . . .	59
4.10	MD form factor for extensible kraft papers . . . . .	60
4.11	CD mechanical properties for extensible kraft papers. . . . .	62
4.12	CD form factor for extensible kraft papers . . . . .	63
4.13	Geometric mechanical properties for extensible kraft papers. . . . .	64
4.14	Effect of temperature and atmosphere on viscoelastic behavior. . . . .	66
4.15	Single creep-recovery cycle under different atmospheres. . . . .	68
4.16	Multiple creep-recovery cycles under increasing RH. . . . .	71
4.17	Multiple creep-recovery cycles under increasing temperature. . . . .	73
4.18	Structure and temperature maps for kraft paper strip $\square$ . . . . .	75
4.19	Structure and temperature maps for kraft paper strip $\triangle$ . . . . .	76
4.20	Structure and temperature maps for kraft paper strip $\circ$ . . . . .	77
4.21	Air permeance vs. optical transparency for kraft paper. . . . .	78
4.22	Optical transparency vs. temperature for kraft paper. . . . .	78
4.23	Air permeance vs. temperature for kraft paper. . . . .	79
4.24	Structure and temperature maps for extensible kraft paper strip $\diamond$ . . . . .	81
4.25	Structure and temperature maps for extensible kraft paper strip $\nabla$ . . . . .	82
4.26	Structure and temperature maps for extensible kraft paper strip $\triangleright$ . . . . .	83
4.27	Air permeance vs. optical transparency for extensible kraft paper. . . . .	84
4.28	Optical transparency vs. temperature for extensible kraft paper. . . . .	84
4.29	Air permeance vs. temperature for extensible kraft paper. . . . .	85

# List of Tables

3.1	Trial plan for studying effects of Clupak process parameters. . . . .	36
3.2	Analysis procedure for Clupak compaction trial. . . . .	36
3.3	DMA programs for studying kraft and extensible kraft paper. . . . .	37
4.1	Data of paper sheets prepared in laboratory scale trial. . . . .	48
4.2	Properties for sheets produced with rubber recoiling of 7%. . . . .	52
4.3	Properties for sheets produced with rubber recoiling of 14%. . . . .	52
4.4	Behavior during single creep-recovery cycle. . . . .	69
4.5	Multiple creep-recovery cycles under dry atmosphere. . . . .	70
4.6	Multiple creep-recovery cycles under increasing temperature. . . . .	72
4.7	Tensile index and breaking strain for kraft paper. . . . .	74
4.8	Tensile index and breaking strain for extensible kraft paper. . . . .	80

# List of abbreviations

<b>PM</b>	Paper machine
<b>MD</b>	Machine direction
<b>CD</b>	Cross machine direction
<b>ZD</b>	Thickness direction
<b>TEA</b>	Tensile energy absorption
<b>MTS</b>	Material testing system
<b>P</b>	Primary wall
<b>S1</b>	Outer layer of secondary wall
<b>S2</b>	Middle layer of secondary wall
<b>S3</b>	Inner layer of secondary wall
<b>RH</b>	Relative humidity
<b>N<sub>2</sub></b>	Dry nitrogen atmosphere
<b>DMA</b>	Dynamic mechanical analysis
<b>tan δ</b>	Loss tangent
<b>IR</b>	Infrared
<b>MWIR</b>	Mid-wavelength infrared
<b>PTFE</b>	Polytetrafluoroethylene
<b>ANOVA</b>	Analysis of variance
<b>r<sup>2</sup></b>	Coefficient of determination

## Introduction

### 1.1 Sack kraft paper

Sack kraft paper produced from long softwood fibers is mainly used as a material for industrial bags. Figure 1.1 shows various powdered goods which are stored and transported by using these bags. The distribution of end-use applications depends strongly on the region as can be seen in Figure 1.1. In North America and Europe the bags are filled with wide variety of goods, whereas in Asia, Africa, and Middle East the main focus is on cement and building materials [JOSEFSSON, 2013; PÖYRY, 2011].

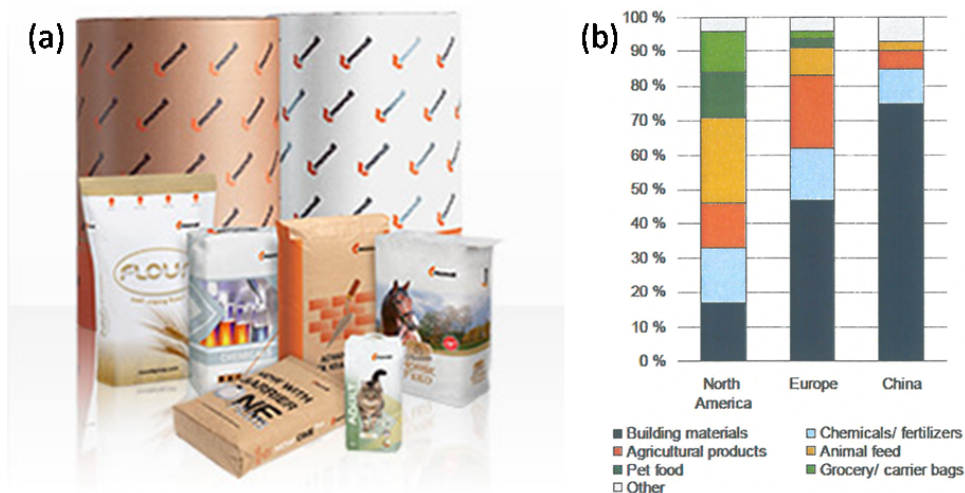


**Figure 1.1** End-use applications of industrial bags made of sack kraft paper. (a) Examples of sack kraft paper rolls and industrial bags filled with various powdered goods. (b) Distribution of end-use applications in different regions [MONDI, 2015A; PÖYRY, 2011].

The regional distribution of demand for sack kraft paper between the years 1990 and 2010 is shown in Figure 1.2 in kilotons. It can be seen that the emerging markets are in South-East Asia, Oceania, Africa and Middle East [JOSEFSSON, 2013; PÖYRY, 2011]. Especially in these markets the handling of the bags sets high requirements for the mechanical properties of sack kraft paper. Due to a low degree of automation, rough manual handling, dropping of bags and long/complicated distribution chains, sack kraft paper undergoes various stresses during its lifetime. Besides, the prevailing climate in these emerging market regions is often very hot and humid which further increases the challenge for mechanical performance [JOSEFSSON, 2013; MADDERN, 2003]. In order to withstand all these stresses without breaking, the paper needs to absorb a high amount of energy in machine direction (MD) and cross machine direction (CD). Figure 1.3 illustrates this need for even energy absorption in MD and CD by showing two examples of bag drops. It can be seen from the upper picture sequence that the energy absorption of the extensible kraft paper used in the bag was not high enough in CD, and thus the bag failed. The extensible kraft paper used in the bag which is shown in the lower picture sequence was in turn capable of absorbing the energy evenly in both MD and CD, and thus the bag stayed unbroken. The high tensile energy absorption (TEA) is created through high stretch of the paper [IHRMAN, 1964; MADDERN, 2003; MONDI BAG APPLICATION CENTRE, 2008]. Thus, sack kraft paper is normally made extensible in both directions [JOSEFSSON, 2013; MADDERN, 2003] and is then called extensible kraft paper in this study. Sack kraft paper which is not made extensible in MD is in turn called kraft paper in this study. High CD stretch is achieved through the combination of high consistency refining and free shrinkage of the paper web in the drying section of a paper machine. In MD the high stretch is in turn achieved by compacting the moist paper web with an extensible unit, such as e.g. a Clupak or Expanda unit, in the drying section of a paper machine [BURROW, 1965; IHRMAN AND ÖHRN, 2003; MADDERN, 2003; MONDI, 2015B]. This work focuses on the Clupak extensible unit. Besides TEA, air permeance is an important property for sack kraft paper, because the air conveying the powdered good into the bag during the filling process needs to be effectively removed through the paper. The amount of low consistency refining mainly defines the level of air permeance. The compaction hardly affects air permeance [BURROW, 1965; MADDERN, 2003].

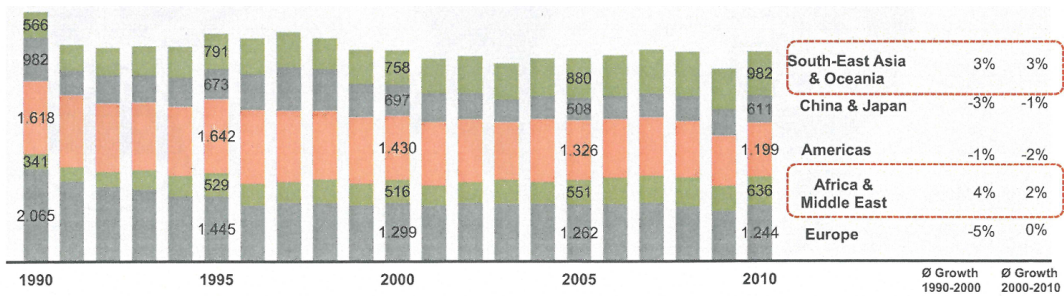


**Figure 1.2** Regional distribution of demand for sack kraft paper between years 1990 and 2010 in kilotons [JOSEFSSON, 2013; PÖYRY, 2011].

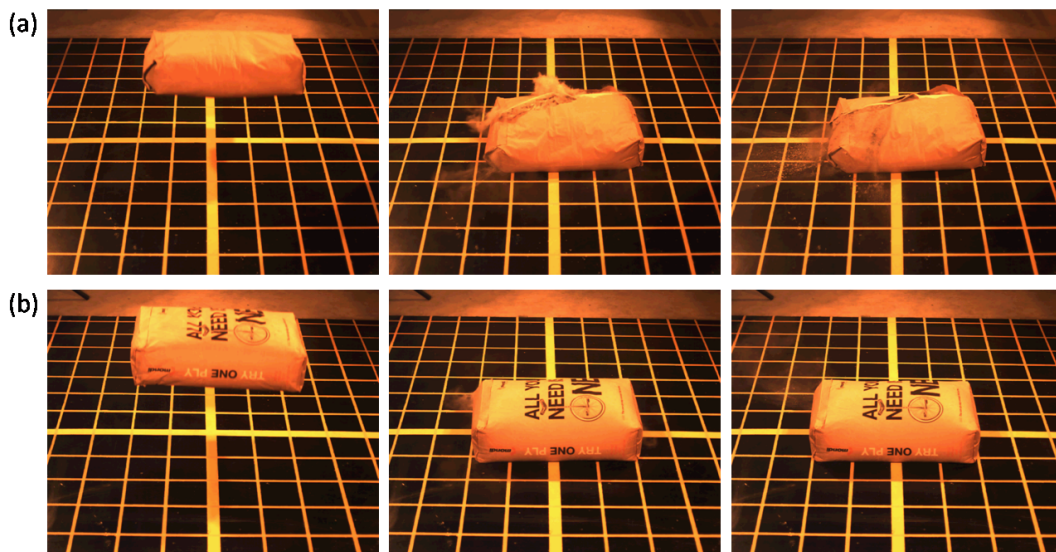


**Figure 1.3** Dropping of industrial bags made of extensible kraft paper. (a) Energy absorption of extensible kraft paper was not high enough in CD, and thus the bag failed. (b) Energy absorption of extensible kraft paper was high in MD and CD, and thus the bag stayed unbroken [MONDI BAG APPLICATION CENTRE, 2008].

## 1.2 Objective

Improved cost efficiency and reduced environmental load are among the main drivers in developing the extensible kraft paper production further. This means reducing the amount of water, energy and raw materials in the production while still fulfilling the requirements for structural and mechanical properties of paper. The current work aims to contribute in the pursuit of these goals by gaining an extensive understanding of the Clupak process as well as the structural and mechanical properties of extensible

kraft paper. Based on this extensive understanding, a broad foundation for generating new ideas to improve the production process and properties of extensible kraft paper is created.

To create this broad foundation, the aim is to study the extensible kraft paper from three different perspectives. First, the effects of Clupak process parameters on structural and mechanical properties of extensible kraft paper are studied in laboratory and mill scale trials. Due to the inflexibility and limited accessibility of the industrial scale Clupak process, a new laboratory method for preparing extensible kraft paper was developed. Thus, simulation of the industrial scale production with wider variation of process parameters became possible, which in turn enables further optimization of the Clupak process and relevant unit processes to produce extensible kraft paper with improved properties. Second, the stresses that kraft paper and extensible kraft paper undergo as the bag material during their lifetime are evaluated using measurements of time-dependent mechanical properties, i.e. viscoelasticity, creep and creep recovery. These mechanical properties are dependent on the atmosphere, temperature and loading history [KETOJA, 2008; KOLSETH AND DE RUVO, 1983] which may all vary greatly during the end-use of bags (see Section 1.1). Thus, the time-dependent mechanical behavior during the end-use is estimated by measuring the viscoelastic, creep and creep recovery behavior of both papers under different constant as well as dynamically changing atmospheres and temperatures, which in turn enables the detection of critical conditions where the probability for failure is high. Third, kraft paper and extensible kraft paper are studied and compared by linking local structural properties, i.e. basis weight and density, to local tensile damage. In this way, it is possible to gather information regarding critical local events which ultimately lead to the rupture of paper, and furthermore, to compare these critical events between the two papers. Finally, the aim is to combine the knowledge gained from these three research approaches to create ideas how the structure of extensible kraft paper as well as the production process could be improved in the future.

### 1.3 Outline

A base for pursuing the goals of this thesis is created in the following Chapter 2 where the essential background information taken from a literature survey is presented. This literature review is started by describing the general structural and mechanical properties of paper after which the focus is directed to the Clupak extensible unit and its working principle. This is in turn followed by a description how the MD compaction with an extensible unit changes the structure and mechanical properties of paper. The effect of structural non-uniformity of paper on the local and global mechanical properties is then discussed. Finally, the key findings and learnings of

the literature review are concluded, and based on these, the more precise research questions for the following experimental studies are defined.

Materials and methods for studying the defined research questions are presented in Chapter 3. This presentation is started by describing the method for preparing extensible kraft paper on the laboratory scale and a special emphasis is given to the description of the purpose-built MD compaction apparatus. Subsequently, an experimental plan for simulating the production of extensible kraft paper with the developed laboratory method as well as a procedure for analyzing the prepared papers are given. This is in turn followed by an experimental plan for studying the extensible paper production on the mill scale including also a procedure for analyzing the produced papers. The procedure for analyzing the time-dependent mechanical properties of kraft paper and extensible kraft paper is then presented. Finally, an analysis sequence for measuring local structural properties and local tensile damage of kraft paper and extensible kraft paper including also a description for linking these measured local properties to each other is given.

The results gained from the experimental studies are presented and analyzed in Chapter 4. First, the outcomes of the extensible paper production on the laboratory and mill scale are discussed and compared. This is in turn followed by a discussion and comparison of the measured time-dependent mechanical properties of the kraft paper and extensible kraft paper. An analysis and comparison how the local structural properties correlate with the local tensile damage within the kraft paper and extensible kraft paper strips are then given. Finally, key findings and learnings of the experimental studies are concluded.

Based on the key findings and learnings of the literature review as well as experimental studies, Chapter 5 concludes this thesis by giving an outlook on potential improvements as well as future research to further improve the production process and properties of extensible kraft paper.

## Background

This chapter, consisting of four sections, creates a base for the experimental study by presenting the essential background information. The description is started by a general introduction of paper in Section 2.1. It includes a description of structure, stress versus strain curve, viscoelastic-plastic behavior as well as creep, creep recovery and stress relaxation behavior of paper. The focus of the description is then changed to the Clupak extensible unit and extensible kraft paper in Section 2.2. It in turn consist of a description of history, structure and working principle of the Clupak extensible unit as well as a description of the structure and mechanical properties of extensible kraft paper. Subsequently in Section 2.3, the description deals with the structural inhomogeneity of paper and its effect on the local and global mechanical properties. Finally, Section 2.4 concludes the most important findings and learnings from the three previous sections and defines the important research questions for the experimental studies.

### 2.1 Structure and mechanical properties of paper

#### 2.1.1 Structure

Paper is a fibrous material belonging to the field of polymers. Its structural hierarchy is presented in Figure 2.1 [FELLERS, 2009B]. Industrially produced papers consist of a network of fibers oriented predominantly into MD and held together by the combination of the following physical bonding mechanisms: hydrogen bonding, van der Waals forces, Coulomb forces, capillary forces, mechanical interlocking and interdiffusion [HIRN AND SCHENNACH, 2014; NORMAN, 2007]. The structure of the fibers includes a fiber wall surrounding a hollow lumen. The fiber wall consist of a primary wall layer P and secondary wall layers S1, S2 and S3. However, the P and S1 layers are

partly lost during pulping and stock preparation. The S2 layer is the thickest layer, and thus largely defines the mechanical properties of the fibers. All layers consist of microfibrils embedded into an amorphous matrix including mainly hemicelluloses and lignin. In the S2 layer the microfibrils are oriented in a right-handed spiral manner around the fiber axis with a constant fibril angle [KAJANTO ET AL., 1998]. However, this angle is locally disturbed through the axial compression of fibers caused mostly by the mechanical treatment of wood and pulp as well as the drying of paper [SETH, 2005]. The microfibrils in turn consist of crystalline, amorphous and paracrystalline (not fully amorphous) regions of cellulose molecules [KULASINSKI ET AL., 2014; VISH-TAL AND RETULAINEN, 2014].

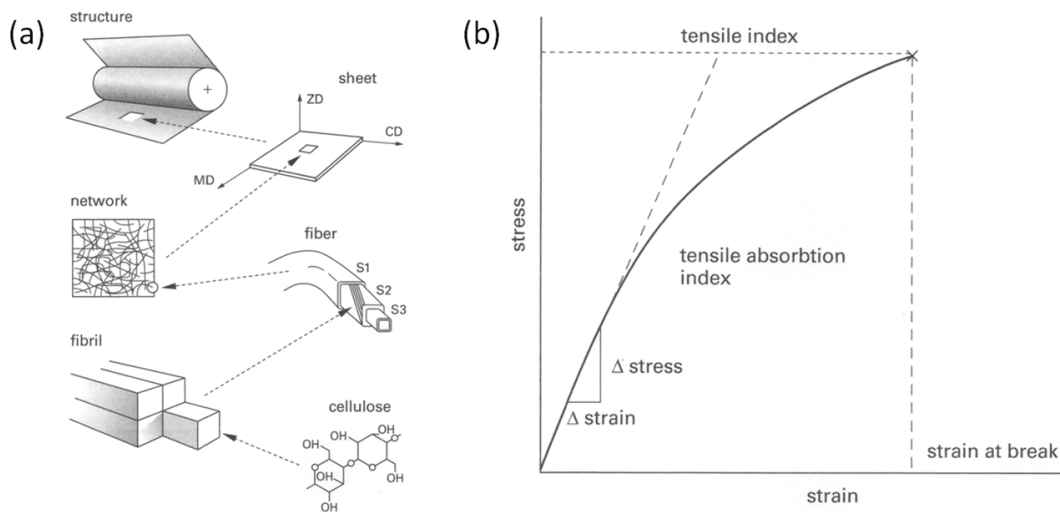


**Figure 2.1** Structural hierarchy of paper (a) and general stress versus strain curve for paper (b) [FELLERS, 2009A,B].

### 2.1.2 Stress versus strain curve

The general form of the stress versus strain curve for the above-described paper structure is shown in Figure 2.1. In the case of paper, the specific stress (indexed stress) is often used instead of stress to describe the loading intensity in order to take the varying density into account. The stress is calculated as follows:

$$\sigma = \frac{F}{b \cdot t} \quad (2.1)$$

where  $F$  is the tensile force (load),  $b$  the width and  $t$  the thickness of the sample. The specific stress is achieved by replacing the thickness term ( $t$ ) in Equation 2.1 with the basis weight of the sample:

$$\sigma^w = \frac{F}{b \cdot w} \quad (2.2)$$

where  $w$  is the basis weight of the sample. Furthermore, tensile strength and tensile index are defined as the maximum stress and maximum specific stress reached at the point of rupture, respectively. The longitudinal (loading direction) strain is in turn expressed in a following way:

$$\varepsilon = \frac{\Delta l}{l} \quad (2.3)$$

where  $\Delta l$  is the length change and  $l$  the original length in the longitudinal direction of the sample. Simultaneously with the longitudinal strain, the paper contracts in the transverse direction. The ratio of transverse strain to longitudinal strain is called Poisson's ratio:

$$\nu = -\frac{\varepsilon_t}{\varepsilon} \quad (2.4)$$

where  $\varepsilon_t$  is the transverse strain [FELLERS, 2009A]. For industrially produced papers stretched in MD the Poisson's ratio is generally around 0.3, and if stretched in CD, the Poisson's ratio is in turn generally around 0.13 [PAETOW AND GÖTTSCHING, 1990]. The slope of the linear part of the stress versus strain curve is called elastic modulus:

$$E = \frac{\Delta \sigma}{\Delta \varepsilon} \quad (2.5)$$

The tensile stiffness index ( $E^w$ ) is in turn calculated by replacing the stress term ( $\sigma$ ) in Equation 2.5 with the specific stress ( $\sigma^w$ ) [FELLERS, 2009A]:

$$E^w = \frac{\Delta \sigma^w}{\Delta \varepsilon} \quad (2.6)$$

Finally, the area under the stress versus strain curve defines the *TEA* of the sample and is calculated with the following integral:

$$TEA = \int_0^{\varepsilon_b} \sigma \, d\varepsilon \quad (2.7)$$

where  $\varepsilon_b$  is the longitudinal breaking strain. Similarly with the tensile stiffness index, the *TEA* index ( $TEA^w$ ) is calculated by replacing the stress term ( $\sigma$ ) in Equation 2.7 with the specific stress ( $\sigma^w$ ) [ALAVA AND NISKANEN, 2008; FELLERS, 2009A]:

$$TEA^w = \int_0^{\varepsilon_b} \sigma^w \, d\varepsilon \quad (2.8)$$

### 2.1.3 Viscoelastic-plastic behavior

The exact shape of the stress versus strain curve depends on the deformation conditions as well as on the fiber properties in the network. Important deformation conditions affecting on the curve are strain rate, temperature, moisture content and sample size (discussed in Section 2.3). The effect of strain rate on the curve is shown in Figure 2.2. It can be seen that the paper becomes more ductile with decreasing strain rates which is most probably caused by the more even redistribution of stresses due to the longer time available [KETOJA, 2008; VISHTAL AND RETULAINEN, 2014]. This illustrates the viscoelastic nature of paper, i.e. it responds to an applied stress in a time-dependent manner. The viscous (time-dependent) behavior of paper is caused by the deformations in the amorphous components in the fiber wall and also in the interfiber bonds. These deformations are in turn increased with the decreasing strain rates due to the increased flow tendency (liquid-like behavior) of the paper structure. Furthermore, increased temperature and moisture content soften the amorphous components and weaken the interfiber bonds leading also to the increased flow tendency under stress as illustrated by the enhanced ductility in Figure 2.2 [JONES, 2002; KETOJA, 2008; VISHTAL AND RETULAINEN, 2014].

The viscoelasticity of paper can be approximated to be linear, i.e. the strain response at any time is directly proportional to the stress (superposition principle). This enables the usage of a dynamic mechanical analysis (DMA) for studying the viscoelastic nature of paper. In DMA, a small sinusoidal stress is applied to a paper sample. Due to the linear viscoelasticity, the oscillatory strain response of the sample to the applied sinusoidal stress occurs with a time delay as shown in Figure 2.3. This time delay is described with the phase difference angle  $\delta$ . The delay of strain for purely viscous materials is large, and thus the value for  $\delta$  is  $90^\circ$ . For purely elastic materials the strain occurs in turn without any delay, and thus the value for  $\delta$  is  $0^\circ$ . Viscoelastic materials, such as paper, have the values for  $\delta$  between  $0^\circ$  and  $90^\circ$  [KETOJA, 2008; KOLSETH AND DE RUVO, 1983]. The overall response of paper to the stress is quantified with the following complex number called dynamic (complex) modulus:

$$E^* = E' + iE'' \quad (2.9)$$

where  $E'$  is the real part called storage modulus,  $i$  the imaginary unit ( $\sqrt{-1}$ ) and  $E''$  the imaginary part called loss modulus. The dynamic modulus is illustrated by the diagram in Figure 2.3 and its absolute value is calculated with the following equation:

$$|E^*| = \sqrt{E'^2 + E''^2} = \frac{\sigma_{max}}{\varepsilon_{max}} \quad (2.10)$$

where  $\sigma_{max}$  is the maximum stress and  $\varepsilon_{max}$  the maximum strain. The storage modulus describes the elastic response, i.e. mechanical energy is stored and recovered, of paper to the stress and is calculated as follows:

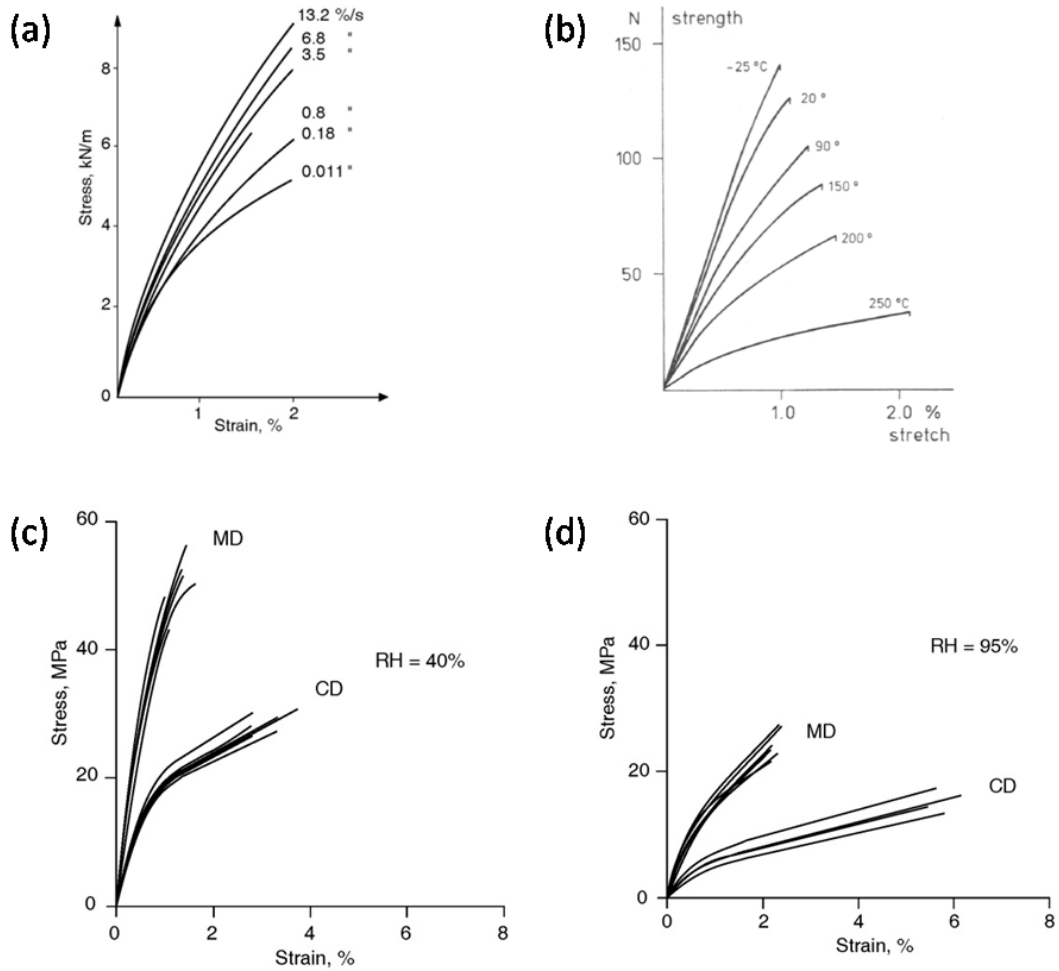


**Figure 2.2** Effect of strain rate (a), temperature (b) and relative humidity (c & d) on the stress versus strain curve of paper. The strain rate effect was studied with machine glazed paper, the temperature effect with fluting and the moisture effect with paperboard (the relative humidities correspond with the moisture contents of 6.6 and 20%) [ALAVA AND NISKANEN, 2008; ANDERSSON AND SJÖBERG, 1953; KETOJA, 2008; YEH ET AL., 1991].

$$E' = |E^*| \cdot \cos \delta = \frac{\sigma_{max} \cdot \cos \delta}{\varepsilon_{max}} \quad (2.11)$$

where  $\sigma_{max} \cdot \cos \delta$  is the maximum elastic stress. The loss modulus describes in turn the viscous response, i.e. mechanical energy is lost, of paper to the stress and is calculated with the following equation:

$$E'' = |E^*| \cdot \sin \delta = \frac{\sigma_{max} \cdot \sin \delta}{\varepsilon_{max}} \quad (2.12)$$

where  $\sigma_{max} \cdot \sin \delta$  is the maximum viscous stress. Furthermore, loss tangent is used to evaluate the viscoelastic response of paper to the stress. It is a measure of energy lost to energy stored and is calculated as follows:

$$\tan \delta = \frac{E''}{E'} \quad (2.13)$$

As with the  $\delta$ , materials with low loss tangent (low  $\delta$ ) are highly elastic and lose little mechanical energy during the viscoelastic evaluation with DMA. High loss tangent (high  $\delta$ ) refers in turn to highly viscous materials which lose a lot of mechanical energy during the same evaluation [KETOJA, 2008; KOLSETH AND DE RUVO, 1983; WALKER, 2001].

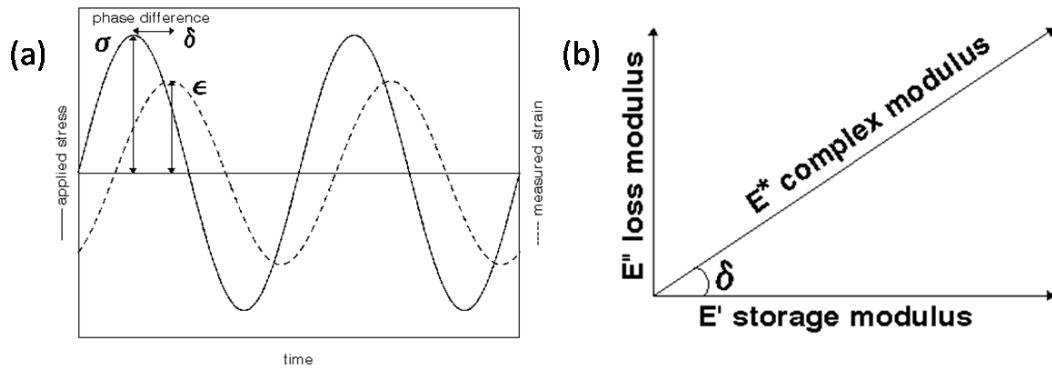


**Figure 2.3** Principle of studying viscoelasticity with DMA (a) and diagram for determining the viscoelastic properties (b) [ANASYS, 2015].

The effect of increasing temperature during DMA on the  $E'$ ,  $E''$  and  $\tan \delta$  of paper under dry nitrogen ( $N_2$ ) atmosphere is shown in Figure 2.4. It can be seen that the  $E'$  decreases (stored and recovered mechanical energy is reduced) with increasing temperature. This occurs due to the temperature induced softening of the amorphous fiber wall components and weakening of the interfiber bonds - as already discussed above. Also the loading history, i.e. previously induced viscoelastic deformations, most probably has an influence on the decreasing  $E'$ . Simultaneously with the decreasing  $E'$ , the more distinctive temperature and loading history induced changes in the fiber network cause the transient  $E''$  peaks (mechanical energy loss peaks). By knowing the development of  $E'$  and  $E''$ , the overall temperature and loading history dependent development of viscoelasticity can be evaluated for paper by calculating the  $\tan \delta$  value with Equation 2.13 [KETOJA, 2008; WALKER, 2001].

However, the viscoelastic deformation dominates the behavior of paper structure only before reaching the end of the linear part, i.e. yield point, of the stress versus strain curve. After that the deformation of the paper structure becomes significantly plastic (irreversible). The plastic deformation occurs through irreversible intrafiber

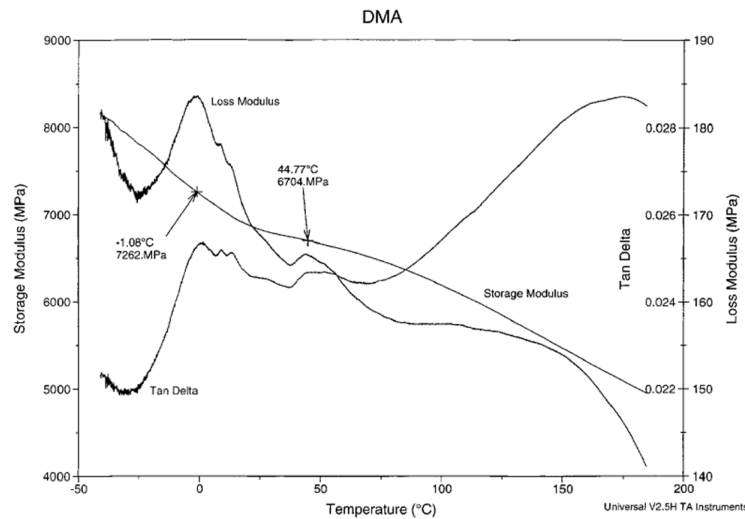


**Figure 2.4** Effect of increasing temperature during DMA on the storage modulus ( $E'$ ), loss modulus ( $E''$ ) and loss tangent ( $\tan \delta$ ) of paper under dry ( $N_2$ ) atmosphere [WALKER, 2001].

deformations, i.e. the amorphous components flow and the misalignments of the microfibrils with respect to the fiber axis are drawn out (decrease in the fibril orientation angle), and gradual opening of the interfiber bonds - complete opening of the bonds is however rare. Eventually the initiation of final rupture takes place through a burst of bond failures. Consequently, paper is considered to be a viscoelastic-plastic material [ALAVA AND NISKANEN, 2008; KETOJA, 2008; SETH, 2005; VISHTAL AND RETULAINEN, 2014].

Besides the deformation conditions, the shape of the stress versus strain curve is also influenced by the fiber properties in the network. These properties are largely dependent on the drying conditions in MD and CD. Fibers have a much higher tendency to shrink laterally during drying due to the anisotropic structure of the fiber wall. Consequently, the neighboring fibers shrink axially at the bonded interfiber crossings through the formation of microcompressions. These are closely packed dislocations in the fiber wall where the orientation angle of the microfibrils is locally increased. As the machine made paper is dried under tension in MD, the MD shrinkage of the fibers at the bonded segments is restrained, which in turn subjects the free fiber segments in MD under axial tensile stress. Thus, these free fiber segments are straightened through the irreversible intrafiber deformations and become capable of bearing the load together with the bonded fiber segments, i.e. the fiber network is activated. This activation leads to a stiff and brittle paper in MD (see Figure 2.8). In CD, the shrinkage of the paper is in turn only partially restrained allowing the CD shrinkage of the fibers at the bonded segments. This shrinkage is enhanced by

the MD orientation of the fibers and the Poisson contraction due to the MD tension. Consequently, the load bearing ability of the paper is reduced and the paper becomes ductile in CD (see Figure 2.8) [SETH, 2005; VAINIO, 2007; VISHTAL AND RETULAINEN, 2014].

#### 2.1.4 Creep, creep recovery and stress relaxation

Paper undergoes approximately constant tension over an open draw in MD during drying. Consequently, the paper deforms due to creep which means that the paper stretches in a time-dependent manner under constant stress. The creep behavior of paper can be studied with a creep compliance as a function of creep time:

$$J(t) = \frac{\varepsilon(t)}{\sigma} \quad (2.14)$$

The paper relaxes after removing the stress. Immediately after the stress removal, part of the strain is elastically recovered. This is followed by a viscoelastic (delayed) recovery and finally there is only a plastic strain of the paper left [KETOJA, 2008]. The creep recovery behavior of paper can be studied with a recoverable compliance as a function of creep time, i.e. the part of the creep compliance which is recovered during the elastic and viscoelastic recovery, as follows [GREGOROVA ET AL., 2013]:

$$J_R(t) = J(t) - J_{NR}(t) = \frac{\varepsilon(t) - \varepsilon_{NR}(t)}{\sigma} \quad (2.15)$$

where  $J_{NR}(t)$  is the non-recoverable compliance as a function of creep time and  $\varepsilon_{NR}(t)$  the non-recoverable (plastic) strain as a function of creep time. Furthermore, the relaxation ability of paper as a function of creep time can be calculated as follows [GREGOROVA ET AL., 2013]:

$$R(t) = \frac{J_R(t)}{J(t)} \quad (2.16)$$

Besides the creep during the open draw, paper may also experience stress relaxation in MD during drying when supported by a cylinder. This means that the stress within paper decreases in a time-dependent manner under constant strain. The stress relaxation behavior can be studied with a relaxation modulus as a function of stress relaxation time [KETOJA, 2008]:

$$E(t) = \frac{\sigma(t)}{\varepsilon} \quad (2.17)$$

The microscopic changes in the paper structure during the creep and stress relaxation are similar to the changes during the stress versus strain test. Thus, the creep and stress relaxation of paper are also similarly sensitive to the prevailing conditions. Figure 2.5 shows that the creep rate increases with the applied stress. Besides, in-

creased RH and temperature also lead to faster creep, as also shown in Figure 2.5, and the creep rate increases further under varying RH, i.e. the creep rate is higher under cyclic RH in comparison to the highest RH of the cycle kept constant [BREZINSKI, 1956; CONSIDINE ET AL., 1989; KETOJA, 2008]. Thus, the creep under cyclic RH is called accelerated creep. Proposed mechanisms for the accelerated creep under cyclic RH are inhomogeneous stress distribution and mechanosorption [KETOJA, 2008]. The inhomogeneous stress distribution within a paper sample is probably caused either by temporary moisture gradients during the sorption or by heterogeneous response to the even moisture. More precisely, the temporary moisture gradients create stress gradients through hygroexpansion gradients. The heterogeneous response to the even moisture is in turn created by the hygroexpansion incompatibility between fibers bonded together with different axial alignments in a sheet. Both options, temporary moisture gradients during the sorption and heterogeneous response to the even moisture, induce locally higher creep rates in the regions where the stresses are concentrated. This ultimately leads to the faster overall creep of the paper sample. Mechanosorption explanation, i.e. the moisture absorption of paper is higher under tensile stress in comparison to compressive stress, for the accelerated creep is supported by the fact that the abrupt changes in the moisture content cause a transient reduction in the stiffness of paper samples [COFFIN AND HABEGER, 2001; HABEGER AND COFFIN, 2000; KETOJA, 2008]. Similarly with the creep rate, the stress relaxation rate of paper also increases with the applied initial stress and moisture content [JOHANSON AND KUBAT, 1964; KETOJA, 2008].

In practice, e.g. during drying or during end-use in industrial bags (see Section 1.1), paper often undergoes stress and strain sequences instead of single stress and strain events. The final state of the stress and strain depends then on the duration and order of the applied stresses and strains in the sequence. This means that the mechanical behavior of paper is history dependent - as already briefly discussed in connection with Figure 2.4 [KETOJA, 2008].

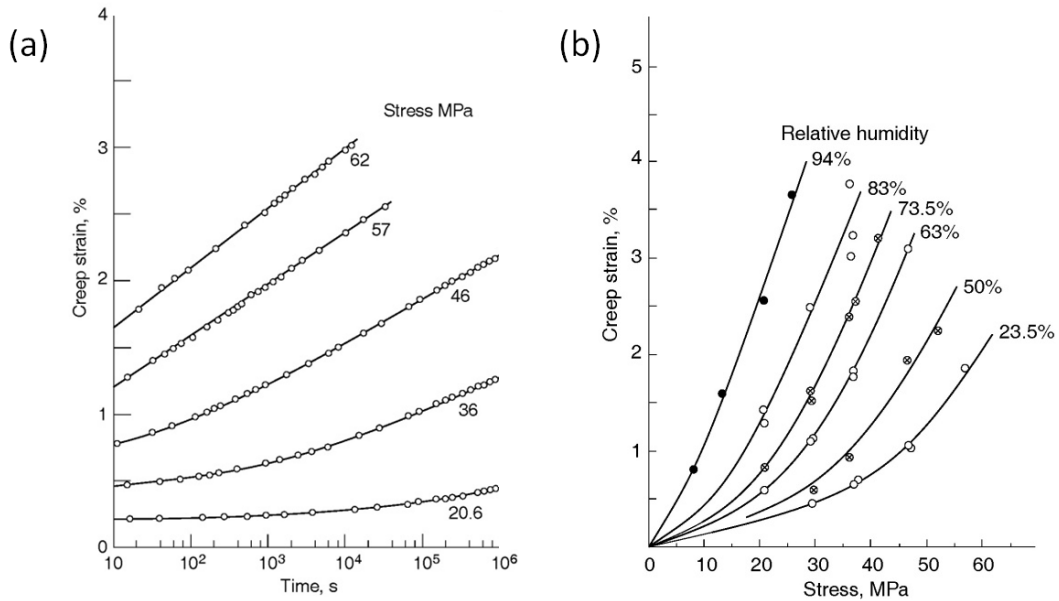


**Figure 2.5** Effect of applied stress and RH on the creep behavior of alpha pulp handsheets. (a) Creep rate at different stress levels. (b) Creep rate (creep time 24 h) at different stress levels and RHs [BREZINSKI, 1956; LESKELÄ AND SIMULA, 1998].

## 2.2 Clupak process and extensible kraft paper

### 2.2.1 Introduction

The American businessman and inventor Sanford Lockwood Cluett (1874-1968) invented the Clupak process which enabled the production of paper with high TEA also in MD - crucial for the high performance of industrial bags (see Chapter 1.1) [SHOUDY, 1959; WIKIPEDIA, 2015A]. He started to develop the process on the laboratory scale in 1940s and in 1953 the process was patented [CLUETT, 1953; SHOUDY, 1959]. In 1954 West Virginia Pulp and Paper Co. initiated a project to study the industrial possibilities of the laboratory Clupak extensible unit developed by Cluett. This led to a design and build of the pilot scale Clupak extensible unit in 1955. The extensible kraft paper made by using this unit performed well as a material in industrial bags, and thus the first industrial scale Clupak extensible unit was designed and installed on a kraft paper machine at the Charleston mill, South Carolina, USA in 1957 [SHOUDY, 1959]. Nowadays, the Clupak extensible unit is a standard unit process in paper machines producing extensible kraft paper [CLUPAK, 2014].

An alternative to the Clupak process is the Expanda process. These two processes have the same compaction principle using an elastic medium. Furthermore, the properties of the final paper products are similar. The difference in the design of these two processes is that the Clupak unit uses a rubber blanket as the elastic medium for

compaction whereas in the Expanda unit the elastic medium is a rubber fixed to a roll [BURROW, 1965; IHRMAN AND ÖHRN, 2003]. Nowadays, the Clupak process is dominating over the Expanda process in the production of extensible kraft paper, and thus the current work has a primary focus on the Clupak process. However, the results from both Clupak and Expanda experiments are presented in the following literature review due to the similar final paper properties achieved with these two processes.

### 2.2.2 Clupak extensible unit and its compaction mechanism

The principle of the Clupak extensible unit is presented in Figure 2.6. The unit is normally located in the drying section of a paper machine with the solids content of the paper web being between 60-65% [CLUPAK, 2014]. It includes a nip which consists of a rubber blanket having to pass through a gap between a heated cylinder and a nip bar. This nip can be considered as a Venturi section formed by the rotating heated cylinder and the static water lubricated nip bar in which the endless rubber blanket is accelerated. The paper web follows the dimensional changes of the rubber surface in the nip due to friction forces between paper and rubber. This is a consequence of a high radial nip pressure, which also prevents paper from buckling, and a simultaneous slippage of the paper on the cylinder surface. The slippage occurs due to the combination of highly polished cylinder surface and the steam film generated between the paper and the cylinder. The steam film is created through evaporation of water sprayed on the hot cylinder surface [BURROW, 1965].

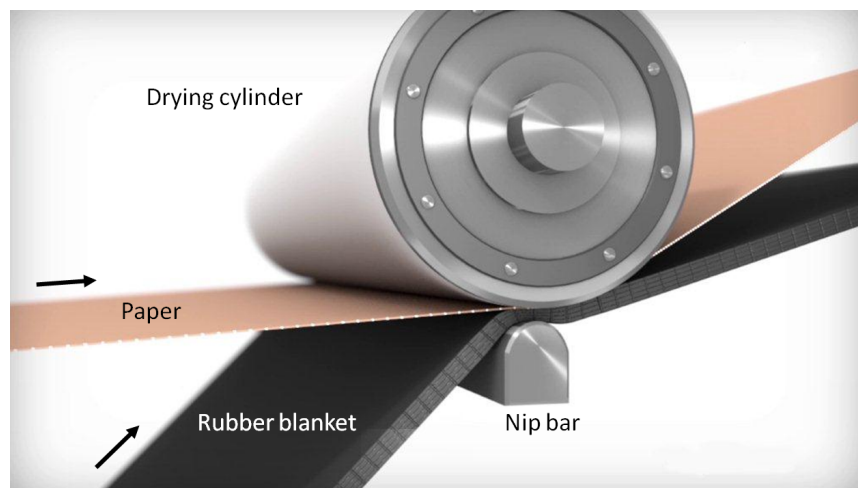


**Figure 2.6** Principle of the Clupak extensible unit [MONDI, 2015B].

The dimensional changes of the rubber surface are induced by bending and by the Venturi effect. First, the surface of the rubber blanket closer to the paper web is stretched through bending over the nip bar and it is further stretched because of

the Venturi effect. The stretched rubber surface then comes into contact with the moist paper web. After passing the center of the nip, the stretched rubber surface starts to recoil due to the deceleration caused by Venturi effect and bending of the rubber in the opposite direction. The paper web compacts in MD while following the shrinkage of the rubber surface in the second half of the nip and these events in the nip become more pronounced with increasing nip width. The nip width increases with the increasing radial nip pressure and rubber thickness as well as decreasing rubber hardness. The final compaction level is adjusted by controlling the speed difference of the paper web between inlet and outlet of the Clupak nip [BURROW, 1965; IHRMAN AND ÖHRN, 2003].

### 2.2.3 Structure and mechanical properties of extensible kraft paper

Figure 2.7 shows how the compaction in MD induces a microcreping effect in the paper network through curling of the fibers [IHRMAN AND ÖHRN, 2003]. These curls can be partly linked to kinks which are formed due to large-scale deformations like nodes which are regions with highly localized compressive strain in the fiber wall of the curled cellulosic fibers. The orientation angle of helically wound cellulose fibrils is increased and/or the fibrils are completely disoriented in these fiber wall regions - depending on the severity of the compaction [DUMBLETON, 1971, 1972; PAGE ET AL., 2003; SETH, 2005]. Figure 2.7 also shows how the microcreping effect becomes more pronounced, i.e. the scale of deformations increases, when the solids content during the MD compaction is increased. Besides the curling of fibers some bonds which have already been formed between fibers break [IHRMAN AND ÖHRN, 2003].

The induced microcreping effect increases the ductility of paper in a similar manner as the drying shrinkage in CD, decreased strain rate as well as increased temperature and moisture content (see Section 2.1.3). Figure 2.8 illustrates this by showing examples of the specific stress versus strain curves in MD for kraft paper and extensible kraft paper. In comparison to kraft paper, extensible kraft paper has reduced load carrying ability under tensile load in MD due to the introduced deformations, i.e. tensile stiffness index and tensile index of the paper are decreased. Upon reaching the yield point the elongation of extensible kraft paper occurs by straightening out the microcreped structure and simultaneous weakening/breaking of the bonds which have been formed between curled fibers, as shown in Figure 2.9. This elongation behavior differs considerably from the plastic deformation of other paper grades (e.g. kraft paper) in a way that the weakening/breaking of the bonds is much lower if the paper is produced without inducing the microcreping effect (see Section 2.1.3). The elongation of extensible kraft paper upon reaching the yield point corresponds with the long center part of the stress versus strain curve with low strain hardening. The straightened fibers bear the load more efficiently which in turn leads to increased strain hardening before rupture of the fiber network. Thus, the stress ver-

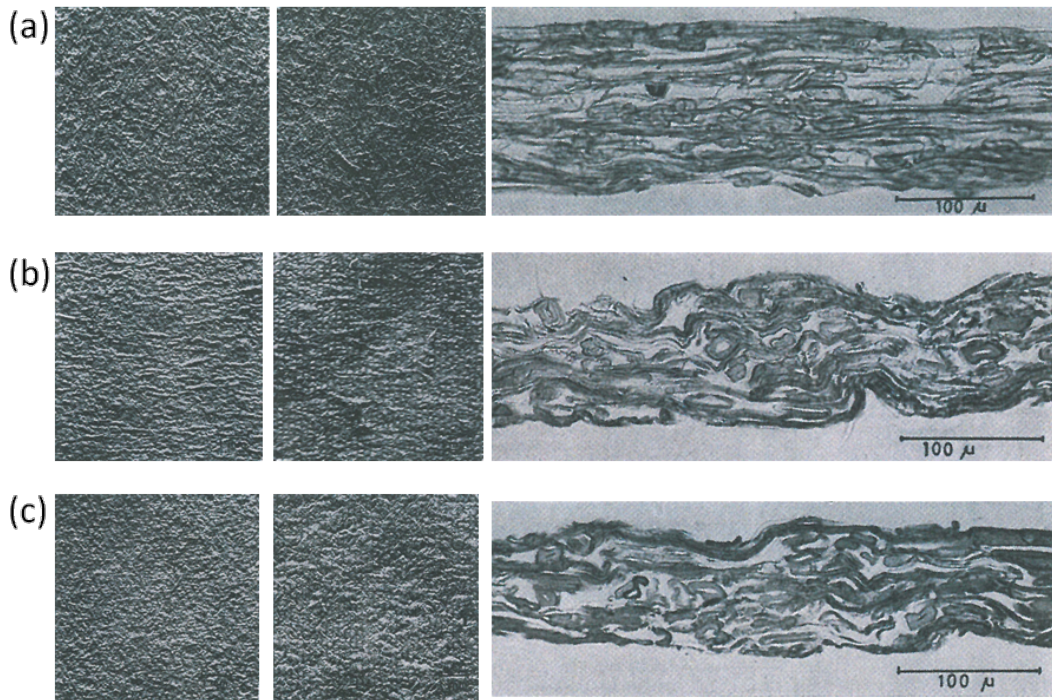


**Figure 2.7** Surfaces and cross section of kraft paper and extensible kraft papers. The images for each paper sample (a-c) are described from left to right. (a) Top side, wire side and cross section of kraft paper. (b) Rubber surface side, cylinder surface side and cross section of extensible kraft paper with highly pronounced microcreped structure. (c) Rubber surface side, cylinder surface side and cross section of extensible kraft paper with less pronounced microcreped structure. The extensible kraft papers were produced with the Expanda process [IHRMAN AND ÖHRN, 2003].

sus strain curve becomes sigmoidally shaped. Altogether this leads to higher strain of the paper but the tensile strength is decreased due to disturbed interfiber bonding after straightening out of the microcreped structure [BURROW, 1965; DUMBLETON, 1971, 1972; IHRMAN AND ÖHRN, 2003; POPPEL, 1996; SETH, 2005].

All the MD mechanical properties mentioned above have an effect on the area under the stress versus strain curve, i.e. the TEA of paper. When the stress versus strain curves of kraft paper and extensible kraft paper are compared, it is obvious that the strain dominates the development of TEA [BURROW, 1965; IHRMAN AND ÖHRN, 2003]. For example the kraft paper presented in Figure 2.8 has TEA index of 1.6 J/g in MD whereas the extensible kraft paper has TEA index of 3.6 J/g in MD.

In order to study the shape of the stress versus strain curve quantitatively, a form factor  $\kappa$  can be used. It is defined as the ratio of area under the curve to the theoretical maximum area with the corresponding tensile strength and strain at break values, and is expressed as:

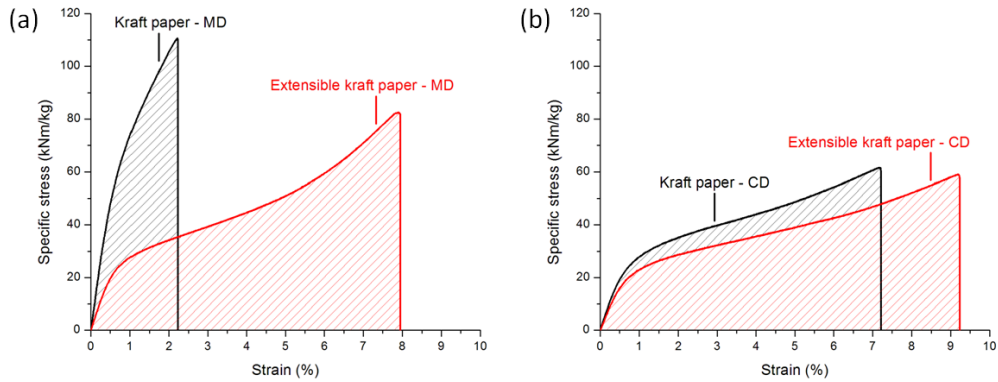


**Figure 2.8** Specific stress versus strain in MD (a) and CD (b) for kraft paper and extensible kraft paper with basis weight of  $80 \text{ g/m}^2$ .

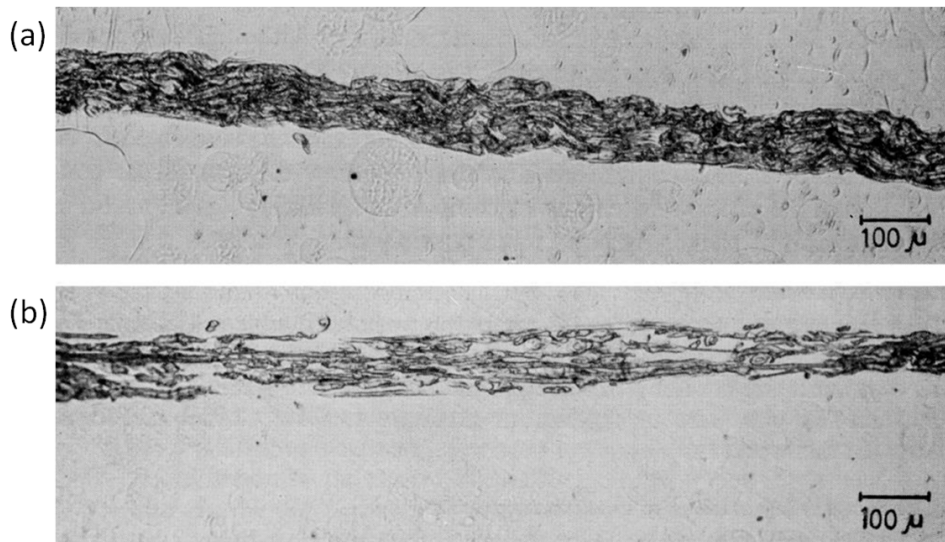


**Figure 2.9** Cross section of extensible kraft paper produced with the Expanda process before (a) and after (b) straightening out of the microcreped structure [IHRMAN AND ÖHRN, 2003].

$$\kappa = \frac{TEA}{\sigma_b \cdot \epsilon_b} \quad (2.18)$$

where  $\sigma_b$  is the tensile strength and  $\epsilon_b$  the strain at break. The form factor is especially useful for studying extensible kraft papers in MD due to the importance of a sufficiently high yield point. The higher yield point leads to the higher deformation load in the long center part of the sigmoidally shaped stress versus strain curve. Thus, the

form factor as well as TEA reach considerably higher values in comparison to the sigmoidally shaped stress versus strain curve with the same tensile strength and strain at break but lower yield point. Kraft papers are in turn so stiff and brittle that the changes in the yield point do not cause such a strong variation in the form factor and TEA if the tensile strength and strain at break stay the same. Due to the sigmoidally shaped stress versus strain curve, the form factor of extensible kraft paper is lower in comparison to kraft paper [BURROW, 1965; IHRMAN AND ÖHRN, 2003]. For example the kraft paper presented in Figure 2.8 has a form factor of 0.64 in MD whereas the extensible kraft paper has a form factor of 0.56 in MD. The form factor of extensible kraft paper in MD is sensitive to changes in some papermaking parameters, e.g. fiber orientation and draw during drying. A more oriented paper leads to a lower form factor and higher TEA. A tighter draw of paper web in turn increases form factor while strain at break decreases [IHRMAN AND ÖHRN, 2003]. This can be connected to the increased fiber network activation described in Section 2.1.3.

All three major Clupak process parameters, i.e. the speed difference between inlet and outlet of the nip, nip width and solids content of paper during the compaction, have effects on the final mechanical properties of paper. The increased speed difference between inlet and outlet of the nip and the increased nip width without outlet draw enhance the mechanical properties characteristic for extensible kraft paper. Decreased solids content during the compaction in turn leads to the lower strain whereas TEA is less affected [IHRMAN AND ÖHRN, 2003].

The Clupak process affects also on CD mechanical properties of paper. Strain and TEA increase whereas elastic modulus and form factor decrease in CD as a consequence of the MD compaction, i.e. in the same way as in MD but less pronounced. Figure 2.8 demonstrates this by showing examples of the specific stress versus strain curves in CD for kraft paper and extensible kraft paper. In Figure 2.8, the kraft paper and extensible kraft paper have TEA indices in CD of 2.9 J/g and 3.4 J/g and form factors of 0.66 and 0.63, respectively. However, the tensile strength in CD is not greatly affected by the MD compaction [BURROW, 1965; IHRMAN AND ÖHRN, 2003].

## 2.3 Link between structural and mechanical properties

### 2.3.1 Effect of structural non-uniformity on deformation

Besides the microcreped structure as well as the other mentioned factors affecting on the mechanical behavior of paper (see Section 2.1.3), it is also important to take into account the heterogeneous structure of the fiber network (the structure is explained in Section 2.1.1) when analyzing the mechanical performance. During the paper web forming process fibers, fiber fragments, mineral fillers and chemical additives settle stochastically in the web formed on the wire. As a result, basis weight varies in the plane of the web. This kind of basis weight variability in small-scale (0.1-20 mm)

is called formation and its uniformity is the most important property of paper from the practical point of view. Poor formation may lead to paper strength problems [ALAVA AND NISKANEN, 2006; NISKANEN AND PAKARINEN, 2008; NORMAN, 2007]. Weak correlation between local basis weight and local deformation has been found, i.e. regions with lower basis weight deform more [WONG ET AL., 1996]. On the other hand, the connection between formation and stress versus strain behavior of paper is often fairly weak or completely missing [ALAVA AND NISKANEN, 2008; KIMURA ET AL., 1985; NORMAN AND WAHREN, 1976]. The extent to which formation affects on the local and global deformation (global deformation is the strain measured with a tensile tester) of paper depends on spatial variations in various other structural factors such as fiber orientation, bonding degree, internal stresses due to drying shrinkage or wet strain, fines and filler content and fiber density [ALAVA AND NISKANEN, 2008; KORTEOJA ET AL., 1996, 1998; NORMAN AND WAHREN, 1976]. Furthermore, the degree by which high basis weight regions reduce or increase stress and strain concentration on the neighboring low basis weight regions has an effect on the local and global deformation behavior. Low basis weight regions having two high basis weight region neighbors perpendicular to the loading direction could have a protective effect. On the other hand, turning the regions 90 degrees could cause a high concentration of stress and strain to the low basis weight region [KIMURA AND SHIMIZU, 1985; THORPE, 1981; WONG ET AL., 1996]

Formation combined with spatial variations in the other structural factors leads to local tensile stiffness variations within paper. Most probably local strain hardening varies also in a similar manner. When paper is subjected under tensile load, parts with lower stiffness (weak parts) stretch more than parts with higher stiffness (strong parts) [HAGMAN AND NYGÅRDS, 2012; KORTEOJA ET AL., 1996, 1997, 1998; NORMAN, 1966; OSTOJA-STARZEWSKI AND CASTRO, 2003]. Figure 2.10 illustrates this by showing strain profiles of paperboard deformed in CD along the blue line drawn in the strain map. The local strain behavior (strain map) was measured with a speckle photography during tensile testing of the paperboard strip. The nonuniformity of the strain profile increases with increasing global strain of the paper - especially beyond elastic deformation of the paper [HAGMAN AND NYGÅRDS, 2012; KORTEOJA ET AL., 1997]. Damage in the highly strained regions through breakage of interfiber bonds causes redistribution of stresses to the unbroken regions, and thus increases the strain heterogeneity in the paper. Here, it must be stressed that the high local strain indeed precedes the local bond failures and not the other way round. With further straining, one of the damaged regions grows to a macroscopic crack which causes total failure by propagating through the paper [ALAVA AND NISKANEN, 2008; BORODULINA ET AL., 2012; CONSIDINE ET AL., 2005].

Structural non-uniformity, and thus local strain variability of paper affects elastic modulus only weakly due to the fact that the elastic modulus is proportional to the average elastic energy in paper [ALAVA AND NISKANEN, 2008]. However, higher vari-

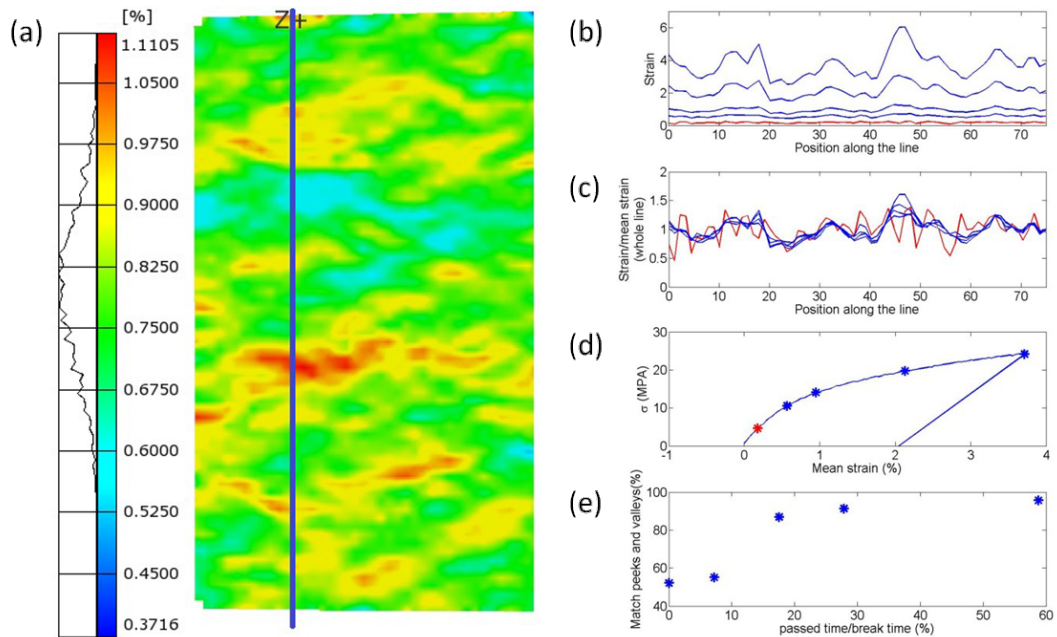


**Figure 2.10** Local strain behavior (measured with a speckle photography) of a  $100 \times 50 \text{ mm}^2$  paperboard strip in CD during tensile test. (a) Strain field in the early stage of the plastic deformation. (b) Strain profiles along the blue line shown in (a) during different stages of the deformation. (c) Strain profiles normalized against the mean of the blue line. (d) Stress versus strain curve showing the positions of the strain profiles. (e) Comparison of the peak and valley positions of the strain profiles during different stages against the strain profile just prior to break [HAGMAN AND NYGÅRDS, 2012].

ation in local strains decreases the yield point of paper as the highly strained regions start to yield earlier. This leads to the situation where a smaller portion of the paper area yields plastically before the rupture. In other words, the strain and damage are heavily localized into the low stiffness and strain hardening regions. Figure 2.11 demonstrates this by showing the effect of structural non-uniformity (formation) on the local and global (external) strain behavior. The analysis was performed by measuring the formation map with a  $\beta$ -radiography and correlating it with the strain map (local strain behavior) which was in turn determined with a digital image correlation during tensile testing (global strain behavior). It can be also clearly seen from Figure 2.11 that the difference between local and global strain in the failure zone increases with the structural non-uniformity. Eventually, uneven distribution of the global strain within the paper leads to lower breaking strain and tensile strength [ALAVA AND NISKANEN, 2008; HAGMAN AND NYGÅRDS, 2012; KORTEOJA ET AL., 1996, 1997, 1998].

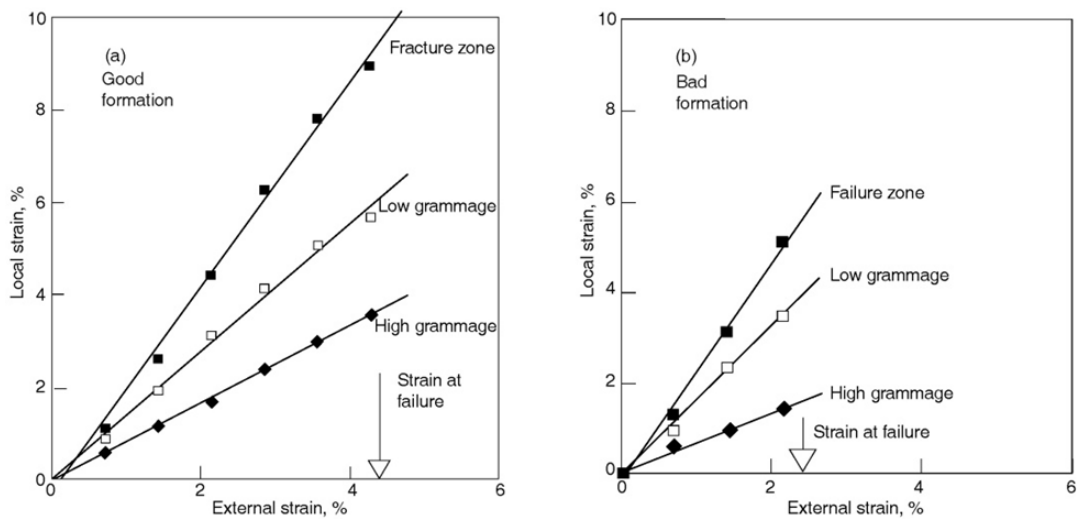


**Figure 2.11** Local versus global (external) strain for copy papers with good formation (a) and bad formation (b) made with pilot scale paper machine. The mean local strain for low grammage (basis weight) regions (basis weight values belonging to the lowest 2.5%), high grammage regions (basis weight values belonging to the highest 2.5%) and failure zone during the deformation were followed separately. The formation maps were measured with a  $\beta$ -radiography whereas a combination of tensile tester and digital image correlation was used to measure the global and local strains. [ALAVA AND NISKANEN, 2008; KORTEOJA ET AL., 1998].

### 2.3.2 Effect of sample size on deformation

Size and length to width ratio of the tested paper also affect on the strain behavior due to the fact that the highly straining regions are relatively constant in size [HAGMAN AND NYGÅRDS, 2012]. In other words, the global strain is distributed differently to the highly straining regions when the paper dimensions are changed. This can be seen in Figure 2.12 where strain distributions for paperboard with different sizes are presented in MD. The strain maps were measured with a speckle photography during tensile testing of the paperboard strips. It is more likely in the case of narrow samples that a highly straining region crosses the whole paper strip. The breaking strain subsequently decreases. Figure 2.12 further shows how the decrease in length to width ratio leads to earlier yield, decreased strain hardening and increased strain at break when the ratio is controlled by keeping either length or width constant [HAGMAN AND NYGÅRDS, 2012]. Thus, the sample size also clearly affects on the shape of the stress versus strain curve in addition to the microcreeping effect (see Section 2.2.3) and other factors described in Section 2.1.3.

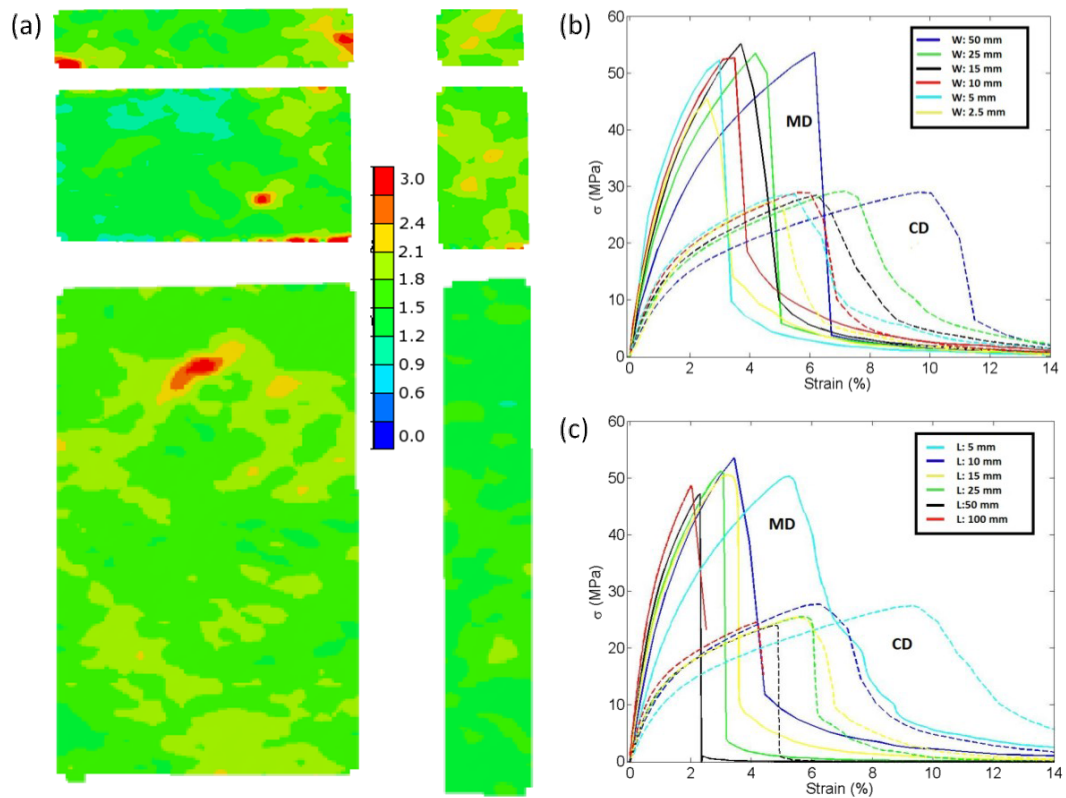


**Figure 2.12** Size dependence of local and global strain behavior for paperboard during tensile test. The strain maps (local strain behavior) were measured with a speckle photography during tensile testing (global strain behavior). (a) Local strain behavior (%) for following strip sizes in MD (row by row):  $10 \times 50$ ,  $10 \times 15$ ,  $25 \times 50$ ,  $25 \times 15$ ,  $100 \times 50$  and  $100 \times 15 \text{ mm}^2$ . (b) Stress versus strain in MD and CD for strips with constant length of 10 mm and varying width. (c) Stress versus strain in MD and CD for strips with constant width of 15 mm and varying length [HAGMAN AND NYGÅRDS, 2012].

### 2.3.3 Deformation studies with infrared thermography

Tensile deformation of paper has also been studied with infrared (IR) thermography [ALAVA AND NISKANEN, 2008; DUMBLETON ET AL., 1973; EBELING, 1976; YAMAUCHI, 2012]. This method is based on the fact that thermal energy is absorbed or dissipated depending on the nature of deformation, as shown in Figure 2.13. The absorption of thermal energy occurs during the elastic/viscoelastic tensile deformation of paper. This is called Kelvin's thermoelastic effect in thermodynamics. Removal of the applied load in the elastic/viscoelastic region of the stress versus strain curve leads to the release of the absorbed thermal energy which means that the elastic/viscoelastic behavior of paper is thermodynamically reversible. When the tensile deformation of paper changes from the elastic/viscoelastic to plastic after the yield point, the thermal

energy is dissipated instead. This dissipation of thermal energy continues also after removal of the applied load in the plastic region of the stress versus strain curve which in turn means that the plastic behavior of paper is thermodynamically irreversible. As the reloading elastic modulus in the plastic region of the cyclic stress versus strain curve shown in Figure 2.13 is approximately equal to the initial elastic modulus, the dissipation of thermal energy occurs mainly due to the irreversible intrafiber deformations and gradual opening of the interfiber bonds (see Section 2.1.3). Only a minority of the interfiber bonds open completely due to the fact that the amount of fiber segments bearing the load must remain almost constant in order to achieve similar values for the initial and reloading elastic moduli (see also Section 2.1.3) [ALAVA AND NISKANEN, 2008; DUMBLETON ET AL., 1973; EBELING, 1976; YAMAUCHI, 2012]. However, the behavior of extensible kraft paper in MD differs considerably in this respect due to the much stronger weakening/breaking of the bonds during the pullout of the microcreped structure (see Section 2.2.3 and especially Figure 2.9).

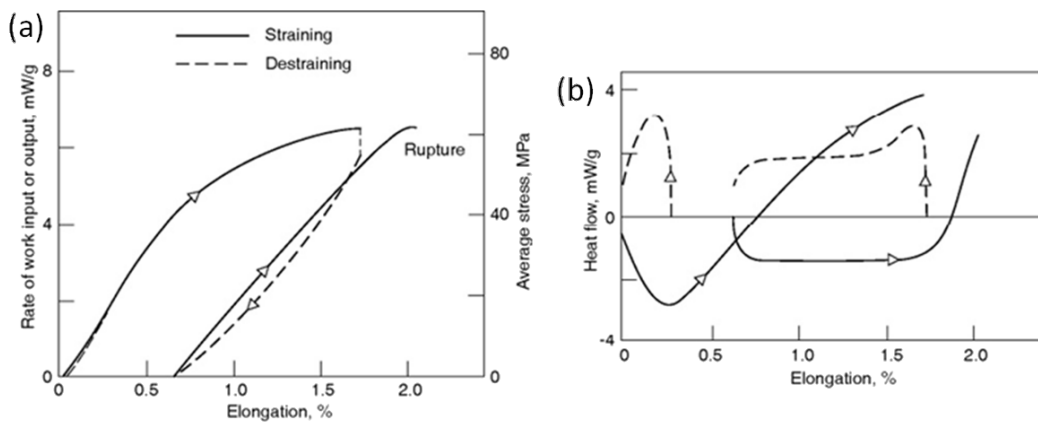


**Figure 2.13** Cyclic stress versus strain (elongation) curve (a) and simultaneous thermodynamic behavior (b) for rag paper in CD. The stress is directly proportional to the rate of mechanical work input or output when the strain rate is constant. The measurements were performed with a tensile tester and a microcalorimeter [ALAVA AND NISKANEN, 2008; EBELING, 1976].

The local plastic deformations within a paper sample can be followed by observing the thermal distribution during deformation [DUMBLETON ET AL., 1973; HYLL ET AL., 2012B; YAMAUCHI, 2012]. When paper sample with good formation is subjected under tensile load while simultaneously recording thermal images with an IR camera, the thermal distribution of paper appears to be fairly uniform until the moment of rupture. In the case of paper with poor formation, the thermal distribution may become uneven already in the early stage of the plastic deformation. The first three cases in Figure 2.14 demonstrate this by showing the thermal distribution images during deformation, formation image and breaking load/strain values. In these three cases the

initiating point of the final rupture can be predicted in the early stage of plastic deformation by observing the regions with highest temperature. When compared with the paper with good formation, the breaking load is lower in these three cases. The fourth case in Figure 2.14 differs from the other three because the thermal distribution is fairly even throughout the deformation although the formation is poor. The breaking load is also higher similar to the papers with good formation. Thus, it can be deduced that poor formation does not necessarily cause heavy localization of damage and the breaking load is more dependent on the distribution of plastic deformation within the paper [YAMAUCHI, 2012; YAMAUCHI AND MURAKAMI, 1993, 1994]. This also illustrates the fact described in Section 2.3.1 that the spatial variations in various other structural factors than formation have an effect on the local and global deformation of paper.

However, Figure 2.14 indicates that the final rupture of paper occurs in the region with low basis weight and high temperature [YAMAUCHI AND MURAKAMI, 1994]. Similarly, Figure 2.15 showing the formation, strain distribution and rupture line of two paper strips illustrates that the final rupture originates from the region with low basis weight. The formation maps and the strain distribution maps were measured with a  $\beta$ -radiography and a combination of tensile tester and video image correlation, respectively. Besides, local strain is also high in this region [WONG ET AL., 1996]. The critical scale of deformation which leads to the rupture of paper is evaluated to be approximately 1 mm [HRISTOPULOS AND UESAKA, 2004]. After the initiation, the rupture line proceeds perpendicular to the load independently of the formation. From the rupture line in Figure 2.15 it can be also seen that the two parts in the rupture initiation region are overlapping whereas the rest of the line is clearly separated. This indicates that the plastic deformation was higher in this region [WONG ET AL., 1996].

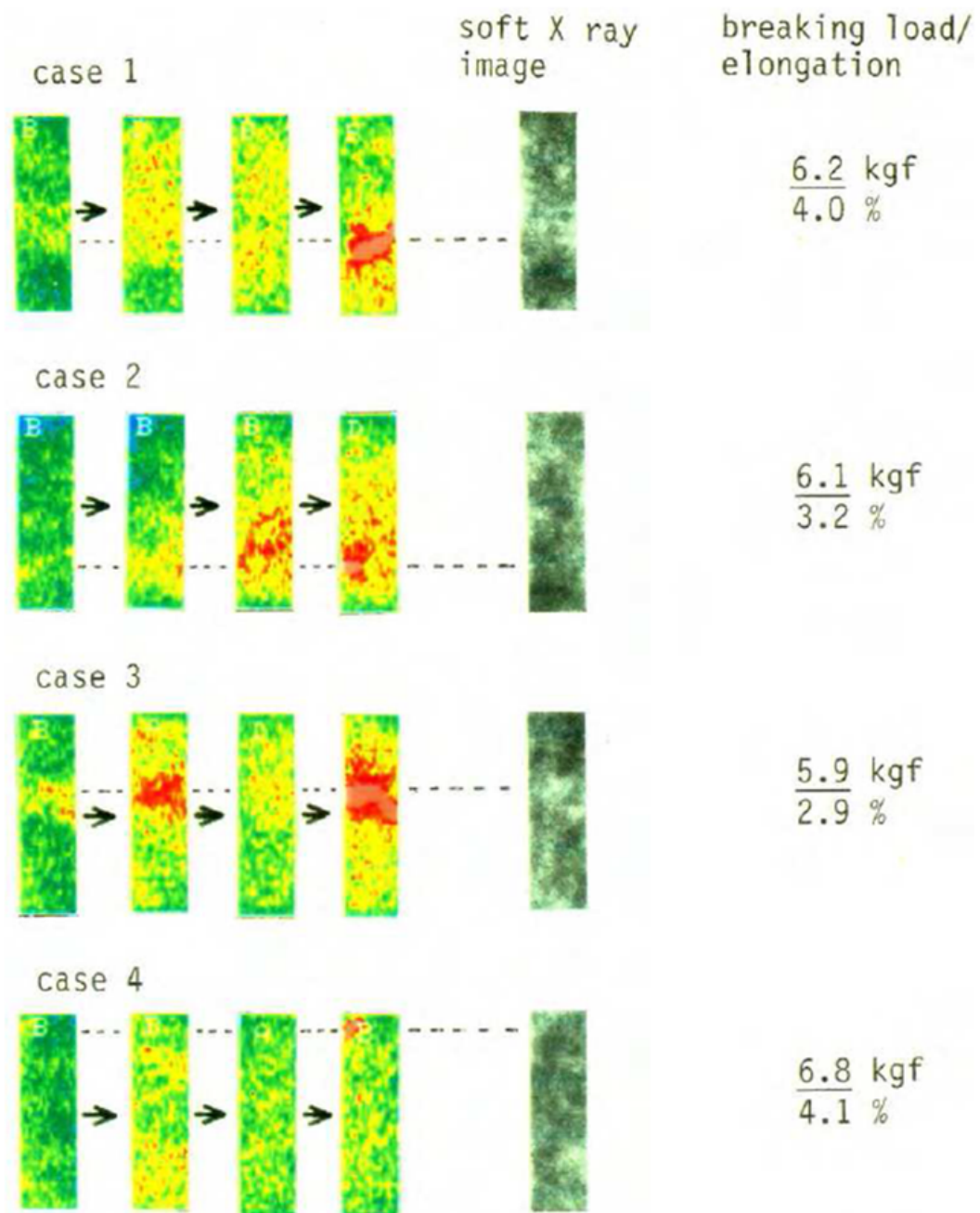


**Figure 2.14** Temperature rise distribution map, formation map and breaking load/strain values for four  $50 \times 15 \text{ mm}^2$  laboratory made bleached kraft paper strips. The measurements were performed with a soft X-ray method (formation maps) and a combination of tensile tester (breaking loads/strains) and IR camera (temperature rise distribution maps). The formation was made poor intentionally [YAMAUCHI AND MURAKAMI, 1994].

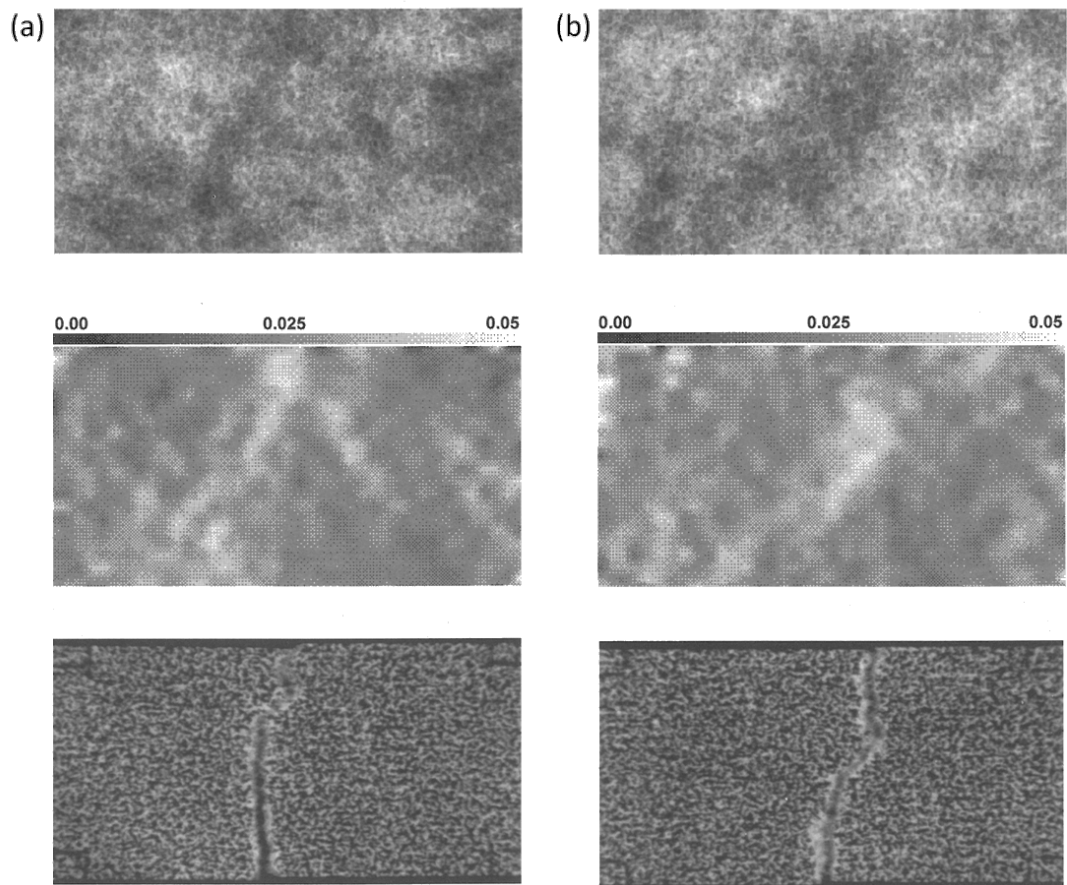


**Figure 2.15** Formation map, strain distribution map and rupture line (from top to down) for two (a & b)  $50 \times 20 \text{ mm}^2$  laboratory made unbleached kraft paper strips. The measurements were performed with a  $\beta$ -radiography (formation maps) and a combination of tensile tester and video image correlation (Strain distribution maps). Dark regions correspond with low basis weight in the formation maps whereas light regions correspond with high strain in the strain distribution maps. [WONG ET AL., 1996].

## 2.4 Conclusions

This literature survey offered an in-depth description of the causality between structural and mechanical properties of paper - especially from the perspective of extensible kraft paper. However, some important issues remain still unclear.

First, the structure and MD mechanical properties of extensible kraft paper can be controlled by altering the final compaction level and the solids content during the compaction with a Clupak extensible unit. The increased level of final compaction leads to a stronger microcreeping effect in the paper network. As a consequence,

MD breaking strain and TEA increase whereas MD elastic modulus, tensile strength and form factor decrease. The decreased solids content during MD compaction in turn decreases the scale of deformations leading to the decreased MD breaking strain whereas MD TEA is less affected. In order to compensate the substantial loss in TEA caused by decreased breaking strain, MD tensile strength and/or form factor must increase. Based on this, the following important research question can be addressed: Is it possible to decrease the solids content during MD compaction in a way that the reduction of TEA could be avoided by compensating the reducing breaking strain with increasing tensile strength and/or form factor? The answer for this question is searched in the experimental studies with laboratory and industrial scale trials. The increased load carrying ability achieved in this way without sacrificing the TEA would offer high potential for the reduction in water, energy and raw material consumption during the production of extensible kraft paper.

Second, paper is a viscoelastic-plastic material and thus becomes more viscous/ductile with increasing moisture content and temperature due to the softening of amorphous components in the fiber wall and weakening of the interfiber bonds. Besides, the mechanical behavior of paper is history dependent. These are all important factors to be taken into account in practice as the RH, temperature as well as duration and order of applied stresses/strains may all vary greatly during the end-use of industrial bags made of kraft paper or extensible kraft paper. Thus, the practical mechanical performances of kraft paper and extensible kraft paper are estimated and compared in the experimental studies by measuring the viscoelastic, creep and creep recovery behavior under different constant as well as dynamically changing atmospheres and temperatures. It is already known that the viscous behavior becomes stronger and creep rate increases with increasing RH and temperature. Furthermore, the creep rate increases under cyclic RH (accelerated creep). In order to increase the knowledge of practical mechanical performance further, the following research questions can be addressed: How does the viscoelastic behavior of kraft paper and extensible kraft paper differ under different atmospheres when the temperature increases dynamically? How does the creep and creep recovery behavior of kraft paper and extensible kraft paper differ when exposed to different combinations of atmospheres, temperatures and creep-recovery histories (effect of history dependency)? By finding answers to these questions, the knowledge how the microcreped structure affects the practical mechanical performance of industrial bags can be deepened. Furthermore, the critical conditions where the probability for bag failure is especially high can be detected in a more detailed manner.

Third, the structure of paper is heterogeneous and its deformation behavior is dependent on the formation in combination with other structural non-uniformities. Increased spatial variability in the structural factors leads to higher variation of local stiffness and strain hardening within paper. Thus, the strain and damage are heavily localized into the regions with low stiffness and strain hardening. These regions

are relatively constant in size and one of them with low basis weight gives rise to a macroscopic crack which causes paper rupture. The critical scale for rupture initiation within the region is approximately 1 mm. Based on this, the following research questions can be addressed: Which kind of local structure actually causes the high localization of strain and damage within a paper sample? How does the microcreped structure of extensible kraft paper change the strain and damage distribution within the sample? It is already known that the weakening/breaking of the bonds during the plastic deformation of extensible kraft paper in MD is much stronger in comparison to the kraft paper. In the case of kraft paper, substantial breakage of the bonds occurs only in the regions where the rupture line initiates and proceeds during the final rupture of the sample. Thus, it could be possible that the distribution of strain and damage is more even during the deformation of extensible kraft paper. In order to find answers to the addressed research questions, local basis weight and density are linked to the local tensile damage. This enables deepening of the knowledge how kraft paper as well as extensible kraft paper deforms, and thus offers new possibilities for the optimization of the structure of both papers.

In the following Chapter 3, methodologies and experimental plans for studying the research questions described above are presented.

## Materials and methods

Methodologies and experimental plans for studying the defined research questions are presented in this chapter which is further divided into four sections. A method and a plan for studying the effect of solids content during MD compaction on the structural and mechanical properties of extensible kraft paper on the laboratory scale are introduced in Section 3.1. The contents of this section are also largely described by LAHTI ET AL. [2014]. This study is enlarged in Section 3.2 by introducing an industrial scale plan for studying the effects of Clupak process parameters on the extensible kraft paper properties. A plan for estimating the practical mechanical performance of kraft paper and extensible kraft paper through measurements of viscoelastic, creep and creep recovery properties while exposed to different combinations of atmospheres, temperatures and loading histories is then presented in Section 3.3. The contents of this section are also largely described by GREGOROVA ET AL. [2013]. Finally, the local paper properties are analyzed in Section 3.4. More precisely, a method and a plan for studying the relationship between local basis weight, density and tensile damage of kraft paper and extensible kraft paper are presented. The contents of this section are in turn largely described by HIRN AND LAHTI [2015].

### 3.1 Laboratory scale study of extensible kraft paper

#### 3.1.1 Sample preparation

Unbleached softwood kraft pulp taken from the paper production line after low-consistency refining was used in this laboratory scale study. The pulp properties were at the following level: a Kappa number of 45 (ISO 302), a fiber length of 2.5 mm (ISO 16065-1) and a Schopper-Riegler degree of 18 °SR (ISO 5267-1). The process steps for preparing extensible paper in the laboratory are presented in Figure 3.1. The

stock preparation and sheet forming were performed according to ISO 5269-2 (Rapid-Köthen method; FRANK-PTI, Birkenau, Germany) with the exception of using an air suction time of 1 min after the removal of suspension water. Subsequently, the formed sheet was couched onto the carrier board, removed from the screen and covered with the plotter board. The sheet was then consolidated in a Rapid-Köthen dryer at a temperature of 42°C and a suction pressure of 92 kPa for 12 min. In order to achieve different solid contents after the consolidation, the plotter board was removed from the sheet followed by either direct transfer to the MD compaction step or by fully restrained pre-drying in a drum dryer (AMC, Queensbury, NY, USA). The pre-drying temperature was 59°C held for 2 or 3 min.

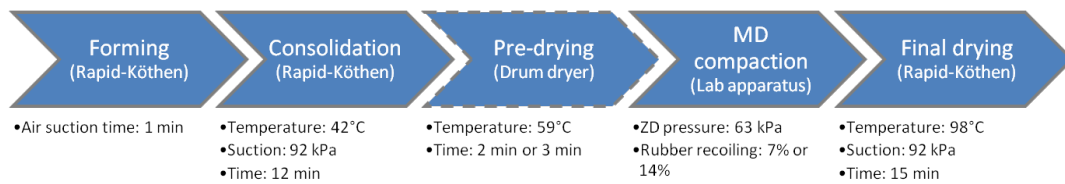


**Figure 3.1** Process steps for preparing extensible paper in the laboratory. Pre-drying was not performed for the sheets with lowest solids content during MD compaction. Pre-drying and final drying were fully restrained.

Inspired by Dumbleton's [DUMBLETON, 1971, 1972] work (apparatus for drying fibers under longitudinal compression), a custom-built apparatus for compacting the moist paper sheet in MD was designed. Photographs of the apparatus in unloaded and loaded state are shown in Figure 3.2 whereas the working principle of the apparatus is presented in Figure 3.3. Cleaned and grinded silicone rubber blankets with a hardness of 60° Shore A (ISO 868), an elastic modulus of 1.64 MPa, a Poisson's ratio of 0.49 and a thickness of 2 mm are used. The lower rubber blanket was stretched with a bench vise to a level resulting later in a rubber blanket recoiling of 7% or 14%. Then the moist paper sheet was placed onto the stretched lower rubber blanket followed by removal of the carrier board. The compaction direction (MD) was marked onto the paper sheet with a permanent marker pen and a stretched upper rubber blanket was placed onto the paper sheet. The sandwich of the two stretched rubbers with the paper in between was then placed between two pressure plates. In order to keep the influence of frictional effects during the MD compaction minimized, special care was taken to guarantee the smooth sliding of the rubbers between the pressure plates. This was done by equipping the upper pressure plate with a 5 mm thick polytetrafluoroethylene (PTFE) plate coated with graphite powder. A graphite powder coated web made out of PTFE impregnated glass fibers was in turn placed on the lower pressure plate. Furthermore, both rubber surfaces in touch with the pressure plates were coated with talc powder. Pressure in the thickness direction (ZD) was applied to generate sufficient friction between the paper sheet and the rubber sheets

by placing four springs with a spring rate of 14.62 N/mm to the corners of the upper pressure plate and compressing the springs between nut and bolt. The total ZD force was adjusted to the level of 2 kN, and thus the total ZD pressure (area of the circular paper sheet was  $316.16 \text{ cm}^2$ ) on the paper sheet was 63 kPa. In order to distribute the ZD pressure evenly across the paper sheet, a plano-convex shaped sheet made out of paper and tape was positioned between the upper pressure plate and the PTFE plate. The paper sheet was then compacted in MD by the rubber recoiling of 7% or 14% with the bench vise resulting in a shear stress of 2 kPa or 4 kPa on both sides of the paper sheet, respectively. The recoiling speed of the rubber blankets was approximately 2 mm/s. Due to the rubber's Poisson's ratio (see Section 2.1.2) of 0.49, the shear stress in CD was approximately 1 kPa or 2 kPa on both sides of the paper sheet, respectively. The MD compaction was not performed in case of the reference paper sheets. After compaction the ZD pressure was relieved and the compacted paper sheet was lifted from the lower rubber blanket with a carrier board. Finally the paper sheet was dried fully restrained in a Rapid-Köthen dryer with a temperature of  $98^\circ\text{C}$  and a suction pressure of 92 kPa for 15 min.

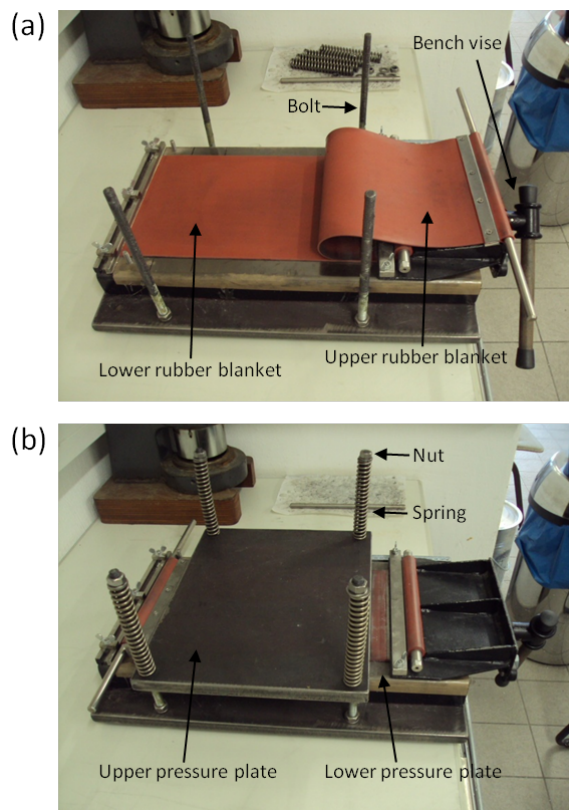


**Figure 3.2** Photographs of the MD compaction apparatus in unloaded (a) and loaded (b) state.

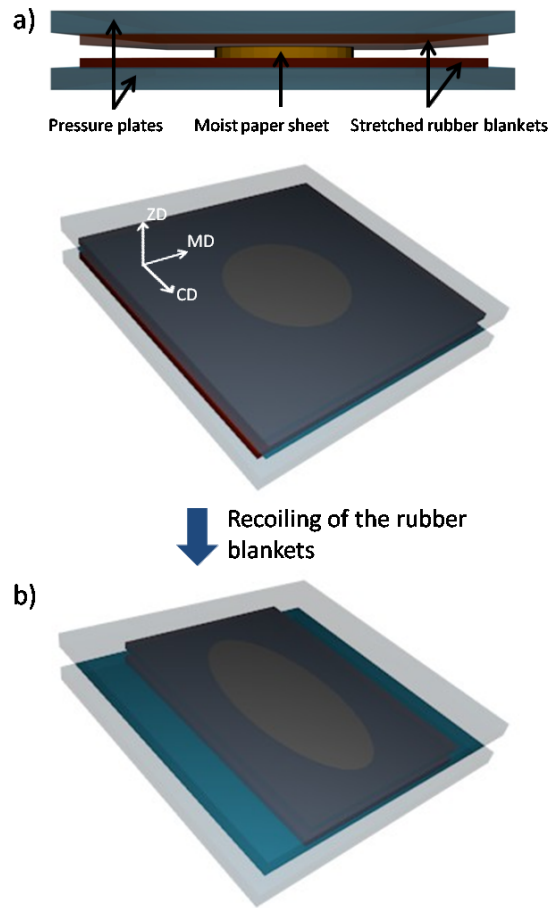


**Figure 3.3** Principle of the MD compaction apparatus. (a) Side and top view before the MD compaction. (b) Top view after the MD compaction. Besides MD compaction, extension occurs in CD.

### 3.1.2 Sample analysis

The mass of the paper sheet was measured directly after the MD compaction and again after the final drying (ovendry) to calculate the solids content of the paper sheet during the MD compaction. Before testing the prepared paper sheet was conditioned in a standard climate of 23°C and 50% RH. The compacted paper sheet has an ellipsoidal shape due to the MD compaction. The length of major (CD) and minor (MD) axis was measured to calculate the strain caused by the MD compaction in MD and CD. Furthermore, these strain values were used to calculate the plastic Poisson's ratio (Poisson's ratio based on permanent deformation) and the area of the paper sheet. The area together with the mass of the paper sheet measured after conditioning was used to calculate the basis weight of the paper sheet. Subsequently, six strips were

cut in MD from the paper sheet to determine the specific stress versus strain curves according to ISO 1924-3. Besides, form factors were calculated by using Equation 2.18. Finally, averages and standard deviations were calculated for the determined properties within individual sheets.

## 3.2 Industrial scale study of extensible kraft paper

### 3.2.1 Sample preparation

An industrial scale trial to study the effects of Clupak process parameters on the structural and mechanical properties of unbleached extensible kraft paper with a basis weight of  $80 \text{ g/m}^2$  was performed in a European kraft paper mill. Clupak nip pressure and solids content of paper web during the compaction were the parameters varied. The values for these variable parameters are shown in Table 3.1. The order of the trial points was chosen to make the adjustment of the parameters as easy as possible. Furthermore, the first and the last trial point were the same in order to study the effect of uncontrollable parameters, e.g. changes in the pulp quality, deviations in the machine settings, etc. One paper machine (PM) reel having a width of 4.2 m was produced on each trial point. The range of nip pressure and solids content during the compaction was chosen in a way that no final product broke was produced. The nip pressure was varied by controlling the pressure of 10 air springs below the nip bar. The solids content during the compaction was in turn adjusted by controlling the steam pressures of the drying groups before and after the Clupak extensible unit. Other controllable parameters of the papermaking process were kept constant during the trial. The machine speed was 630 m/min. The speed difference of the paper web between inlet and outlet of the Clupak nip was  $-40.5 \text{ m/min}$  which corresponds to a web draw of  $-6.2\%$ . In other words, the paper web was compacted  $6.2\%$  with the Clupak process. The compaction of the paper web on the pope reel was reduced by the draws after the Clupak extensible unit to the level of  $4.8\%$ .

### 3.2.2 Sample analysis

The sampling was performed by cutting 29.5 cm wide strips across the CD of the PM reel. The amount of collected strips was 13-15 per trial point. All the strips were analyzed with L&W Autoline 300 automatic paper testing system (Lorentzen & Wettre, Stockholm, Sweden). The measured/calculated paper properties relevant for this study with the corresponding method codes are presented in Table 3.2. The codes are used for the identification of the methods. Detailed descriptions of the methods are presented in the L&W Autoline 300 operating instruction manual [LORENTZEN & WETTRE]. Strain at break, tensile index and TEA index in MD and CD (Code 80-510) were measured 24 times across the strips at regular intervals whereas the other

Trial point	Solids content (%)	Pressure per air spring (kN/m)
P1	60	20
P2	60	35
P3	62	35
P4	62	20
P5	57.5	20
P6	57.5	35
P7	60	20

**Table 3.1** Trial plan for studying the effects of Clupak nip pressure, which was adjusted by controlling the pressure of 10 air springs below the nip bar, and solids content of paper during the Clupak compaction on the structural and mechanical properties of extensible kraft paper.

properties (Codes 80-538, 80-545, 80-515 and 80-516) were measured 12 times across the strips at regular intervals. The results from tender side, middle part and drive side were analyzed separately, i.e. the number of analyzed tender side-middle part-drive side measurements was 6-12-6 (Code 80-510) or 3-6-3 (others), respectively. This means that the total number of measurements per trial point was (tender side-middle part-drive side) 90-180-90 (Code 80-510) or 45-90-45 (others). Finally, averages and standard deviations were calculated for the individual trial points.

Property	Code
Basis weight	80-538
Small and large scale optical formation	80-545
Wire and upper side roughness	80-515
Air permeance	80-516
Strain at break in MD and CD	80-510
Geometric strain at break	-
Tensile index in MD and CD	80-510
Geometric tensile index	-
TEA index in MD and CD	80-510
Geometric TEA index	-
Form factor in MD and CD	-

**Table 3.2** Measured/calculated properties for the paper strips produced in the industrial scale Clupak compaction trial with the corresponding method codes. The codes are used for the identification of the methods. The analysis was performed with L&W Autoline 300 automatic paper testing system. Small and large scale optical formation corresponded with nonuniformities up to 1 mm and 1-50 mm, respectively [LORENTZEN & WETTRE]. Form factors were calculated using Equation 2.18. The geometric values were defined by calculating the geometric mean of the MD and CD values.

### 3.3 Analysis of viscoelasticity, creep and creep recovery

#### 3.3.1 Analysis of viscoelasticity

Viscoelastic behavior of industrially produced kraft paper and extensible kraft paper strips with a basis weight of  $80 \text{ g/m}^2$  were studied in MD with a dynamic mechanical analysis combined with relative humidity in a film-tension mode. Before starting the DMA, the strip was mounted in the DMA Q800 instrument (TA Instruments, New Castle, DE, USA) in a way that the area between the clamps of the instrument was  $5 \times 18 \text{ mm}^2$ . Both papers were measured with two different DMA programs shown in Table 3.3 and in each case three parallel measurements were performed. The first DMA program included dynamically increasing temperature under dry ( $N_2$ ) atmosphere whereas the atmosphere in the second DMA program was humid (50% RH). Consequently, it became possible to analyze the combined effect of atmosphere, dynamically increasing temperature and previous DMA cycles (effect of loading history) on the storage modulus and loss tangent (see Section 2.1.3) of both papers.

Program	1	2
Atmosphere	$N_2$	50% RH
Temperature ( $^{\circ}\text{C}$ )	-120 to 300	5 to 80
Heating rate ( $^{\circ}\text{C}/\text{min}$ )	3	1
Frequency (Hz)	1	1
Amplitude ( $\mu\text{m}$ )	20	20
Mode	Film-tension	Film-tension

**Table 3.3** DMA programs for studying the combined effect of atmosphere and dynamically increasing temperature on the storage modulus and loss tangent of kraft paper and extensible kraft paper.

#### 3.3.2 Analysis of creep and creep recovery

Besides the analysis of viscoelasticity, creep and creep recovery behavior of the kraft paper and extensible kraft paper strips ( $80 \text{ g/m}^2$ ) were also studied in MD with the DMA Q800 instrument by using the same strip size. Both papers were measured with five different creep-recovery programs described in Figure 3.4 and in each case two or three parallel measurements were performed. A creep stress of 10 MPa was selected for all of the programs as it clearly illustrates the difference in the creep and creep recovery behavior between the kraft paper and extensible kraft paper. The first and second program included single creep-recovery cycle under constant temperature. The atmosphere during the first program was dry ( $N_2$ ) whereas the second program included a constant humidity (50% RH). The number of creep-recovery cycles was multiplied in the third program which was performed under dry atmo-

### 3. Materials and methods    Analysis of viscoelasticity, creep and creep recovery 3.3

sphere and constant temperature. The atmosphere in the fourth program including multiple creep-recovery cycles was changed to dynamically increasing RH while the temperature was kept constant. Finally, the fifth program consisted of multiple creep-recovery cycles, dynamically increasing temperature and constant humid atmosphere. Through these five programs, it became possible to analyze the combined effect of different atmospheres, temperatures and previous creep-recovery cycles (effect of loading history) on the creep compliance, recoverable compliance and relaxation ability (see Section 2.1.4) of both papers.

### 3. Materials and methods Analysis of viscoelasticity, creep and creep recovery 3.3

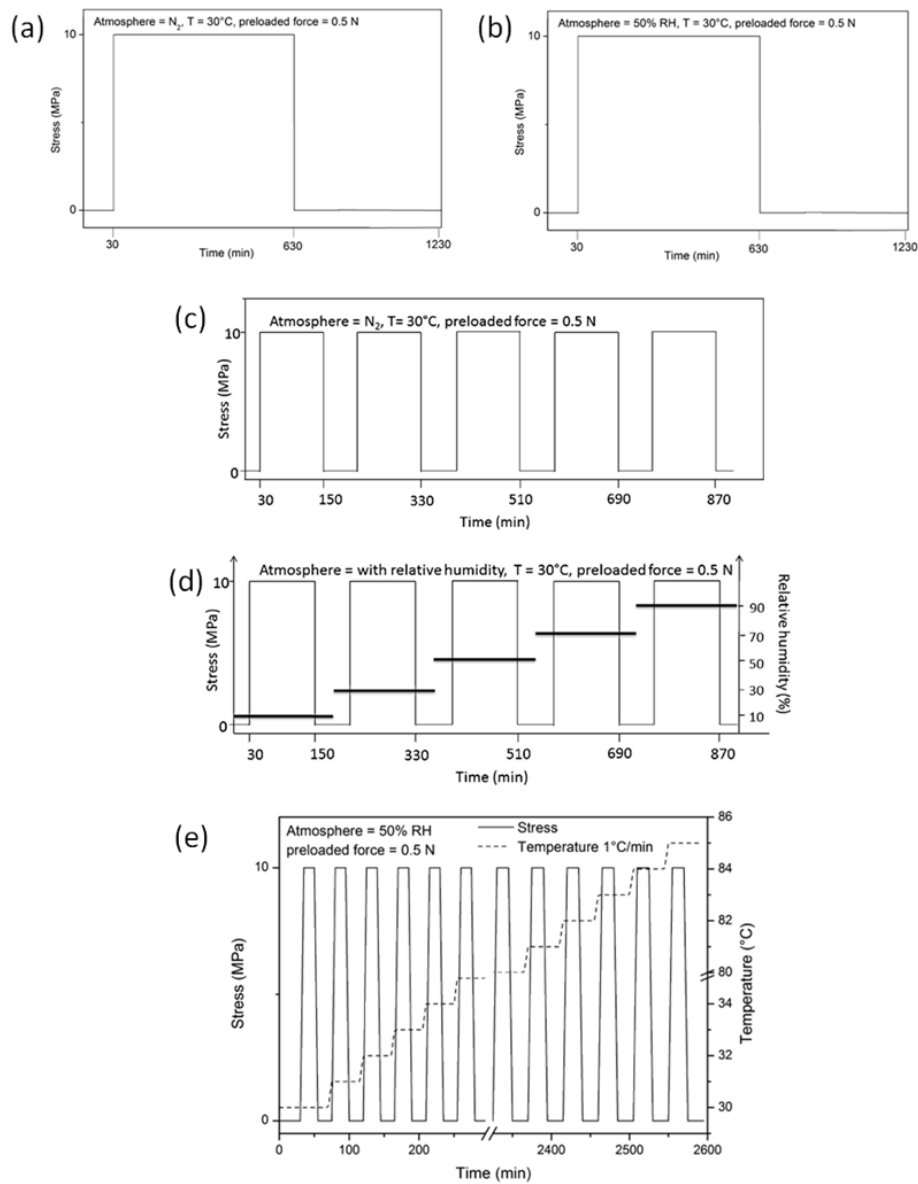


**Figure 3.4** Programs for studying the combined effect of different atmospheres, temperatures and previous creep-recovery cycles (effect of loading history) on the creep compliance, recoverable compliance and relaxation ability of kraft paper and extensible kraft paper. (a) Single creep-recovery cycle under dry atmosphere and constant temperature. (b) Single creep-recovery cycle under constant humidity and constant temperature. (c) Multiple creep-recovery cycles under dry atmosphere and constant temperature. (d) Multiple creep-recovery cycles under dynamically increasing RH and constant temperature. (e) Multiple creep-recovery cycles under constant humidity and dynamically increasing temperature.

## 3.4 Linking structural and mechanical properties

### 3.4.1 Measurement procedure

An industrially produced A4 unbleached kraft paper sheet and an industrially produced A4 unbleached extensible kraft paper sheet with basis weight of  $120 \text{ g/m}^2$  were the starting point in this study for analyzing local paper properties. Before the measurement procedure was started, an area of  $180 \times 180 \text{ mm}^2$  was marked with small holes (landmarks) on the A4 sheets. The marked areas are illustrated with white filled squares in Figure 3.5. First, air permeance map and optical transparency map of the marked sample areas were measured. Subsequently, the marked sample areas were cut into the  $50 \times 100 \text{ mm}^2$  strips and the tensile tests (80 mm distance between the tensile tester clamps) with simultaneous temperature map measurements were performed. Finally, the measured data was processed and analyzed through registration and point wise correlation [HIRN ET AL., 2008] by using the marker dots highlighted with white filled circles in the corners of the individual strips.

### Air permeance map measurement

Local air permeance measured with a small-scale air permeance measurement equipment [VOMHOFF AND BOUVENG, 2010] (Innventia, Stockholm, Sweden) was used together with local basis weight in the evaluation of local density of the paper sample. More precisely, low basis weight with low air permeance refers to high density as a low amount of fiber layers can effectively resist the air flow through the paper, i.e. the porosity is low. On the other hand, high basis weight with high air permeance refers to low density because a high amount of fiber layers is not able to effectively resist the air flow through the paper, i.e. the porosity is high.

The measurement principle of the local air permeance is shown in Figure 3.6. The paper sample (area within the hole markers) was measured between two perforated plates with coaxial holes having a diameter of 2 mm. The holes were arranged hexagonally and the distance between the centers of the adjacent holes was 2.67 mm. The local air permeance of the paper sample was measured from each hole with the measurement head. The measurement head consisted of the measurement probe and the pressure chamber. The actual measurement was performed by positioning the probe coaxially with the hole and measuring the air flow through the probe with flow meters. The task of the air flow in the pressure chamber was to minimize the lateral leakage flows by equalizing the pressure in the chamber and in the probe [VOMHOFF AND BOUVENG, 2010]. The total amount of local air permeance measurements per paper sample was 4758.

Every other cell of the measured air permeability matrix was empty because of the 0.67 mm wide unmeasured region between the adjacent holes. These empty cells were filled through interpolation, i.e. average of the row-wise adjacent local air permeance

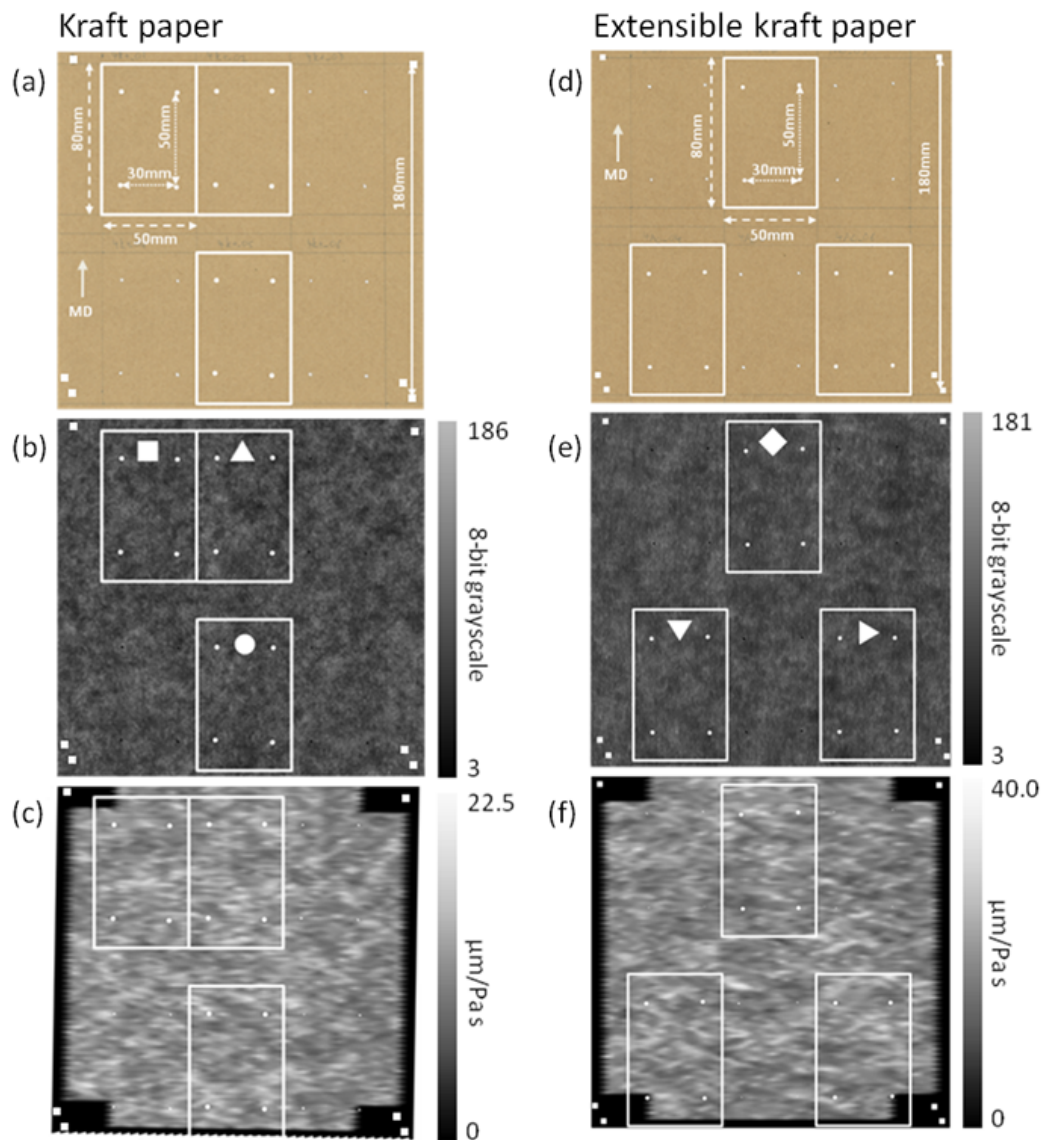


**Figure 3.5** Photographs (a & d), optical transparency maps (b & e) and air permeance maps (c & f) for kraft paper and extensible kraft paper samples. Holes (landmarks) used for registration of the total square-shaped sample area are highlighted with white filled squares. Three strips from both samples selected for the registration and correlation analysis after the tensile tests with simultaneous temperature map measurements are highlighted with white lines (area between the tensile tester clamps) and named with following white symbols:  $\square$ ,  $\triangle$ ,  $\circ$ ,  $\diamond$ ,  $\nabla$  and  $\triangleright$ . Dots (landmarks) used for registration of the strips are highlighted with white filled circles. Black refers to the non-measured regions on the edges of the air permeance maps (c & f).

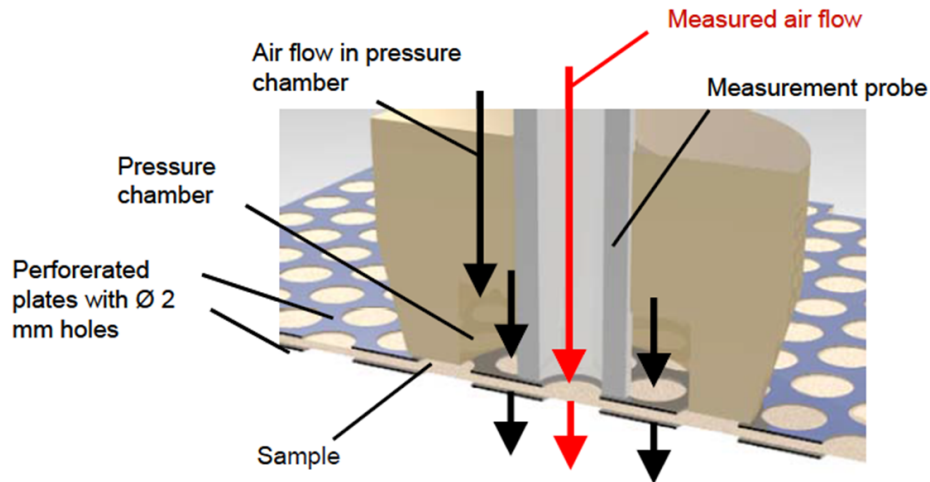


**Figure 3.6** Measurement principle of local air permeance of paper [VOMHOFF AND BOUVENG, 2010].

values were used as an estimation for the air permeance of the area in between. The averages were calculated and the resulting full matrix plotted with a resolution of  $257 \mu\text{m}/\text{pixel}$  by using a Python (Python Software Foundation) script. Figure 3.5 shows the plotted air permeance map for kraft paper and extensible kraft paper.

### Optical transparency map measurement

After the determination of the air permeance map, the paper sample ( $180 \times 180 \text{ mm}^2$ ) was divided with a pencil into six strips, and furthermore, four dots (landmarks) were placed using a felt pen with metallic ink into the corners of each strip for registration. The dots and the dimensions of the strips are illustrated in Figure 3.5 for the kraft paper and the extensible kraft paper. The sample area was then scanned (Creo *iQsmart*<sup>3</sup>) in a reflection and transmission mode with a resolution of  $43 \mu\text{m}/\text{pixel}$ . The optical transparency map obtained in the transmission scan (presented in Figure 3.5 for the kraft paper and the extensible kraft paper) was used as a measure for formation. This was possible because local basis weight is highly correlated to optical transparency for uncalendered papers consisting of components with similar optical properties - which is the case for the papers analyzed. In other words, very small variation in the local light scattering and absorption coefficients enabled good correlation between the local light transmission and the local basis weight [KOMPPA AND EBELING, 2003; NORMAN, 2007].

**Tensile test with simultaneous temperature map measurement**

After the structural measurements, the paper sample area was cut into the strips. The tensile testing of these strips in MD was performed with a Material Testing System (MTS Systems, Eden Prairie, MN, USA) including a load cell with a maximum load of 2500 N. The simultaneous temperature map measurements, in order to study the localization of tensile damage (see Section 2.3.3), were performed with a high speed SC6000 mid-wavelength (3-5  $\mu\text{m}$ ) infrared (MWIR) camera (FLIR Systems, Wilsonville, OR, USA). The paper strips were conditioned and the testing was performed in a standard climate of 23°C and 50% RH. First, a paper strip was fixed between the MTS clamps having a distance of 80 mm, i.e. 10 mm on both sides of the strip was inside the clamp. The camera was then positioned in front of the clamped paper strip. In order to minimize the effect of ambient radiation from the surroundings, the MTS was covered with paperboard sheets. The MWIR emittance of kraft paper has been previously measured to be  $0.76 \pm 0.03$  with Directional Emittance Measurement Method [HYLL ET AL., 2012B]. This method is based on the reference emitter methodology and was developed by Hyll et al. [HYLL, 2012; HYLL ET AL., 2012A]. The emittance value of 0.75 was chosen for the kraft and extensible kraft paper in this study. Subsequently, an image of the clamped paper strip was obtained as shown in Figure 3.7. The measurement procedure was started by initiating the camera recording with a resolution of 255  $\mu\text{m}/\text{pixel}$  and a frequency of 73 Hz. Shortly after this, the tensile test of the paper strip was started through movement of the upper clamp with a speed of 3.2 mm/s. The load versus displacement data were collected during the tensile test at a frequency of 102 Hz. In total six kraft paper and six extensible kraft paper strips were tested. Finally, three kraft paper and three extensible kraft paper strips where the rupture initiated within the area marked by the dots were selected for the registration and correlation analysis. The selected kraft paper strips were named with  $\square$ ,  $\triangle$  and  $\circ$  whereas the selected extensible kraft paper strips were named with  $\diamond$ ,  $\nabla$  and  $\triangleright$  (see Figure 3.5).

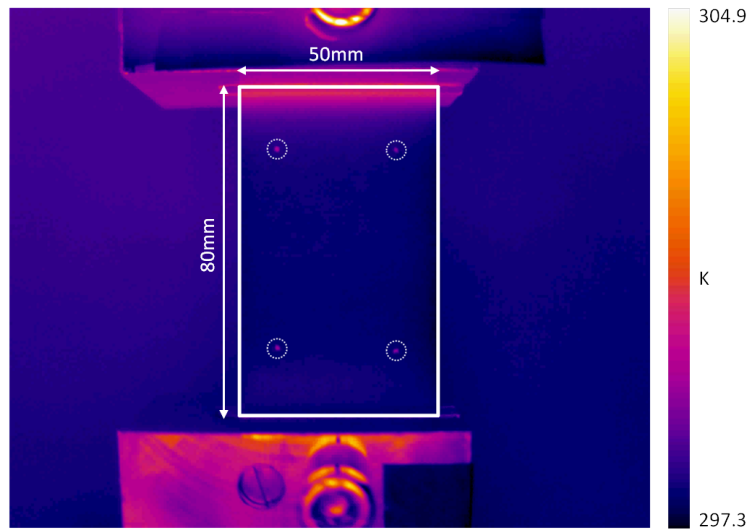


**Figure 3.7** IR image of a paper strip before tensile test. The sample area between MTS clamps is marked within the rectangle and marker dots (landmarks) are highlighted with dashed circles.

### 3.4.2 Data processing

First, the dots (landmarks) marked with felt pen on the paper strips were transcribed digitally to the air permeance maps in GIMP 2.8 (GNU Image Manipulation Program, The GIMP Development Team) by superimposing the air permeance map and the optical transparency map followed by the addition of the dots. The air permeance maps were then divided into the strips corresponding with the area between the clamps ( $50 \times 80 \text{ mm}^2$ ) by using a Bash script based on the ImageMagick convert tool (GNU, Unix shell). Due to the operations in GIMP, the air permeance data was replaced with 8-bit grayscale data. In order to get the air permeance data back, the ratio between air permeance and gray scale was calculated from the original air permeance map with the help of GIMP. This was possible because both scales were linear. The strip matrices including the gray scale data were then divided with the calculated ratio in MATLAB R2011b (MathWorks, Natick, MA, USA).

The optical transparency maps were also divided into identical strips with the air permeance images by using the Bash script. No further processing of the data was performed because the 8-bit grayscale values were used as a measure for local basis weight.

The processing of the temperature map was started by extracting the first image, the last image prior to rupture and the first image after rupture as data (MATLAB) matrices from the recorded IR image sequence. The last image prior to rupture and the first image after rupture were resized to the same size as the first image ( $50 \times 80$

$mm^2$ ) with a MATLAB script to compensate for the elongation of the sample due to straining during the tensile test. Thus the original geometry was restored which is necessary for image registration. The script was based on the `imresize` function in the Image Processing Toolbox [MATHWORKS, 2015]. First, the distances between the dots in MD and CD were calculated for the last image prior to rupture, the first image after rupture and the first image by using the coordinates of the dots. These distances were used to calculate the scales for the dimensional changes in MD and CD. The last image prior to rupture and the first image after rupture were then resized to the same size as the first image by multiplying the size vector with the corresponding scale vector.

### 3.4.3 Registration and correlation analysis

The landmark based registration of the measured and processed strip images was performed using a software developed by Hirn et al. [HIRN ET AL., 2008] (IPZ Datamap Registration Tool, Institute of Paper, Pulp and Fibre Technology, Graz University of Technology, Austria). First, the corresponding air permeance image, optical transparency image, temperature image prior to rupture and temperature image after rupture were imported into the registration software. This was followed by the definition of the coordinate system of the images, i.e the  $x$ ,  $y$  coordinates of the dot markers (landmarks) were marked to the images. The origin was in the center of the formed four line coordinate system. The images with defined coordinate system were then aligned through shape preserving coordinate transform, as described in Figure 3.8. More Precisely, the  $x$ ,  $y$  coordinates of the target image were mapped to the  $x'$ ,  $y'$  coordinates of the source images through translation, rotation and scale. The target image had an unrotated coordinate system with the origin at the center. The translation vector  $\mathbf{t}$  connecting the target image origin to the source image origin was used for the translation. The rotation was performed with the rotation angle  $\phi$  between the  $x$ - and  $x'$ -axes. The scale  $s$  was in turn defined by dividing the pixel size in the target image with the pixel size in the source image. The shape preserving coordinate transformation presented in Figure 3.8 can be thus mathematically presented as follows:

$$\begin{pmatrix} x' \\ y' \end{pmatrix} = \mathbf{t} + s \cdot \mathbf{r} \cdot \begin{pmatrix} x \\ y \end{pmatrix} = \begin{pmatrix} t_x \\ t_y \end{pmatrix} + s \cdot \begin{pmatrix} \cos \phi & \sin \phi \\ -\sin \phi & \cos \phi \end{pmatrix} \cdot \begin{pmatrix} x \\ y \end{pmatrix} \quad (3.1)$$

where  $\mathbf{r}$  is the rotation matrix. The pixel size in the target image was set to  $300 \mu\text{m}$  which was slightly larger than the largest pixel size of the source images ( $257 \mu\text{m}$ ). The slightly larger value was chosen in order to reduce the registration error. The registered images were then extracted and exported [HIRN ET AL., 2008].

For the correlation analysis, two regions with different sizes were registered, extracted and exported. First, a large region of  $34 \times 54 \text{ mm}^2$ , i.e. an area including the dot

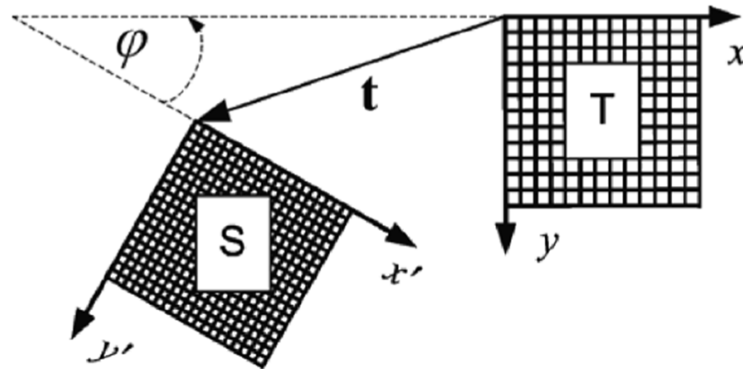


**Figure 3.8** Shape preserving coordinate transformation for registering source images (S) with defined coordinate system to a target image (T). The aligning is based on translation  $t$ , rotation  $\phi$ , and scale  $s$  [HIRN ET AL., 2008].

markers of a strip, was chosen for general qualitative correlation of the local air permeance, optical transparency and temperature. Second, three small high temperature regions and three small low temperature regions of  $2.7 \times 2.7 \text{ mm}^2$  were chosen from the large temperature image prior to rupture for a more accurate analysis. The size of the small region was chosen based on the sizes of the high temperature spots, i.e. local tensile damages, detected from the temperature maps just prior to rupture. More precisely, the size of the small region was proper to capture the patterns of interest from all of the maps being also large enough to take into account the considerably lower measurement resolution of the air permeance map (hole diameter of 2 mm). The selection of the small regions was based on the visual observation of the temperature map just prior to rupture, i.e. three very bright regions (high temperature) and three very dark regions (low temperature) were chosen for the accurate analysis to study the degree of correlation between the measured local properties. Subsequently, air permeance data, optical transparency data and temperature data just prior to rupture were registered, extracted and exported as CSV-files for the analysis. Mean values and standard deviations were then calculated within the small regions in MATLAB. In order to compare the mean values of the small regions to the mean values of the large regions, the relative values were calculated by subtracting the mean value of the large region from the mean value of the small region. These calculated values were then quantitatively analyzed to determine the dependence of local temperature (local tensile damage) on local optical transparency (local basis weight) and local air permeance (local density) by fitting linear regression models, i.e. the local temperature was modeled as a linear function of the local optical transparency and the local air permeance, and conducting an analysis of variance (ANOVA) [NETER ET AL., 1996].

This thesis is continued in the following Chapter 4 by presenting and analyzing the results gained from the above-described experiments.

## Results and Discussion

Results gained from the experimental studies are presented and analyzed, i.e. answers for the defined research questions are discussed, in this chapter which is further divided into five sections. All the discussions in this chapter are based on the background presented in Chapter 2. Section 4.1 and Section 4.2 focus on discussing and comparing the effects of solids content during MD compaction on the structural and mechanical properties of extensible kraft paper on the laboratory and industrial scale. The contents of Section 4.1 are also largely described by LAHTI ET AL. [2014]. The practical mechanical performance of kraft paper and extensible kraft paper is then estimated in Section 4.3 through analysis of viscoelastic, creep and creep recovery properties which were measured while exposing the papers to different combinations of atmospheres, temperatures and loading histories. The contents of this section are also largely described by GREGOROVA ET AL. [2013]. Section 4.4 focuses in turn on discussing and comparing the relationship between local basis weight, density and temperature (local tensile damage) of kraft paper and extensible kraft paper. The contents of this section are also partly described by HIRN AND LAHTI [2015]. Finally, Section 4.5 summarizes all the important findings and learning, and thus outlines the further discussion in Chapter 5.

### 4.1 Laboratory scale trial

#### 4.1.1 Effect of MD compaction on the dimensions of paper sheets

Table 4.1 presents the number of the paper sheets, the solids content of the paper sheets during the MD compaction, and the basis weight of the paper sheets which were prepared in the laboratory scale experiment using different pre-drying and rub-

ber recoiling combinations. Three paper sheets were prepared in two trial points to study the reproducibility of the method.

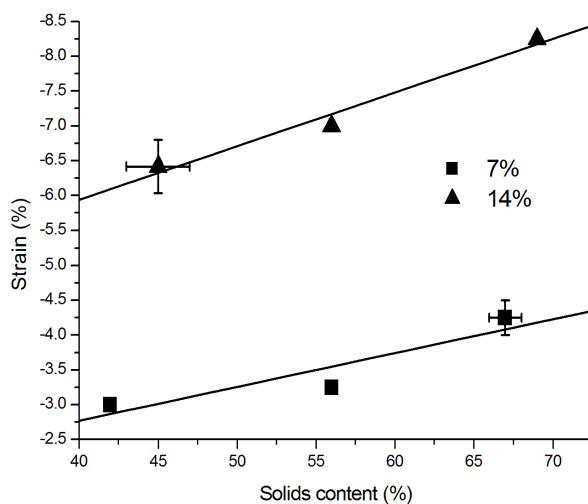
Pre-drying time, drum dryer (min)	Recoiling of rubber blankets (%)	Number of prepared sheets	Solids content during MD compaction (%)	Basis weight ( $g/m^2$ )
-	7	1	42	77
-	14	3	45±2	78±1
2	7	1	56	79
2	14	1	56	78
2	-	1	55	75
3	7	3	67±1	77±1
3	14	1	69	79

**Table 4.1** Data of the paper sheets prepared in the laboratory scale trial.

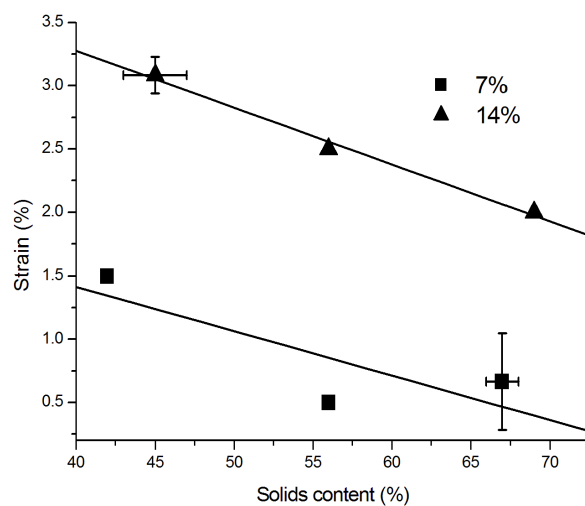
Figure 4.1 and Figure 4.2 show that MD strain increased and CD strain decreased linearly with increasing solids content of the paper sheet during the MD compaction when rubber recoiling was 14%. The strain behavior at a rubber recoiling of 7% exhibits a slightly larger deviation from the linear fit. It could be argued that the fluctuating strain behavior with rubber recoiling of 7% occurred due to a stick-slip phenomenon. In-plane stiffness of the paper sheet partly prevented the paper sheet to follow the rubber blankets and, as a consequence, the rubber blankets partly slid on the paper sheet. In the case of rubber recoiling of 14% the higher shear stresses apparently reduced the effect of a possible stick-slip phenomenon on the paper sheet.

Figure 4.3 presents the plastic Poisson's ratios of the prepared paper sheets. The plastic Poisson's ratio decreased linearly with increasing solids content during the MD compaction at a rubber recoiling of 14%. The plastic Poisson's ratio of the paper sheet with a solids content of 42% during the MD compaction and a rubber recoiling of 7% also fits to this trend. YEH ET AL. [1991] concluded that the Poisson's ratio of paperboard decreases approximately linearly with increasing solids content during tensile testing. This conclusion corresponds well with the results obtained during the MD compactions in the present study. However, the plastic Poisson's ratios of the paper sheets with solids contents of 56% and 67±1% during the MD compaction and a rubber recoiling of 7% deviated clearly from the linearity due to the fluctuations in the strain behavior.

The plastic Poisson's ratio of the paper sheets with solids content of 42% and 45±2% during the MD compaction were 0.5 and 0.48±0.02, respectively. This means that the paper sheets followed the rubber blankets which have a Poisson's ratio of 0.49. These changes in the sheet dimensions were caused by a friction between the paper sheet and the rubber blankets. As a result, microcreping effects were induced in MD and straightening of the free fiber segments, i.e. activation of the fiber network, in



**Figure 4.1** MD strain versus solids content during MD compaction for paper sheets produced with rubber recoiling levels of 7% and 14%.



**Figure 4.2** CD strain versus solids content during MD compaction for paper sheets produced with rubber recoiling levels of 7% and 14%.

CD. Note that the CD behavior of paper is completely different in the industrial scale production as the partial drying shrinkage is allowed. Due to the low solids content, sliding of the fibers on top of each other might have occurred in MD and CD. This is

explained with entanglement friction which provided the sheet's integrity as bonds between fibers were not yet formed [ALINCE ET AL., 2006; DE OLIVEIRA ET AL., 2008; GIMÅKER ET AL., 2011; KETOJA, 2008; TEJADO AND VAN DE VEN, 2010]. The decreasing plastic Poisson's ratio with increasing solids content during the MD compaction can be explained with general material behavior, i.e. materials with decreasing Poisson's ratio have higher resistance against shear and compact more instead [GREAVES ET AL., 2011]. The results with the rubber recoiling of 14% in Figure 4.1 and Figure 4.2 illustrate this behavior.

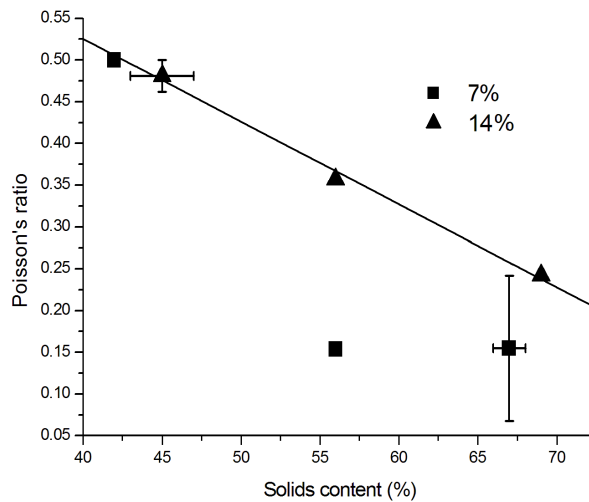


**Figure 4.3** Plastic Poisson's ratio versus solids content during MD compaction for paper sheets produced with rubber recoiling levels of 7% and 14%.

#### 4.1.2 MD mechanical properties of paper sheets

Figure 4.4 and Figure 4.5 present the specific stress versus strain curves measured in MD for the paper sheets produced with rubber recoiling levels of 7% and 14%, respectively. Additionally, the uncompacted reference paper sheet is presented for comparison. The specific stresses were calculated using the data presented in Table 4.1. The reproducibility of the curves measured from a single sheet was at a good level. Also the parallel measurements from three sheets are in good agreement. Less variation between the curves was observed in case of sheets produced with a rubber recoiling of 14%. This can be linked to the more stable MD compaction process at higher rubber recoiling (see Figure 4.1, Figure 4.2 and Figure 4.3).

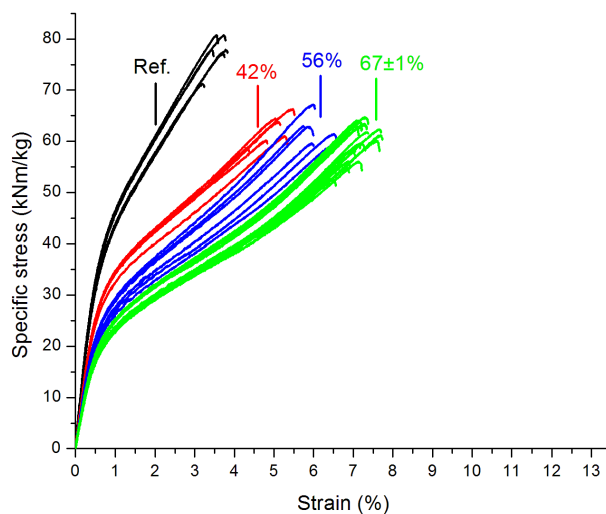


**Figure 4.4** Specific stress versus strain in MD for reference paper sheet and paper sheets produced with solids contents of 42%, 56% and  $67\pm 1\%$  during MD compaction and a rubber recoiling of 7%.

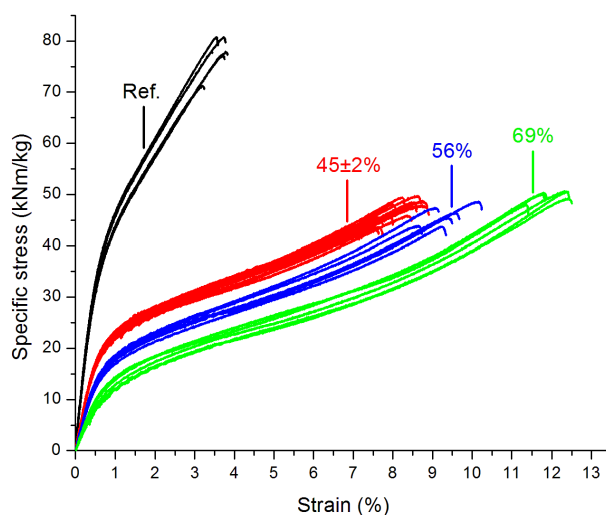


**Figure 4.5** Specific stress versus strain in MD for reference paper sheet and paper sheets produced with solids contents of  $45\pm 2\%$ , 56% and 69% during MD compaction and a rubber recoiling of 14%.

Table 4.2 and Table 4.3 show the mechanical properties presented in Figure 4.4 and Figure 4.5 in a numerical form, respectively. It can be seen that the MD compaction on the laboratory scale results in similar effects on the MD mechanical properties of paper as an extensible unit at industrial scale, i.e. strain at break and TEA index increased while tensile stiffness index and tensile index decreased. The tensile stiffness index was determined through the maximum slope (calculated by linear regression analysis) of the specific stress versus strain curves shown in Figure 4.4 and Figure 4.5 [LORENTZEN & WETTRE, 2003]. Increased rubber recoiling enhanced these effects through higher MD compressive strain (see Figure 4.1) in the same manner as increased speed difference between inlet and outlet of the nip and increased nip width without outlet draw do in the Clupak extensible unit. The influence of the increased rubber recoiling was particularly pronounced with the highest solids content during MD compaction, i.e. higher solids content of paper seems to reinforce the effects of increased rubber recoiling.

Solids content during MD compaction (%)	Strain at break (%)	Tensile index (kNm/kg)	Tensile stiffness index (kNm/g)	TEA index (J/g)	Form factor
Ref.	3.6±0.2	77.7±3.5	7.5±0.2	1.9±0.2	0.68±0.01
42	5.0±0.4	62.4±2.9	6.0±0.1	2.2±0.2	0.70±0.01
56	6.1±0.3	62.2±2.9	5.0±0.2	2.5±0.1	0.65±0.01
67±1	7.1±0.3	60.1±3.5	4.3±0.1	2.7±0.2	0.63±0.01

**Table 4.2** Mean and standard deviation of mechanical properties in MD for reference paper sheet and paper sheets produced with a rubber recoiling of 7%.

Solids content during MD compaction (%)	Strain at break (%)	Tensile index (kNm/kg)	Tensile stiffness index (kNm/g)	TEA index (J/g)	Form factor
Ref.	3.6±0.2	77.7±3.5	7.5±0.2	1.9±0.2	0.68±0.01
45±2	7.9±0.6	46.0±2.3	4.0±0.1	2.5±0.3	0.70±0.01
56	9.3±0.5	45.9±1.9	3.0±0.1	2.8±0.2	0.64±0.01
69	12.0±0.4	49.8±1.0	2.0±0.2	3.4±0.1	0.57±0.01

**Table 4.3** Mean and standard deviation of mechanical properties in MD for reference paper sheet and paper sheets produced with a rubber recoiling of 14%.

Increased solids content of the paper sheet during the MD compaction led to higher strain and lower tensile stiffness index for both rubber recoiling levels. This

occurred because of increased MD compressive strain of the paper sheets (see Figure 4.1). The increased MD compressive strain can be connected to the more pronounced microcreped structure, as illustrated in Figure 4.6, which has lower load carrying ability and higher stretch potential due to the larger scale deformations. This can be seen in the more sigmoidal shaped specific stress versus strain curves. In other words, the yield point lowered and the difference between the center part corresponding to the straightening out of the microcreped structure and the final part corresponding to the deformation of the straightened fiber network became more pronounced. Thus, the form factor also decreased although the sheets with lowest solids content during MD compaction had slightly higher form factors in comparison to the reference sheet due to clearly lower strain hardening and low sigmoidal shape of the curve. Form factor seemed to decrease also with increased rubber recoiling when the solids content during MD compaction was high. Also on the industrial scale production, the higher final MD compaction level decreases the form factor. Despite the reduced load carrying ability of the paper sheets during the straightening out of the larger scale deformations, the tensile indices remained nearly unchanged. The paper sheet produced with a solids content of 69% during MD compaction and a rubber recoiling of 14% was an exception due to a little bit higher tensile index. Anyhow, based on the nearly unchanged tensile indices, it could be argued that the interfiber bonding in the fiber networks was at a similar level after the straightening out of the microcreped structure regardless of the scale of the deformations. In practice, this means that the MD stretch potential of extensible kraft paper can be increased without sacrificing the tensile index by increasing the solids content during MD compaction.

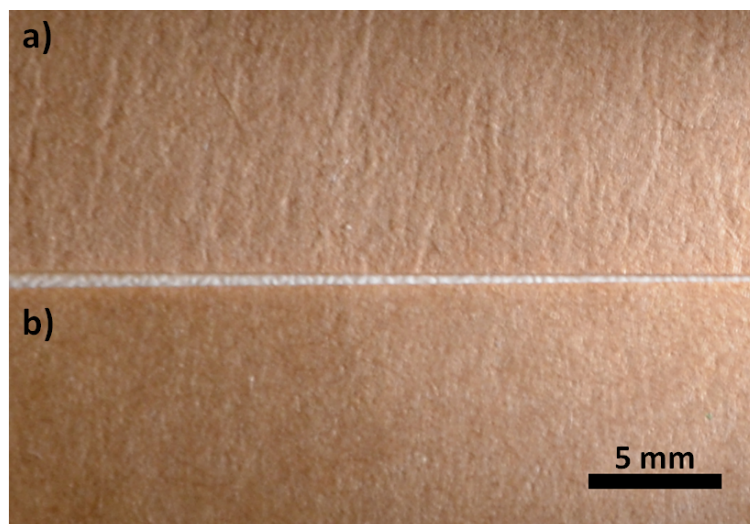


**Figure 4.6** More pronounced microcreped structure of paper due to increased solids content during MD compaction. (a) Solids content of 67% and (b) solids content of 42% during MD compaction at a rubber recoiling of 7%.

As mentioned in Section 2.2.3, lower solids content during MD compaction leads to lower strain whereas TEA is less affected. Similar trend can be observed in the current study. Table 4.2 and Table 4.3 show that the decrease in strain was more pronounced than the decrease in TEA index. As the tensile index remained nearly unchanged, it was the increased form factor that compensated part of the TEA index loss caused by the reduced strain at break. Still, it looks obvious that strain dominated over form factor in the development of TEA index, and thus full compensation of TEA index loss caused by reduced strain was not possible. This also means that the hypothesis stated in the first research question (see Section 2.4) is not feasible based on this laboratory scale study.

#### 4.1.3 Evaluation of the laboratory scale method

Based on the experiments made so far it can be stated that the developed laboratory method offers a feasible way to study the effects of different papermaking variables on the MD mechanical properties of extensible kraft paper. More precisely, the potential of the method lies in the fact that it can be utilized to test new ideas in product and process development, e.g. new chemicals and fiber materials with different MD compaction parameters, without taking risks in the mill production. In this way, more valuable data can be collected to design the mill scale trials properly, and thus reduce the amount of risk taken.

The strongest limitation of the developed laboratory method is that the CD behavior of the paper sheet during the MD compaction differs from the Clupak process. Unlike in the Clupak process, the paper sheet extends in CD during the laboratory MD compaction. Thus, the laboratory scale method cannot be used for simulating the combined MD and CD effect of Clupak compaction on the extensible kraft paper. Furthermore, the laboratory scale method in its current state is fairly time-consuming and difficult to handle. These weaknesses cause limitations to the scaling of the trials.

## 4.2 Industrial scale trial

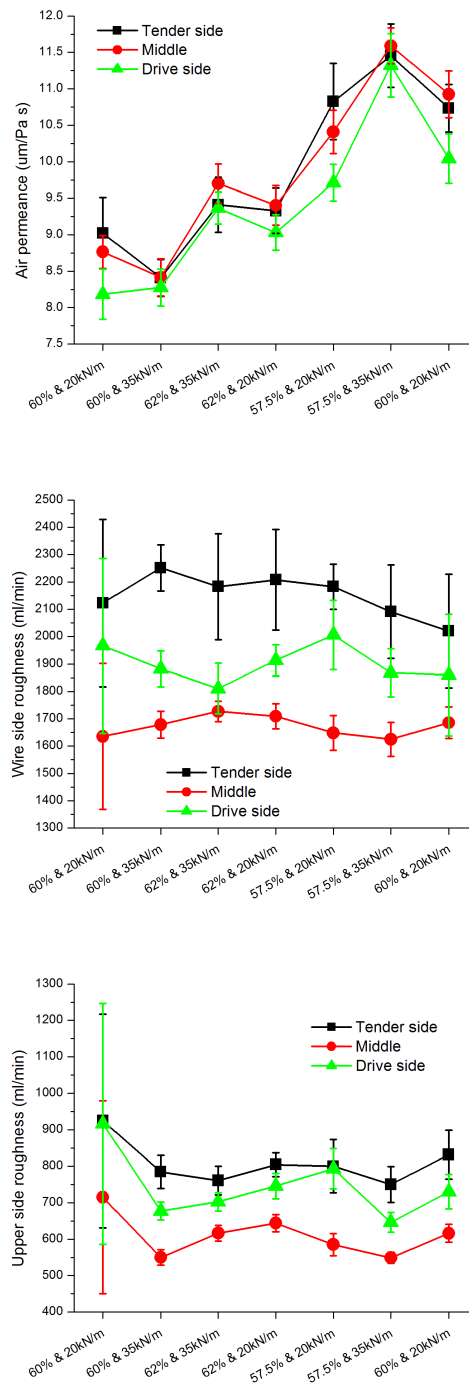
### 4.2.1 Structural properties

Figure 4.7 presents air permeance, wire side roughness and upper side roughness for the extensible kraft papers produced in the industrial scale experiment with different combinations of solids contents during MD compaction and Clupak nip pressures. As the standard deviations are high in comparison to the changes in mean values, the following analysis focuses on observing trends based on mean values. Furthermore, the results are presented in a chronological order due to the fact that uncontrollable parameters had an influence during the trial. This influence can be detected by observing the uncorrelated changes in the structural properties and needs to be taken

into account when analyzing the mechanical properties. The effect of uncontrollable parameters can be especially seen in the air permeance graphs, i.e. the difference between the identical first and last trial point was clear. The porosity (characterized with air permeance) showed an increasing trend during the first six trial points without correlating with the solids content during MD compaction or the Clupak nip pressure. The reason for this kind of development of air permeance could have been a decreasing amount of fines [SCOTT-KERR, 1997].

As the rubber blanket faced the wire side of the paper web, the roughness is considerably higher on that side. Furthermore, the roughness is clearly higher on the edges due to the more pronounced drying-based deformations (wrinkles) caused by less restrained CD drying shrinkage [PAKARINEN ET AL., 2010]. The higher drying shrinkage is demonstrated in Figure 4.11 with the higher CD strain at break on the edges. As the effect of CD drying shrinkage on roughness was lowest in the middle part, the effect of solids content during MD compaction on the microcreped structure can be seen in the wire side roughness levels of this middle part. In other words, the wire side roughness increased with solids content during MD compaction due to more pronounced microcreping effect. The standard deviations of the first trial point were considerably higher in comparison to the others. This most probably occurred because of temporal instabilities in the process.

Figure 4.8 shows basis weight, small scale formation and large scale formation for the extensible kraft papers produced in the experiment. It can be seen that the basis weight stayed at a fairly constant level throughout the trial although the standard deviation of the trial point four was very high - most probably due to temporal instabilities in the process. Small and large scale formation in turn varied during the trial possibly because of fluctuations in the approach flow system and web forming [NORMAN, 2007]. Interestingly, the large and small scale formation improved (higher value refers to better formation [LORENTZEN & WETTRE]) during the first five trial points together with the air permeance. This is contrary to the theory that air permeance increases with worsening formation due to the dominating effect of low basis weight regions [NISKANEN AND PAKARINEN, 2008]. However, the small and large scale formation worsened when the air permeance reached highest value at the sixth trial point. The abnormal relation between the air permeance and formation could have occurred due to uncontrollable parameters, e.g. above-mentioned variations in the fines content and fluctuations in the approach flow system and web forming, although the difference between the identical first and last trial points on both formation scales was negligible - contrary to the air permeance. Still, it needs to be taken into account that the differences between mean values on both formation scales were small in comparison to the standard deviations, and thus the variations were not significant.



**Figure 4.7** Air permeance, wire side roughness and upper side roughness for extensible kraft papers produced with different combinations of solids contents during MD compaction and Clupak nip pressures. Pressure value refers to the pressure per air spring below nip bar (in total 10 air springs).

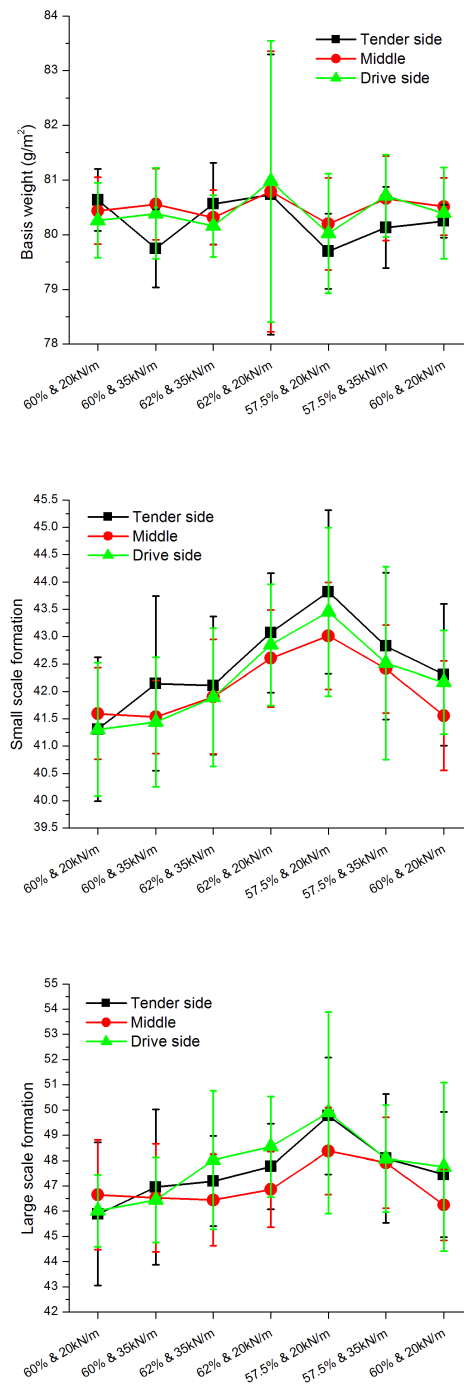


**Figure 4.8** Basis weight, small scale formation and large scale formation (higher value refers to better formation [Lorentzen & Wettre]) for extensible kraft papers produced with different combinations of solids contents during MD compaction and Clupak nip pressures. Pressure value refers to the pressure per air spring below nip bar (in total 10 air springs).

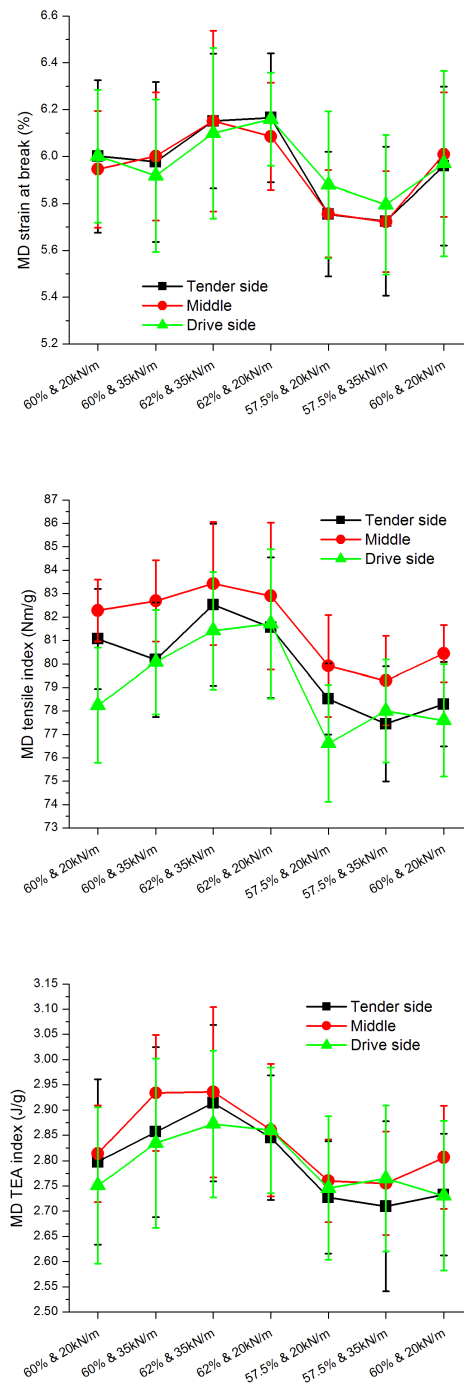
### 4.2.2 MD mechanical properties

Figure 4.9 presents MD strain at break, tensile index and TEA index for the extensible kraft papers produced in the trial. The MD strain at break increased with solids content during the MD compaction whereas the effect of the initial MD compaction level (MD compaction level before the Clupak nip outlet draw) was negligible. As the MD strains at break for the identical first and last trial point were at the same level, the uncontrollable parameters seem to have no effect on this property.

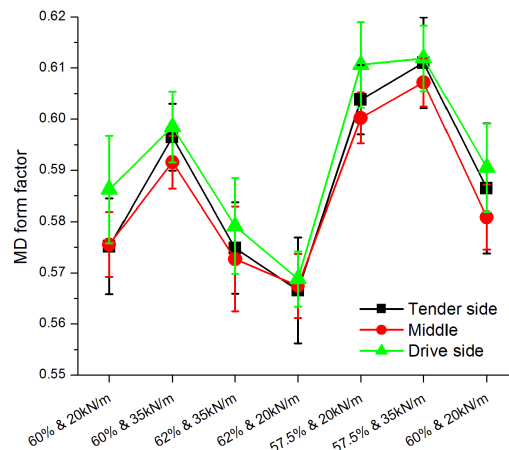
The MD tensile index increased with solids content during MD compaction in a similar manner as the MD strain at break, although the random variation between the Clupak nip pressures was higher within the solids contents during MD compaction. However, it needs to be taken into account that the MD tensile indices of the first trial point were higher in comparison to the last trial point - especially on the tender side and in the middle. Thus, uncontrollable parameters clearly had an influence on this property. It could be argued that the decreased amount of fines increased the porosity [SCOTT-KERR, 1997], and thus the MD tensile index decreased due to weakened bonding [SALMINEN, 2010]. First, the increasing porosity may have slightly weakened the increase in MD tensile index when the solids content during MD compaction increased from 60% to 62%. Second, the further increasing porosity may have reinforced the decrease in MD tensile index when the solids content during MD compaction decreased from 62% to 57.5%.

Figure 4.10 shows that the MD form factor increased with decreasing solids content during MD compaction and with increased Clupak nip pressure. Because of this, the paper produced with the solids content of 60% during MD compaction and the pressure per air spring below nip bar of 35 kN/m (higher Clupak nip pressure) reached similar MD TEA index level as the papers produced with the solids content of 62% during MD compaction, although the MD strain at break and tensile index were higher with the solids content of 62% during MD compaction. In other words, the higher load carrying ability of the microcreped structure of the paper produced with solids content of 60% during MD compaction efficiently compensated the loss of MD TEA index caused by reduced MD strain at break and tensile index. On the other hand, the form factors of the papers produced with the solids content of 57.5% during MD compaction as well as with the solids content of 60% during MD compaction and the pressure per air spring below nip bar of 20 kN/m (lower Clupak nip pressure) were not high enough to compensate the loss of MD TEA index caused by reduced MD strain at break and tensile index. The uncontrollable parameters did not have a large effect on the MD TEA index and form factor because the values for the identical first and last trial point were at the similar level - except the small difference on the tender side.

The relationship between MD strain at break, TEA index and form factor was similar in the laboratory (see Section 4.1.2) and industrial scale trials when the solids



**Figure 4.9** MD strain at break, tensile index and TEA index for extensible kraft papers produced with different combinations of solids contents during MD compaction and Clupak nip pressures. Pressure value refers to the pressure per air spring below nip bar (in total 10 air springs).



**Figure 4.10** MD form factor for extensible kraft papers produced with different combinations of solids contents during MD compaction and Clupak nip pressures. Pressure value refers to the pressure per air spring below nip bar (in total 10 air springs).

content during MD compaction was changed. Thus, the industrial scale trial further supports the statement made in Section 4.1.3 that the laboratory scale method offers a feasible way to simulate the industrial scale process. On both scales, the increased solids content during MD compaction led to higher MD strain at break and TEA index. Form factor decreased instead, and thus lowered the TEA index increasing effect of the higher solids content during MD compaction. On the other hand, MD tensile index behaved somewhat differently on the laboratory scale in comparison to the industrial scale when the solids content during MD compaction was changed. On the laboratory scale, the MD tensile index stayed at the same level. The paper produced with the highest rubber recoiling level and the highest solids content during MD compaction was an exception since the MD tensile index increased. On the industrial scale, the MD tensile index in turn slightly increased with the solids content during MD compaction. As with the laboratory scale trial, the general trend of the results obtained in the industrial scale trial indicate that the avoidance of TEA index loss due to the reduced solids content during MD compaction is unlikely - although it occurred in the case of one trial point. This means that also the industrial scale study did not support the hypothesis stated in the first research question (see Section 2.4). Still, it needs to be remembered that the operational frame in the industrial trial was very narrow, and thus the differences between the mean values were small in comparison to the standard deviations, i.e. the differences were mainly not significant within the operational frame used. Furthermore, the disturbances caused by uncontrollable parameters made the interpretation of the results even more complicated.

However, by thinking the results obtained from the industrial scale trial a little bit

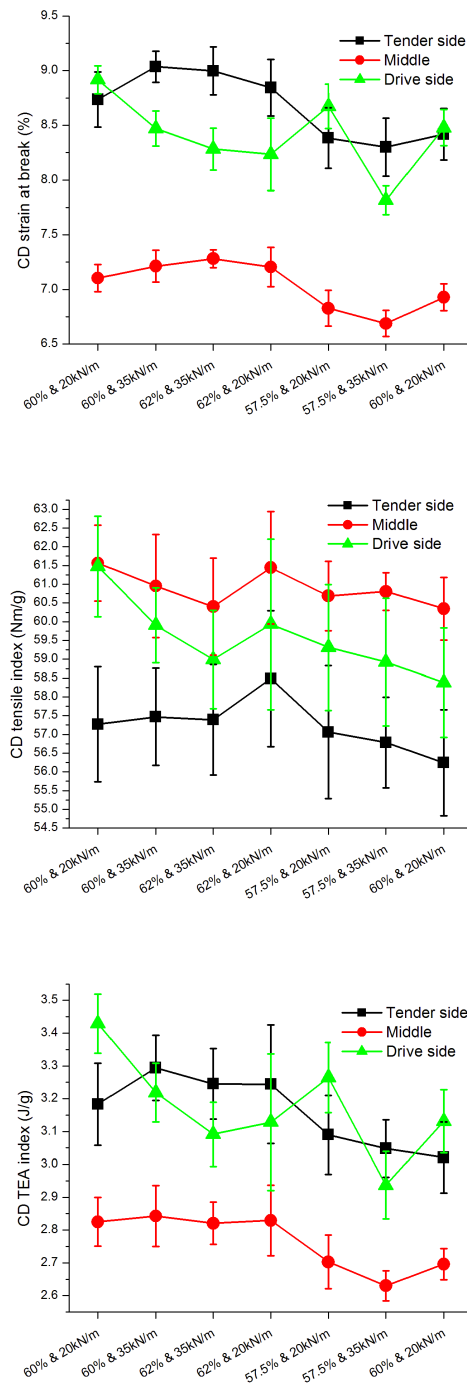
further, it could be argued that the MD strain at break and tensile index increased with solids content during MD compaction because the more pronounced microcreped structure reduced the local stiffness and strain hardening variations. Thus, the stress distribution was more even within the paper sample. As a consequence, the development of heavily localized damage zones which are the potential initiation points for the total failure of the paper sample decreased (see Section 2.3.1). The more even stress distribution may have also been the reason for the increased form factor with higher Clupak nip pressure. More precisely, the combination of higher MD compaction and increased draw after the Clupak extensible unit may have increased the uniformity of the microcreped structure, and thus reduced the variations in local stiffness and strain hardening. The effect of stress distribution is however discussed in a more detailed manner in Section 4.4.

### 4.2.3 CD mechanical properties

Figure 4.11 presents CD strain at break, tensile index and TEA index for the extensible kraft papers produced in the trial. As already mentioned in Section 4.2.1, the CD strain at break was higher on the edges due to the higher CD drying shrinkage. When comparing the wire side roughness (see Figure 4.7) to the CD strain at break, similar trends can be seen - especially in the middle. As the wire side roughness level seemed to correlate with the microcreping effect in the middle, it could be argued that the higher solids content during MD compaction slightly increased the CD strain at break. Due to the difference in the CD strain at break for the identical first and last trial point in the middle, the uncontrollable parameters (e.g. lower fines content) had an effect during the trial. Thus, the CD strain at break reached clearly lower values towards the end of the trial. Similar conclusions could be possibly made on the tender and drive side also, but the deviating CD drying shrinkage covered the effect of MD compaction.

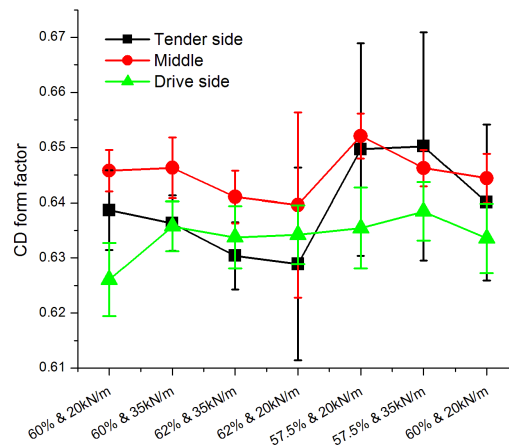
Straightforwardly in relation to the CD strain at break, the CD tensile index was lower on the edges than in the center, i.e. the CD ductility was higher on the edges (see Section 2.1.3). No trend can be seen in the development of the CD tensile index during the trial. The uncontrollable parameters (e.g. lower fines content) may have had a slightly decreasing effect on the CD tensile index towards the end of the trial due to the difference in the identical first and last trial points.

Figure 4.12 shows that the CD form factor slightly increased on the tender side and in the middle with decreased solids content during MD compaction in a similar manner as the MD form factor. In other words, the less pronounced microcreping effect due to the lower solids content during MD compaction increased the load carrying ability of the deforming paper also in CD. However, the effect of higher CD form factor due to the lower solids content during MD compaction on the CD TEA index was negligible (especially in the middle) for the first four trial points - possibly



**Figure 4.11** CD strain at break, tensile index and TEA index for extensible kraft papers produced with different combinations of solids contents during MD compaction and Clupak nip pressures. Pressure value refers to the pressure per air spring below nip bar (in total 10 air springs).

due to the slightly decreased CD strain at break. For the last three trial points, the CD TEA index decreased clearly due to the negative influence of uncontrollable parameters (e.g. lower fines content) on the other mechanical properties, and thus the compensating effect of the higher CD form factor was lower. As in the case of MD mechanical properties, it needs to be remembered that the differences between the mean values were small in comparison to the standard deviations also in CD (the different regions of PM reel analyzed separately), and furthermore, the disturbances caused by uncontrollable parameters complicated the interpretation of the results. Thus, the differences between the trial points in CD were also mainly not significant within the operational frame used.



**Figure 4.12** CD form factor for extensible kraft papers produced with different combinations of solids contents during MD compaction and Clupak nip pressures. Pressure value refers to the pressure per air spring below nip bar (in total 10 air springs).

#### 4.2.4 Geometric mechanical properties

The overall mechanical performances of the extensible kraft papers produced in the trial are presented in Figure 4.13 through geometric mean of the MD and CD strain at break, tensile index and TEA index. The geometric strain at break was higher on the edges due to the higher CD drying shrinkage. Furthermore, the more pronounced microcreeping effect due to the higher solids content during MD compaction increased the geometric strain at break on the tender side and in the middle. A similar trend cannot be seen on the drive side due to the fluctuations in the CD drying shrinkage. The uncontrollable parameters (e.g. lower fines content) had a slightly negative influence on the CD strain at break towards the end of the trial, and thus the geometric strain at break decreased to some extent as well.

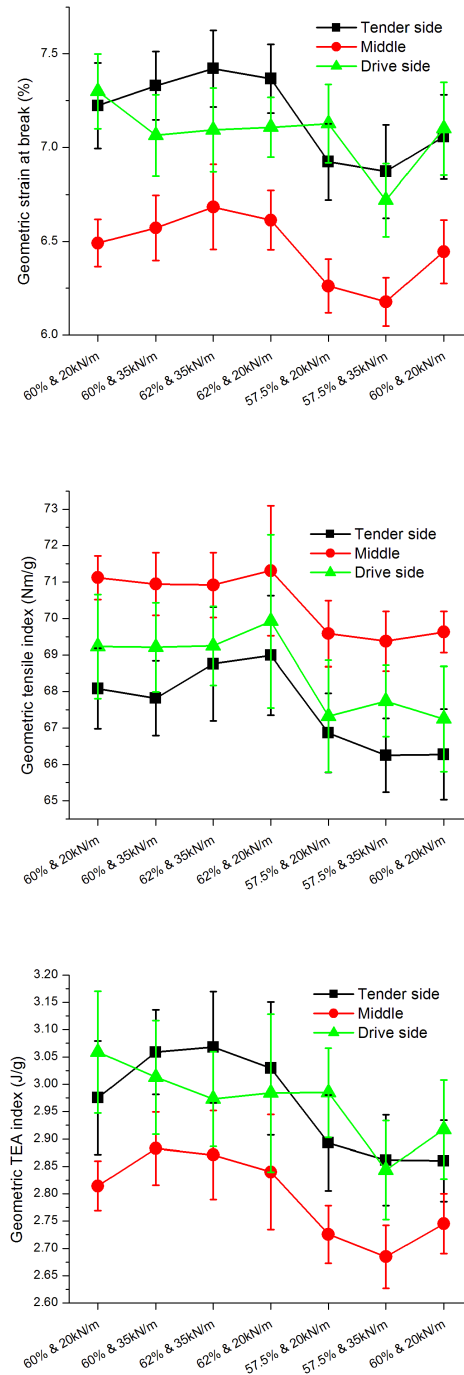


**Figure 4.13** Geometric strain at break, tensile index and TEA index for extensible kraft papers produced with different combinations of solids contents during MD compaction and Clupak nip pressures. Pressure value refers to the pressure per air spring below nip bar (in total 10 air springs).

The geometric tensile index was lower on the edges due to the lower tensile indices in MD and CD. Because of the deviations in MD and CD tensile indices, no clear trend can be seen in the development of geometric tensile index on the drive side and in the middle. On the tender side, the geometric tensile index in turn increased with the solids content during MD compaction due to the more prominently increased MD tensile index. Furthermore, the geometric tensile index clearly decreased towards the end of the trial mainly because of the negative effect of uncontrollable parameters (e.g. lower fines content).

The geometric TEA index reached the highest values on the tender side and in the middle with the solids content of 62% during MD compaction as well as with the solids content of 60% during MD compaction and the pressure per air spring below nip bar of 35 kN/m (higher Clupak nip pressure) in a similar manner as the MD TEA index. As in the case of most other properties, the uncontrollable parameters (e.g. lower fines content) seemed to have a decreasing effect on the geometric TEA index towards the end of the trial (difference between the identical first and last trial points). This can be especially seen in the geometric TEA indices of the papers produced with the solids content of 57.5% during MD compaction, i.e. the geometric TEA indices would most probably have been higher without the negative effect of uncontrollable parameters. Contrary to the tender side and middle part, no trend can be seen on the drive side geometric TEA index due to the fluctuations in the CD TEA index during the trial. Based on the geometric mechanical properties, it could be tentatively argued that the overall mechanical performance of extensible kraft paper improves with increasing solids content during MD compaction. However, as with the MD and CD mechanical properties, the differences between the geometric mean values were small in comparison to the standard deviations (the different regions of PM reel analyzed separately), and furthermore, the disturbances caused by uncontrollable parameters complicated the interpretation of the results. Thus, the overall mechanical performance mainly did not vary significantly between the trial points within the operational frame used.

## 4.3 Viscoelastic, creep and creep recovery behavior

### 4.3.1 Viscoelasticity

The evaluation and comparison of the kraft paper and extensible kraft paper in MD from the practical perspective under different conditions is started from the viscoelastic properties. The developments of storage modulus and loss tangent ( $\tan \delta$ ) of the kraft paper and extensible kraft paper during DMA (frequency 1 Hz and amplitude 20  $\mu\text{m}$ ) with increasing temperature are illustrated under dry nitrogen ( $N_2$ ) and humid atmosphere (50% RH) in Figure 4.14. In harmony with the lower tensile stiffness index and higher ductility (see Figure 2.8), the storage modulus of the extensible kraft

paper was lower and the  $\tan \delta$  higher in comparison to the kraft paper. In other words, the elastic response of the extensible kraft paper was weaker (less mechanical energy was stored and recovered) and it behaved more viscous instead (more mechanical energy was lost) due to the microcreeping effect induced by the MD compaction with the Clupak extensible unit.

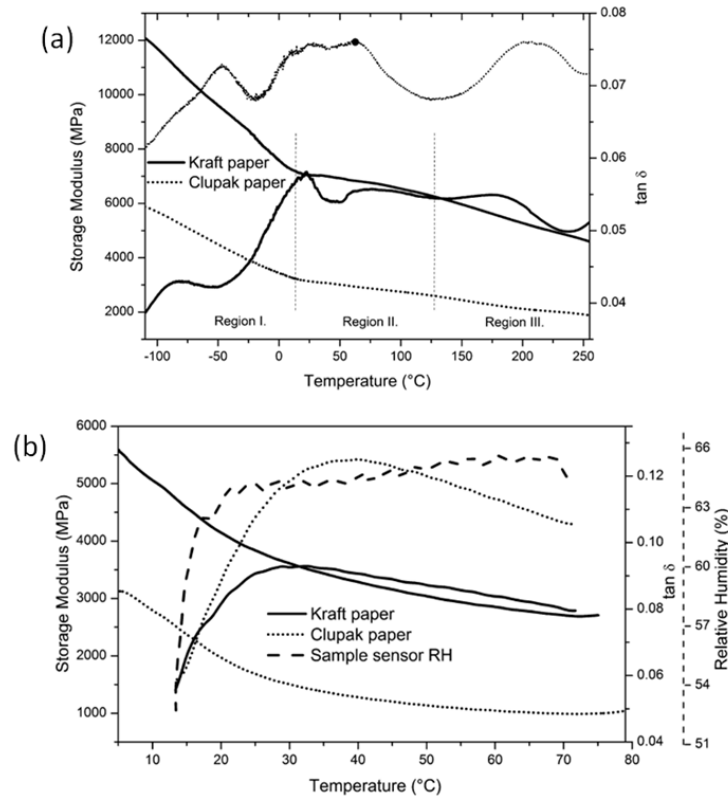


**Figure 4.14** Influence of increasing temperature during DMA (frequency 1 Hz and amplitude 20  $\mu\text{m}$ ) on storage modulus and loss tangent ( $\tan \delta$ ) of kraft paper and extensible kraft paper (Clupak paper) in MD under dry atmosphere (a) and 50% RH (b). Regions with different storage modulus reduction rates under dry atmosphere are illustrated in the graph.

The 50% RH led to the decreased storage modulus and increased  $\tan \delta$  for the kraft paper as well as extensible kraft paper in comparison to the dry atmosphere. Furthermore, the storage modulus of both papers decreased with increasing temperature under both atmospheres (compare with Figure 2.4). These stronger viscous effects can be explained with the temperature and moisture induced softening of the amorphous fiber wall components and weakening of the interfiber bonds. Besides, the loading history most probably also had an influence on the development of storage modulus and  $\tan \delta$ , i.e. the previously induced deformations affected on the following viscoelastic behavior. Similar stronger viscous response of the fiber network due

to the higher temperature and moisture content is also evident in the case of stress versus strain curves (see Figure 2.2). By observing the results more carefully, it can be seen that the decrease in storage modulus was more pronounced, i.e. the elastic response weakened more, for the kraft paper. Furthermore, both papers exhibited three clear transient  $\tan \delta$  peaks in the range of  $-120$  to  $270^\circ\text{C}$  under dry atmosphere. These peaks can be connected to the more distinctive temperature induced changes in the fiber network (see Section 2.1.3) together with the loading history effect. The transient  $\tan \delta$  peak temperatures for the kraft paper were  $-87$ ,  $23$  and  $186^\circ\text{C}$  whereas the peak temperatures for the extensible kraft paper were correspondingly  $-60$ ,  $44$  and  $199^\circ\text{C}$ , i.e. the more distinctive changes in the fiber network due to the combination of increased temperature and loading history effect occurred earlier and thus at lower temperatures for the kraft paper under dry atmosphere. Broad  $\tan \delta$  transitions can be in turn observed in the range of  $15$  to  $70^\circ\text{C}$  for both papers under humid atmosphere. The  $\tan \delta$  reached peak value at a temperature of  $30^\circ\text{C}$  for the kraft paper whereas the peak value for the extensible kraft paper occurred correspondingly at a temperature of  $40^\circ\text{C}$ , i.e. the more distinctive changes in the fiber network occurred earlier and thus at lower temperature for the kraft paper also under humid atmosphere. Based on the above-described less pronounced decrease in storage modulus with increasing temperature and higher transient  $\tan \delta$  peak temperatures, it could be argued that the viscoelastic behavior of extensible kraft paper was less sensitive to the combination of increasing temperature and loading history effect, which probably has something to do with the higher viscosity/ductility of the microcreped paper structure.

### 4.3.2 Creep and creep recovery

The evaluation and comparison of the kraft paper and extensible kraft paper in MD from the practical perspective under different conditions is continued here with the creep and creep recovery properties. The creep (creep stress  $10$  MPa) and creep recovery behaviors of the kraft paper and extensible kraft paper under dry atmosphere ( $N_2$ ) and  $50\%$  RH with a constant temperature of  $30^\circ\text{C}$  are illustrated in Figure 4.15 and Table 4.4. The creep and creep recovery time was  $600$  min. It can be seen that the creep compliance of the extensible kraft paper was higher and the relaxation ability lower under both atmospheres. As the microscopic changes in the paper structure are similar during the creep and the stress versus strain test, the higher creep compliance occurred due to the lower load carrying ability of the microcreped paper structure. The creep mainly occurred by straightening out of the microcreped structure and simultaneous weakening/breaking of the bonds between curled fibers, i.e. mainly through plastic strain (compare with the long center parts of the specific stress versus strain curves shown in Figure 4.5). Thus, the relative share of the elastic and viscoelastic recovery remained small meaning that the recoverable compliance was relatively low. Since the creep compliance was high in combination with the relatively low

recoverable compliance, the relaxation ability of the extensible kraft paper was low in comparison to the kraft paper. Finally, the humid atmosphere strongly increased the creep compliance and decreased the relaxation ability of both papers due to the moisture induced softening of the amorphous fiber wall components and weakening of the interfiber bonds, i.e. the enhanced viscous behavior increased the plastic strain (compare with Figure 2.5).

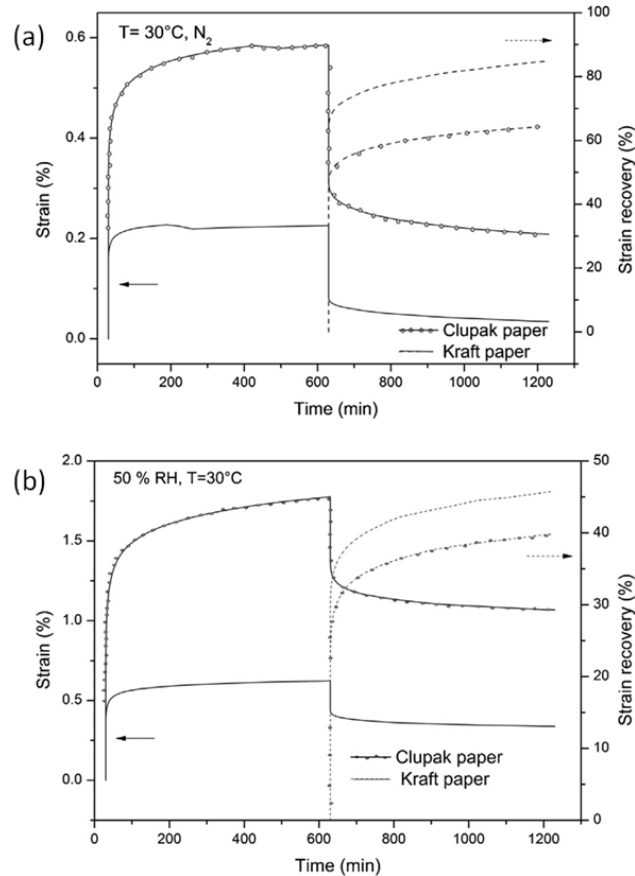


**Figure 4.15** Behavior of kraft paper and extensible kraft paper (Clupak paper) during single creep-recovery cycle (creep stress 10 MPa) under dry atmosphere (a) and 50% RH (b).

Dividing the creep time of 600 min (single creep-recovery cycle) into five 120 min creep cycles (creep stress 10 MPa) with a creep recovery time of 30 min under dry atmosphere with a constant temperature of 30°C affected on the creep compliance, recoverable compliance and relaxation ability of the kraft paper and extensible kraft paper as shown in Table 4.5. As with the single creep-recovery cycle, the creep compliance of the extensible kraft paper was higher and the relaxation ability lower in the first creep-recovery cycle. The creep compliance of the extensible kraft paper was

Sample	Atmosphere	J(600 min) ( $\mu\text{m}^2/\text{N}$ )	$J_R$ (600 min) ( $\mu\text{m}^2/\text{N}$ )	R(600 min)
Kraft paper	$N_2$	235	186	0.79
	50% RH	525	272	0.52
Extensible kraft paper	$N_2$	602	383	0.64
	50% RH	1683	699	0.42

**Table 4.4** Creep compliance ( $J$ (600 min)), recoverable compliance ( $J_R$ (600 min)) and relaxation ability ( $R$ (600 min)) of kraft paper and extensible kraft paper as a function of creep time (600 min) during single creep-recovery cycle (creep stress 10 MPa) under dry atmosphere and 50% RH with a constant temperature of 30°C. The creep recovery time was 600 min.

also higher in the following cycles but the relaxation ability reached approximately the same values as with the kraft paper. After the first cycle, the creep compliance of both papers decreased considerably with the simultaneous strong increase in the relaxation ability. More precisely, the creep compliance decreased and the relaxation ability increased slowly after the first cycle in a way that the creep compliance reached approximately the same value as the recoverable compliance in the cycle before and the difference between creep compliance and recoverable compliance reduced cycle by cycle. In other words, part of the elastic and viscoelastic creep strain of a cycle became plastic in the following cycle and the portion of this plastic transformation became smaller as the cycles went on. The reason for this kind of development was the dependency of mechanical behavior of paper on the loading history, i.e. the deformations induced during the previous creep cycles affected on the creep behavior in the following cycles. Still, majority of the plastic strain in this experiment occurred during the first creep cycle and the creep strain after that was almost entirely elastic and viscoelastic, i.e. the relaxation abilities were close to one. In the case of extensible kraft paper under dry atmosphere, the amount of creep-recovery cycles did not have an effect on the final level of non-recoverable compliance (plastic strain). The non-recoverable compliance reached during the single creep-recovery cycle with a creep time of 600 min was  $219 \mu\text{m}^2/\text{N}$  (calculated based on Table 4.4) whereas the non-recoverable compliance reached during the five consecutive creep-recovery cycles with a total creep time of  $5 \times 120 \text{ min} = 600 \text{ min}$  was  $218 \mu\text{m}^2/\text{N}$  (calculated based on Table 4.5). The kraft paper under dry atmosphere reached in turn higher non-recoverable compliance ( $68 \mu\text{m}^2/\text{N}$ ) already during the first creep-recovery cycle when compared to the non-recoverable compliance reached during the single creep-recovery cycle ( $49 \mu\text{m}^2/\text{N}$ ) under the same conditions in spite of the considerably shorter creep time (120 min vs. 600 min). Structural differences in the kraft paper strips tested could have been the reason for this kind of behavior.

Changing the atmosphere from dry to dynamically increasing RH while main-

Sample	Property	C1	C2	C3	C4	C5
Kraft paper	J(120 min) ( $\mu\text{m}^2/\text{N}$ )	260	191	182	177	173
	$J_R$ (120 min) ( $\mu\text{m}^2/\text{N}$ )	192	181	177	172	171
	R(120 min)	0.74	0.95	0.97	0.97	0.99
Extensible kraft paper	J(120 min) ( $\mu\text{m}^2/\text{N}$ )	510	336	311	291	296
	$J_R$ (120 min) ( $\mu\text{m}^2/\text{N}$ )	337	309	299	291	290
	R(120 min)	0.66	0.92	0.96	1.00	0.98

**Table 4.5** Development of creep compliance (J(120 min)), recoverable compliance ( $J_R$ (120 min)) and relaxation ability (R(120 min)) of kraft paper and extensible kraft paper as a function of creep time (120 min/cycle) during multiple creep-recovery (creep stress 10 MPa) cycles (C) under dry atmosphere with a constant temperature of 30°C. The creep recovery time was 30 min/cycle.

taining the constant temperature of 30°C, creep stress of 10 MPa and 120 min creep cycles with a creep recovery time of 30 min influenced on the cyclic creep-recovery behavior of the kraft paper and extensible kraft paper as shown in Figure 4.16. It can be seen that the creep strain of both papers increased with the RH whereas the amount of strain recoveries remained approximately constant. In other words, the creep compliances increased whereas the recoverable compliances remained approximately constant which means that the relaxation abilities decreased. The extensible kraft paper reacted clearly more sensitively to the increased RH, i.e. the creep compliance increased more strongly with RH. This high sensitivity to the increasing RH was most probably caused by the enhanced viscous behavior together with the deformations induced during the previous creeps (loading history effect), and thus the reduced load carrying ability of the microcreped structure. Also the possible accelerated creep (see Section 2.1.4) related additional stressed may have had a relatively higher influence in the case of extensible kraft paper. As already discussed in connection with the specific stress versus strain curve of the extensible kraft paper, the tensile stiffness index, yield point and strain hardening during the pullout of the microcreped structure (long center parts of the curves shown in Figure 4.5) are all relatively low under the standard climate (23°C and 50% RH). By increasing the temperature and especially RH further, the tensile stiffness index decreases, yield point is lowered and pullout deformation starts to approach ideal plasticity (strain hardening approaches zero). Thus, the creep rate and strain of the extensible kraft paper became very high when the increased RH together with the deformations induced during the previous creeps reduced the yield point to the level equal/lower than the applied creep stress combined with the possible accelerated creep related stresses - the threshold RH was somewhere between 60 and 80% for the loading and climate history applied. The kraft paper is in turn much more stiff and brittle with a considerably higher load carrying ability, and thus the increased RH in combination with the loading history

effect as well as the possible accelerated creep related stresses did not have such a high influence on the creep behavior under the creep stress (10 MPa) applied.

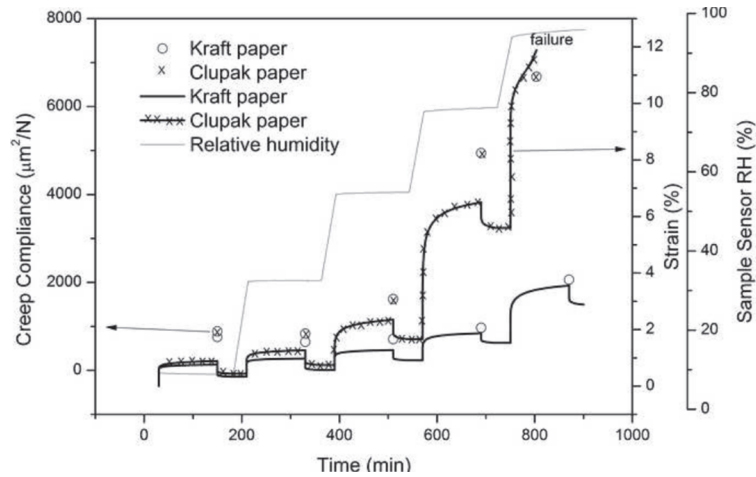


**Figure 4.16** Behavior of kraft paper and extensible kraft paper (Clupak paper) during multiple creep-recovery cycles (creep stress 10 MPa) under dynamically increasing RH with a constant temperature of 30°C.

The dynamical temperature increase under constant humidity of 50% RH affected in turn on the cyclic creep-recovery (creep stress 10 MPa) behavior of the kraft paper and extensible kraft paper as shown in Table 4.6. The creep and creep recovery time was 20 min/cycle. As with the cyclic creep-recovery under dry atmosphere and constant temperature, the creep compliance of the extensible kraft paper was clearly higher in all of the creep-recovery cycles whereas the relaxation ability was considerably lower only in the first creep-recovery cycle. Furthermore, the plastic strain of both papers occurred mainly during the first creep cycle (relaxation abilities were close to one after the first cycle) - especially in the case of kraft paper. After the first creep-recovery cycle with high creep compliance, the creep compliance of both papers, shown in Figure 4.17, decreased first for a short time as under the dry atmosphere and constant temperature. Then, the creep compliance started to increase slowly with temperature due to the temperature reinforced viscous behavior in combination with the deformations induced during the previous creeps - similarly to the dynamically increasing RH. However, this creep strain was, as mentioned above, almost completely elastic and viscoelastic in the case of kraft paper. The extensible kraft paper showed in turn also minor plastic deformation but it was much lower in comparison to the plastic deformation caused by the dynamically increasing RH together with the loading history effect.

Sample	Property	C1 (29°C)	C11 (39°C)	C21 (49°C)	C31 (59°C)	C41 (69°C)	C51 (79°C)
Kraft paper	J(20 min) ( $\mu\text{m}^2/\text{N}$ )	554	319	331	346	363	376
	$J_R$ (20 min) ( $\mu\text{m}^2/\text{N}$ )	349	318	331	345	360	372
	R(20 min)	0.64	1.00	1.00	1.00	0.99	0.99
Extensible kraft paper	J(20 min) ( $\mu\text{m}^2/\text{N}$ )	1140	586	616	653	687	699
	$J_R$ (20 min) ( $\mu\text{m}^2/\text{N}$ )	618	571	597	627	651	661
	R(20 min)	0.54	0.97	0.97	0.96	0.95	0.95

**Table 4.6** Development of creep compliance (J(20 min)), recoverable compliance ( $J_R$ (20 min)) and relaxation ability (R(20 min)) of kraft paper and extensible kraft paper as a function of creep time (20 min/cycle) during multiple creep-recovery (creep stress 10 MPa) cycles (C) under 50% RH with a dynamically increasing temperature. The creep recovery time was 20 min/cycle.

### 4.3.3 Challenges for practical mechanical performance

Based on the description above, the high RH together with the rough loading history seems to be the biggest risk factor for the failure of extensible kraft paper in MD (see Figure 4.16). The conditions in the emerging market regions of extensible kraft paper, e.g. in South-East Asia, fulfill these criteria well. For example the capital of Indonesia, Jakarta, has a tropical monsoon climate with a wet season of eight months per year and a RH close to 80% all-year round [WIKIPEDIA, 2015B]. Furthermore, the extensible kraft paper experiences rough loading paths as a material in industrial bags due to the long and complicated distribution chains with rough manual handling (see Section 1.1). As a consequence, the probability that the stresses exceed the yield point and thus lead to the significant MD plastic deformation of extensible kraft paper along the distribution chain becomes relatively high. For the applied loading and climate history in the current experiment (see again Figure 4.16), the threshold RH after which the MD plastic deformation of extensible kraft paper became significant was somewhere between 60 and 80%, i.e. it was at the same level as the RH in Jakarta. However, it needs to be taken into account that creeps with long duration were applied in the current experiment whereas in practice the strongest stresses are often caused by impacts (bag drops) - as demonstrated in Figure 1.3. Also the stress levels may vary considerably depending on the situation. Thus, the direct comparison of the results gained in laboratory and in practice is difficult.

On the other hand, the high humidity together with the rough loading history does not seem to affect so much on the mechanical performance of kraft paper in MD (see Figure 4.16) due to the considerably higher tensile stiffness index and load carrying ability. Actually, it could be even thought that the ductility of kraft paper could be increased by increasing the RH (see Figure 2.2) in such a way that it would start to behave more like the extensible kraft paper. However in reality, it is very

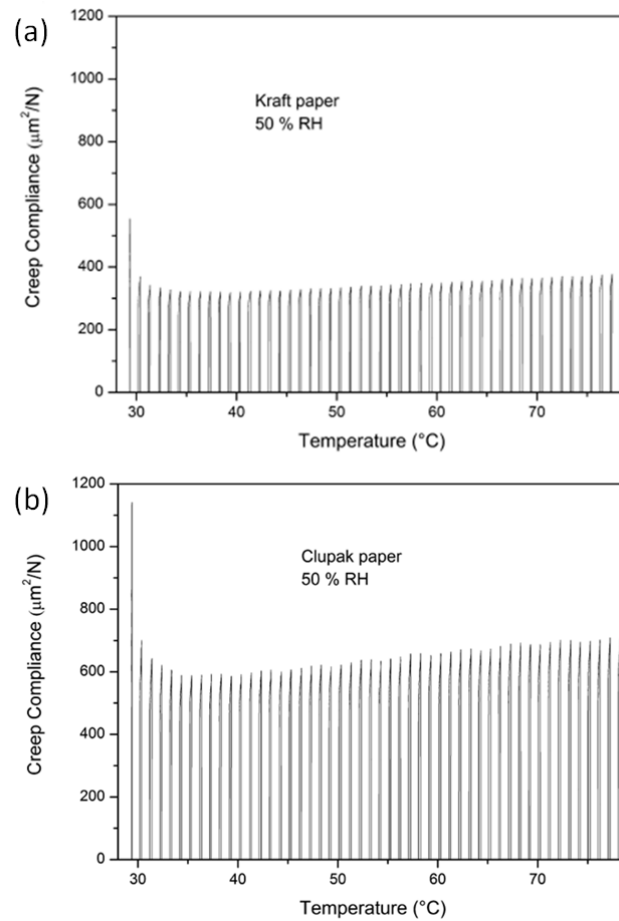


**Figure 4.17** Development of creep compliance of kraft paper (a) and extensible kraft paper (Clupak paper) (b) during multiple creep-recovery cycles (creep stress 10 MPa) under 50% RH with a dynamically increasing temperature. The creep and creep recovery time was 20 min/cycle.

unlikely that the TEA index of kraft paper as well as extensible kraft paper could be increased by increasing the RH due to the detrimental effect of moisture on interfiber bonding. In other words, the moisture induced weakening of the interfiber bonds reduces the tensile index of both papers so much that it most probably overcomes the positive effect of increasing ductility on TEA index. Thus, the illustrated different reaction of kraft paper and extensible kraft paper to the same development of loading and climate demonstrates more importantly the significance of a sufficiently high yield point on the mechanical performance of extensible kraft paper.

## 4.4 Linking local structure and tensile damage

### 4.4.1 Kraft paper

The relationship between local structural properties and local temperature, i.e. local tensile damage (see Section 2.3.3), is first analyzed for the kraft paper. Tensile index and strain at break of the kraft paper strips selected for the registration and correlation analysis are shown in Table 4.7. Kraft paper strip  $\triangle$  had slightly lower tensile index and strain at break than the other two. The overview maps of air permeance, optical transparency and temperature are presented for the strips  $\square$ ,  $\triangle$  and  $\circ$  in Figure 4.18, Figure 4.19 and Figure 4.20, respectively. When comparing the air permeance and optical transparency maps, it seems that the air permeance was generally high in the regions where the basis weight was low and vice versa - as can be expected if the only clearly changing structural factor is basis weight. However, exceptions from this trend can be also seen. For example the regions of the strips  $\square$ ,  $\triangle$  and  $\circ$  marked with solid green circles have low air permeance and basis weight which refers to high density. On the other hand, the regions of the strips  $\square$ ,  $\triangle$  and  $\circ$  marked with dashed yellow circles have high air permeance and basis weight which in turn refers to low density. These results are consistent with the findings of VOMHOFF AND BOUVENG [2010] who concluded that high basis weight regions can occur with both high and low air permeance. The local density variations could have arisen for example from the spatial variations in fiber orientation, bonding degree, internal stresses due to drying shrinkage or wet strain and/or fines content (see Section 2.3.1).

Paper strip	Tensile index (Nm/g)	Breaking strain (%)
$\square$	106	3.2
$\triangle$	99	3.0
$\circ$	105	3.3

**Table 4.7** Tensile index and breaking strain for the analyzed kraft paper strips.

The optical transparency map and the air permeance map seem to roughly correlate with the temperature map before rupture for the strips  $\square$ ,  $\triangle$  and  $\circ$ . However, the local variations in density make the exact prediction of the regional temperature increase fairly complicated. For example high density regions marked with solid green circles and low density regions marked with dashed yellow circles most probably had restraining and promoting effects on the local temperature increase (local tensile damage), respectively. In order to study the contribution of local density and basis weight on the high temperature more accurately, the relative values from three high temperature regions were plotted against each other with solid red symbols in Figure 4.21, Figure 4.22 and Figure 4.23. As a comparison, the relative values from three regions where the temperature was low were added with hollow blue symbols.

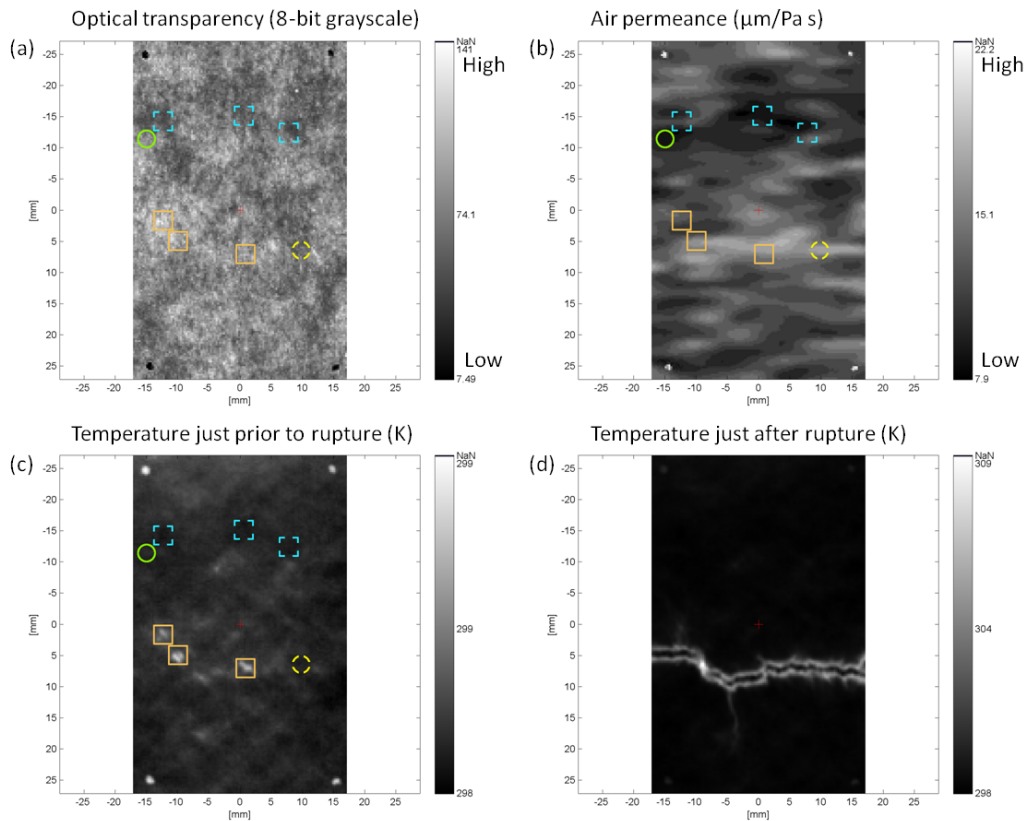


**Figure 4.18** Optical transparency map (a), air permeance map (b), temperature map just prior to rupture (c) and temperature map just after rupture (d). Kraft paper strip  $\square$ : region with low basis weight and high density is marked with solid green circle whereas region with high basis weight and low density is marked with dashed yellow circle. High temperature and low temperature regions selected for a more accurate analysis are marked with solid orange and dashed blue rectangles, respectively.

The regions are marked in Figure 4.18, Figure 4.19 and Figure 4.20. The principles for calculating the relative values as well as selecting the analyzed regions are presented in Section 3.4.3. As can be seen in Figure 4.21, the air permeance was generally above and the basis weight below average level for the high temperature regions and vice versa for the low temperature regions. The difference between low and high temperature regions was more pronounced for the basis weight. In other words, there was no straight relationship between the air permeance and the basis weight which confirms that air permeance does indeed bring additional information regarding the local density. Figure 4.22 and Figure 4.23 show that the standard deviation of the high temperature regions was much higher because the selected region size ( $2.7 \times 2.7 \text{ mm}^2$ ) was larger than the exact region with high temperature. This corresponds well with

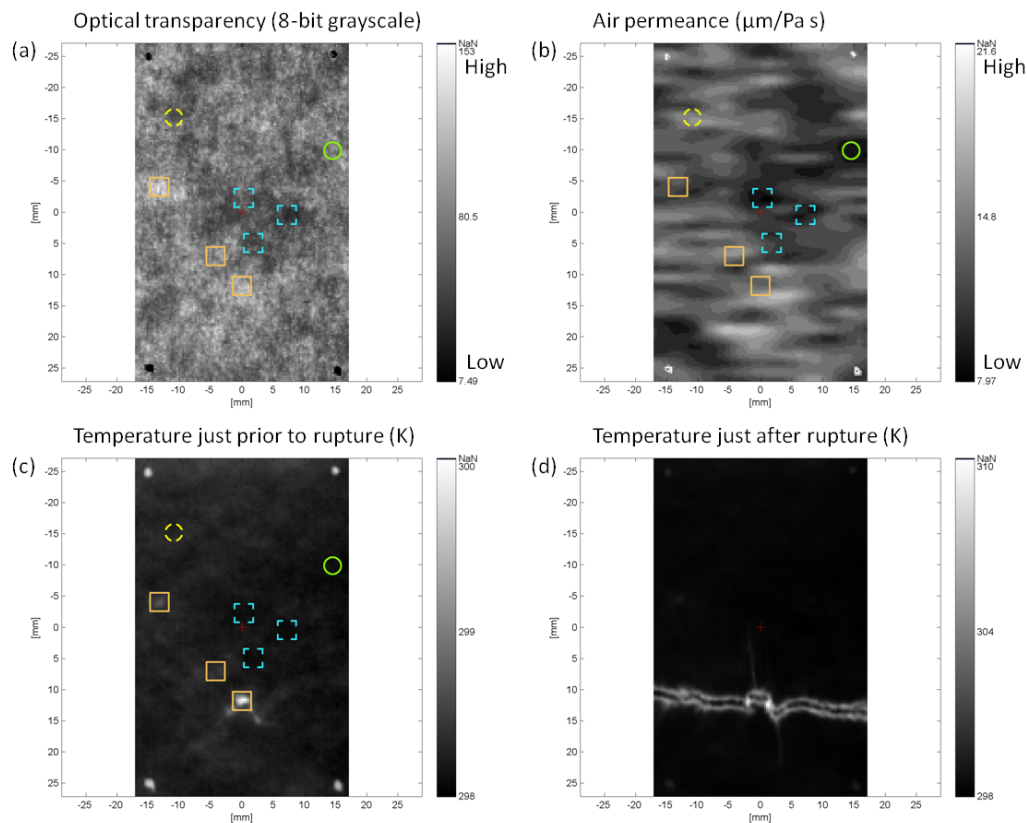


**Figure 4.19** Optical transparency map (a), air permeance map (b), temperature map just prior to rupture (c) and temperature map just after rupture (d). Kraft paper strip  $\triangle$ : region with low basis weight and high density is marked with solid green circle whereas region with high basis weight and low density is marked with dashed yellow circle. High temperature and low temperature regions selected for a more accurate analysis are marked with solid orange and dashed blue rectangles, respectively.

the findings of HRISTOPULOS AND UESAKA [2004] who stated that the critical cluster size for the significant local fracture is approximately 1 mm (see also Section 2.3.3).

Closer observation of Figure 4.21, Figure 4.22 and Figure 4.23 reveals that one of the following three conditions must be met for high local temperature caused by stretching to occur in the paper strip: (1) low local basis weight, (2) low local density (high local air permeance) or (3) low local basis weight and low local density (high local air permeance). This means that the low local basis weight and low local density both cause a reduction in the local stiffness and strain hardening which in turn are prerequisites for the high temperature. The local temperature was highest on the region of the strip  $\triangle$  where both basis weight and density were low (condition 3), i.e. the local stiffness and strain hardening were lowest in this region.

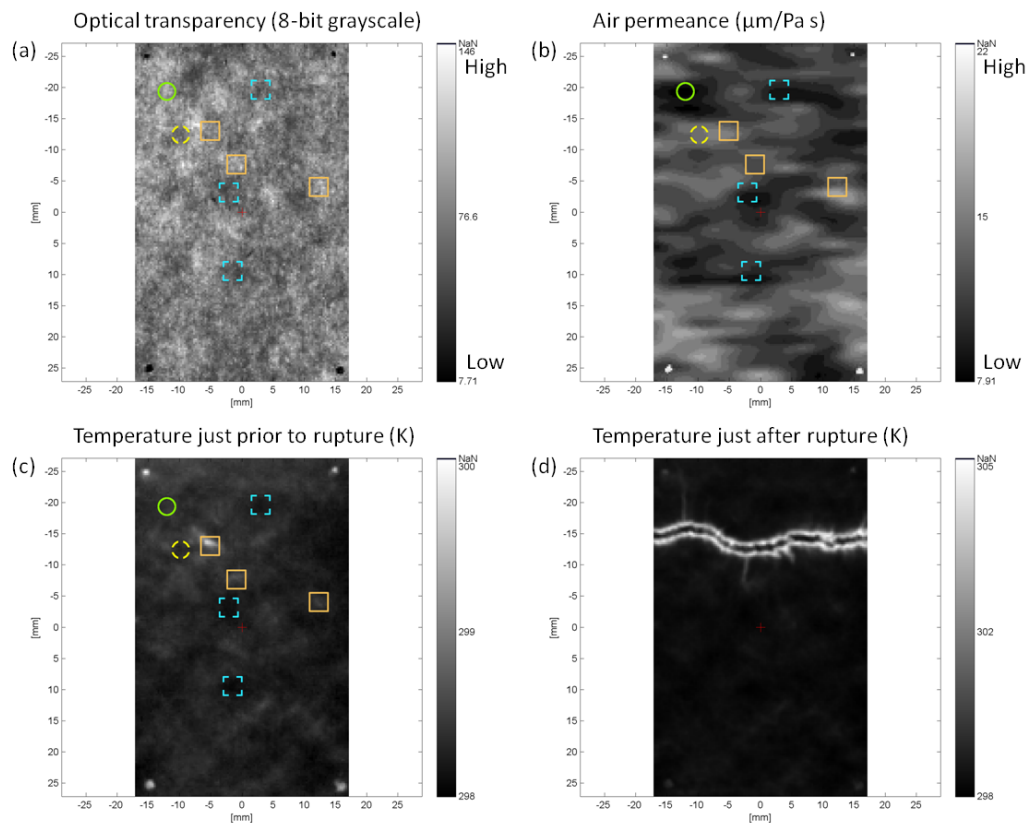


**Figure 4.20** Optical transparency map (a), air permeance map (b), temperature map just prior to rupture (c) and temperature map just after rupture (d). Kraft paper strip  $\bigcirc$ : region with low basis weight and high density is marked with solid green circle whereas region with high basis weight and low density is marked with dashed yellow circle. High temperature and low temperature regions selected for a more accurate analysis are marked with solid orange and dashed blue rectangles, respectively.

When comparing the temperature maps of the strips  $\square$ ,  $\triangle$  and  $\bigcirc$ , it can be clearly seen that the temperature increase in the strip  $\triangle$  was more uneven and heavily localized than in the other two. Thus, the tensile index and strain at break of the strip  $\triangle$ , as previously mentioned (see Table 4.7), were lower in comparison to the strips  $\square$  and  $\bigcirc$ . This is well in line with the previous findings that heavier localization of high temperature, i.e. heavier localization of tensile damage, has a negative impact on breaking load [YAMAUCHI AND MURAKAMI, 1994] and strain at break [KORTEOJA ET AL., 1998] of paper (see also Section 2.3).

The statistical analysis of the data displayed in Figure 4.21, Figure 4.22 and Figure 4.23 (principle of the statistical analysis is presented in Section 3.4.3) further illustrated the heavy influence of local basis weight and local density on local temperature.

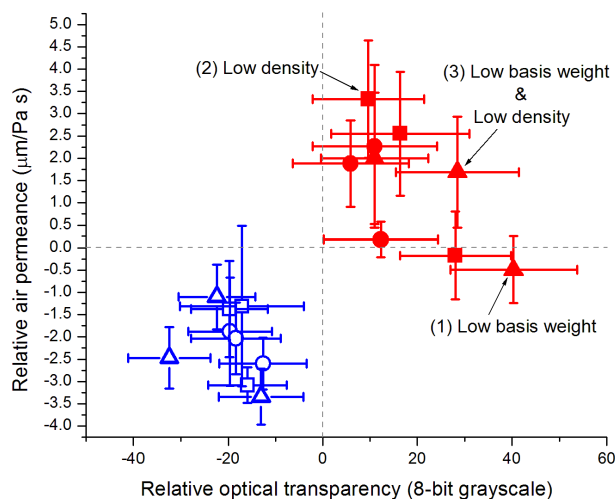


**Figure 4.21** Relative air permeance versus relative optical transparency for high (solid red symbols) and low (hollow blue symbols) temperature regions in the stretched kraft paper strips  $\square$ ,  $\triangle$  and  $\circ$ .

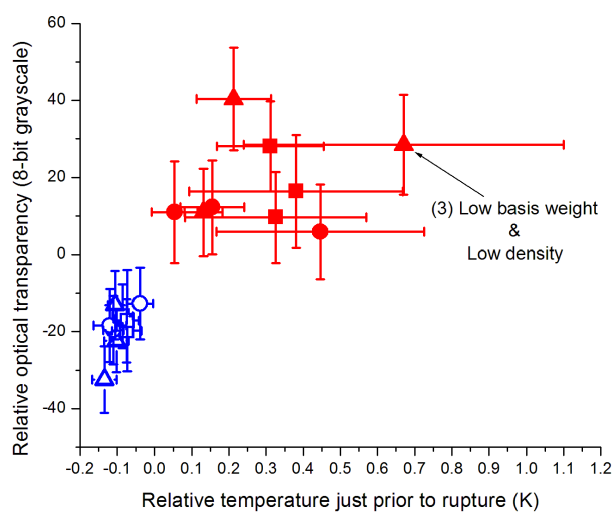


**Figure 4.22** Relative optical transparency versus relative temperature just prior to rupture for high (solid red symbols) and low (hollow blue symbols) temperature regions in the stretched kraft paper strips  $\square$ ,  $\triangle$  and  $\circ$ .

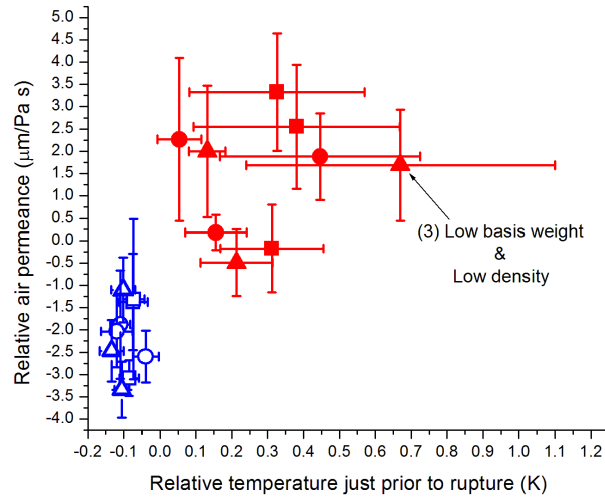


**Figure 4.23** Relative air permeance versus relative temperature just prior to rupture for high (solid red symbols) and low (hollow blue symbols) temperature regions in the stretched kraft paper strips  $\square$ ,  $\triangle$  and  $\circ$ .

Namely, the results revealed that both variables, local optical transparency and local air permeance, independently had a significant impact on local temperature on a 95% confidence limit. This quantitatively proves that high local temperature, i.e. local tensile damage, before failure of the paper strip was indeed not only an effect of low local basis weight but was also an effect of low local density. Furthermore, combined local basis weight and local air permeance explained 76% of total variation in local temperature, i.e. the coefficient of determination of the statistical model was  $r^2=0.76$ . This means that the two variables were able to predict the region with high temperature, i.e. localization of tensile damage, in the paper strip to a degree of 76%. Other possible influence factors, including measurement noise, were responsible for the remaining difference to  $r^2=1$ , which was only 0.24. Finally, it is interesting to mention that local basis weight was only a slightly better predictor for high local temperature ( $r^2=0.66$ ) than local air permeance ( $r^2=0.60$ ). The variables were highly inter-correlated, only a rather small fraction of the information (about 31%) was independent, nevertheless they were both significant on a 95% confidence level.

#### 4.4.2 Extensible kraft paper

Analysis of the relationship between local structural properties and local temperature, i.e. local tensile damage, is continued here with the extensible kraft paper. Tensile index and strain at break of the extensible kraft paper strips selected for the registration and correlation analysis are shown in Table 4.8. Extensible kraft paper strip  $\triangleright$  was the weakest of these three strips. The overview maps of air permeance, optical transparency and temperature are presented in Figure 4.24, Figure 4.25 and Figure 4.26 for the strips  $\diamond$ ,  $\nabla$  and  $\triangleright$ , respectively. Similarly to the kraft paper strips, it can be seen from the air permeance and optical transparency maps of the extensible kraft paper strips that the air permeance was generally high on the regions where the basis weight was low and vice versa. Exceptions of this trend also existed, i.e. regions where both air permeance and basis weight were low and regions where these two properties were high. This means correspondingly that regions where density was clearly higher or lower in comparison to the general trend also existed (compare Section 4.4.1). Examples of these high and low density regions are marked with solid green and dashed yellow circles, respectively, for the strips  $\diamond$ ,  $\nabla$  and  $\triangleright$ . As in the case of the kraft paper strips, the local density variations could have occurred because of the spatial variations in fiber orientation, bonding degree, internal stresses due to drying shrinkage or wet strain and/or fines content (see also Section 2.3.1). Besides, the spatial variations in microcreped structure may also have had an effect.

Paper strip	Tensile index (Nm/g)	Breaking strain (%)
$\diamond$	77	10.4
$\nabla$	79	10.1
$\triangleright$	77	10.0

**Table 4.8** Tensile index and breaking strain for the analyzed extensible kraft paper strips.

Comparison between the temperature maps of the kraft and extensible kraft paper strips clearly demonstrates that the temperature increase caused by stretching was more evenly distributed within the extensible kraft paper strips. It could be argued that the microcreped structure evened out the relative differences between the local tensile stiffnesses, i.e. the local stiffnesses of the strongest regions with high basis weight and low air permeance decreased more than the local stiffnesses of the weaker regions with lower basis weight and higher air permeance, and thus the stresses were more evenly distributed within the strips. A possible reason for the higher stiffness decrease in the strongest regions could have been a stronger microcreping effect in these areas.

As with the kraft paper strips (see Section 4.4.1), the local variations in density complicated the exact prediction of regional temperature increase (local tensile damage) for the extensible kraft paper strips  $\diamond$ ,  $\nabla$  and  $\triangleright$ . Also for these strips, high density

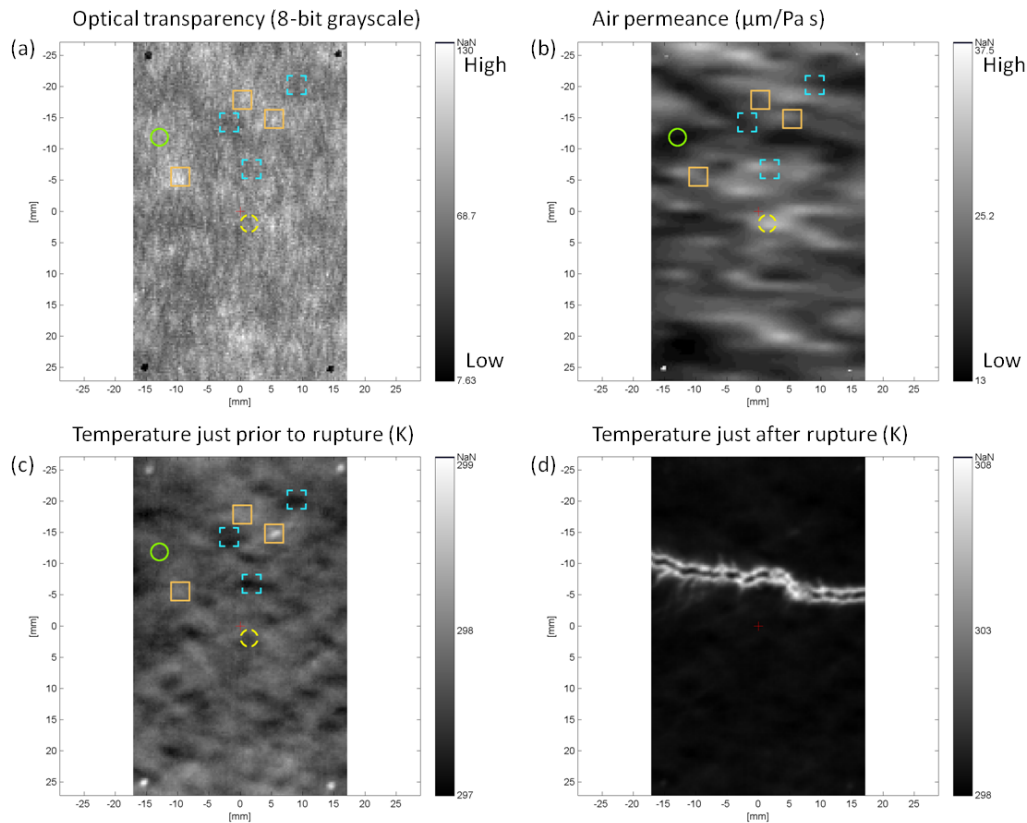


**Figure 4.24** Optical transparency map (a), air permeance map (b), temperature map just prior to rupture (c) and temperature map just after rupture (d). Extensible kraft paper strip  $\diamond$ : region with low basis weight and high density is marked with solid green circle whereas region with high basis weight and low density is marked with dashed yellow circle. High temperature and low temperature regions selected for a more accurate analysis are marked with solid orange and dashed blue rectangles, respectively.

regions marked with solid green circles and low density regions marked with dashed yellow circles most probably restrained and promoted the local temperature increase (local tensile damage), respectively. The microcreped structure complicated the situation even more, and thus the optical transparency map and the air permeance map do not seem to correlate as clearly with the temperature map before rupture for the strips  $\diamond$ ,  $\nabla$  and  $\triangleright$  in comparison to the kraft paper strips. Nevertheless, certain relationship clearly occurred, and thus the relative values from three high temperature regions and three low temperature regions were plotted against each other in Figure 4.27, Figure 4.28 and Figure 4.29 with solid red symbols and hollow blue symbols, respectively. The regions are marked in Figure 4.24, Figure 4.25 and Figure 4.26. As in the case of the kraft paper strips (compare Figure 4.21), the basis weight was generally

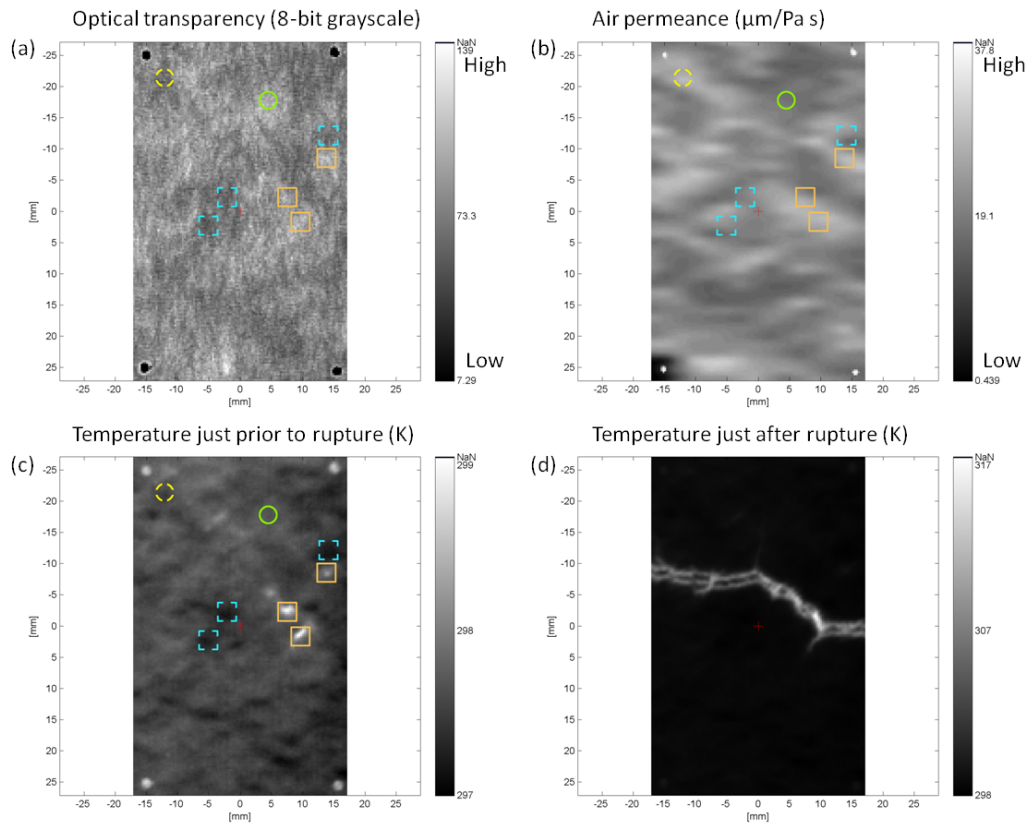


**Figure 4.25** Optical transparency map (a), air permeance map (b), temperature map just prior to rupture (c) and temperature map just after rupture (d). Extensible kraft paper strip: region with low basis weight and high density is marked with solid green  $\nabla$  whereas region with high basis weight and low density is marked with dashed yellow circle. High temperature and low temperature regions selected for a more accurate analysis are marked with solid orange and dashed blue rectangles, respectively.

below average level for the high temperature regions and above average level for the low temperature regions. The air permeance was also generally above average level for the high temperature regions. However, the difference in comparison to the kraft paper strips was that no mean local air permeance values were below the average level. Also contrary to the kraft paper strips, majority of the low temperature regions had air permeance focused around the average level. A possible measurement-related reason for these differences in local air permeance could have been the lateral air leakage due to the rough microcreped surface structure of extensible kraft paper.

As discussed above, the probability for the high local temperature (local tensile damage) caused by stretching to occur is high for both kraft paper and extensible kraft paper when the local basis weight is low and local air permeance high (compare

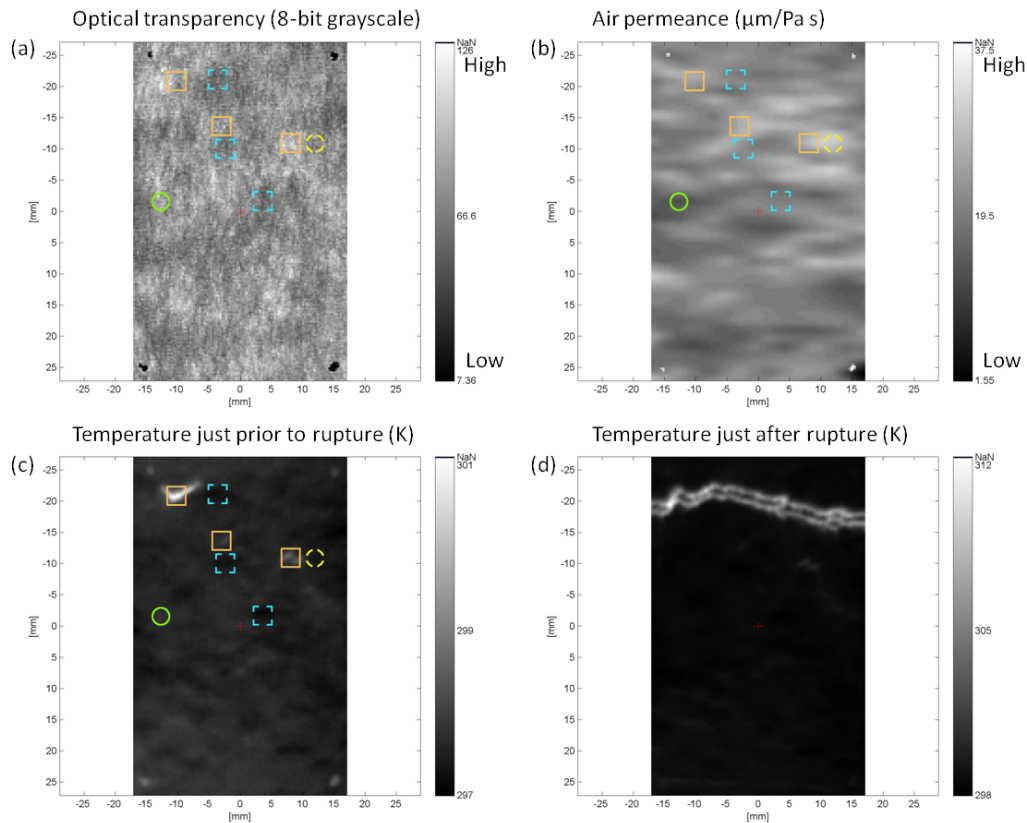


**Figure 4.26** Optical transparency map (a), air permeance map (b), temperature map just prior to rupture (c) and temperature map just after rupture (d). Extensible kraft paper strip  $\triangleright$ : region with low basis weight and high density is marked with solid green circle whereas region with high basis weight and low density is marked with dashed yellow circle. High temperature and low temperature regions selected for a more accurate analysis are marked with solid orange and dashed blue rectangles, respectively.

Figure 4.21 and Figure 4.27). However, the two papers seem to differ regarding the influence of local density on the concentration of high temperature. Low local density had a major influence on the development of high local temperature in certain regions within the kraft paper strips (see Figure 4.21) whereas the influence of local density seemed to be much smaller in the case of extensible kraft paper, i.e. such high temperature regions where both basis weight and air permeance were high did not occur within the extensible kraft paper strips. Possible reason for this difference could have at least partly been the above-mentioned measurement error due to the lateral air leakage, or alternatively, the more even stress distribution caused by the microcreped structure ultimately led to the situation where the high temperature occurred in the regions with low basis weight and high air permeance (average level of density).

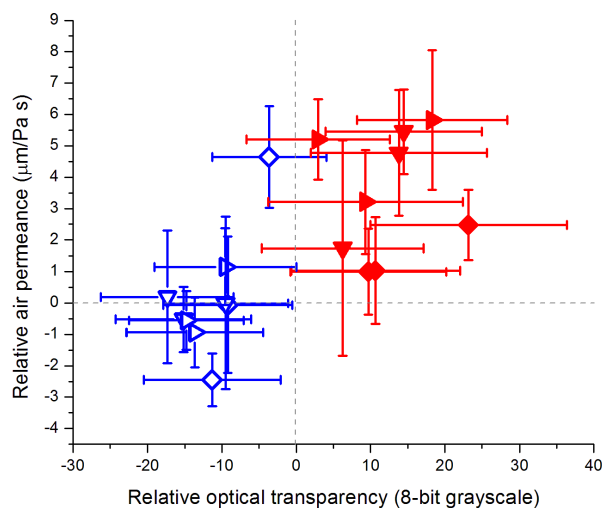


**Figure 4.27** Relative air permeance versus relative optical transparency for high (solid red symbols) and low (hollow blue symbols) temperature regions in the stretched extensible kraft paper strips  $\diamond$ ,  $\nabla$  and  $\triangle$ .

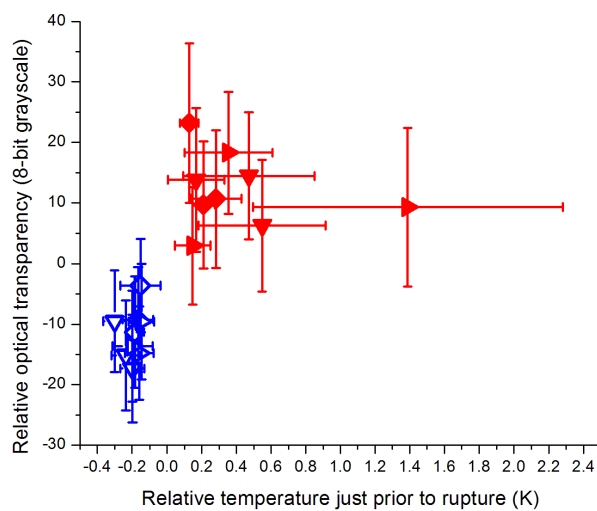


**Figure 4.28** Relative optical transparency versus relative temperature just prior to rupture for high (solid red symbols) and low (hollow blue symbols) temperature regions in the stretched extensible kraft paper strips  $\diamond$ ,  $\nabla$  and  $\triangle$ .

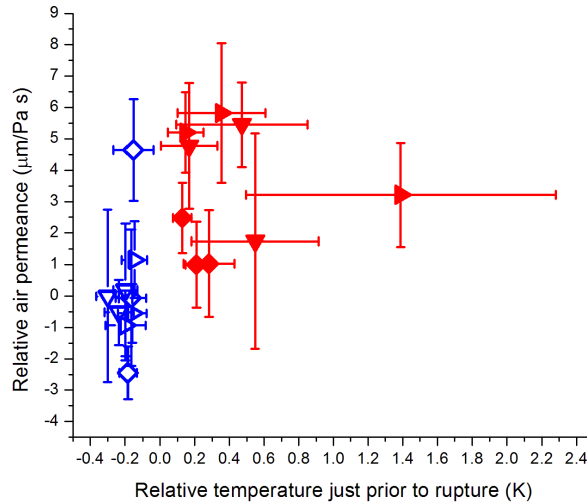


**Figure 4.29** Relative air permeance versus relative temperature just prior to rupture for high (solid red symbols) and low (hollow blue symbols) temperature regions in the stretched extensible kraft paper strips  $\diamond$ ,  $\nabla$  and  $\triangleright$ .

In any case it seems obvious that microcreped structure and its spatial variation, in addition to local basis weight and local density, has a clear effect on the magnitude and variation of local stiffnesses, and thus also affects on the temperature distribution (tensile damage distribution) within extensible kraft paper strips. It is also interesting to mention that the extensible kraft paper strip  $\triangleright$  was weakest (see Table 4.8), similarly with the kraft paper strip  $\triangle$ , due to the heaviest localization of temperature increase (local tensile damage). This further illustrates the fact that even stress distribution is a prerequisite for strong paper.

The heavy localization of temperature increase in the strip  $\triangleright$  had also a clear influence on the results of statistical analysis performed in exactly the same manner as with the kraft paper (see Section 4.4.1). However, according to Grubbs Outlier Test the data point with strong temperature increase was not an outlier from a statistical point of view. When the data point with high temperature increase was taken into account, combined local basis weight and local air permeance explained 43% of total variation in local temperature, i.e. the coefficient of determination of the statistical model with the divergent data point was  $r^2=0.43$ . On the other hand, combined local basis weight and local air permeance were able to explain 71% of total variation in local temperature when the data point with high temperature increase was excluded from the statistical analysis, i.e. the coefficient of determination of the statistical model without the divergent data point was  $r^2=0.71$ . Other possible influence factors, including microcreped structure and measurement noise, were responsible for the remaining

difference to  $r^2=1$ . This difference was 0.57 and 0.29 with and without the divergent data point, respectively. In both cases the coefficient of determination was lower in comparison to the kraft paper ( $r^2=0.76$ ). This is plausible due to the fact that the microcreped structure evened out the temperature increase distribution within the extensible kraft paper strips - as described above. However, it remains unclear whether the influence of microcreped structure on the localization of tensile damage was considerable ( $r^2=0.43$ ) or minor ( $r^2=0.71$ ) due to the instability caused by the large effect of the data point with strong temperature increase. Furthermore, the statistical analysis proved the discussion above that the major difference between the two papers was indeed that the local air permeance of extensible kraft paper did not provide any information about the local temperature increase which was not already given by the local basis weight. This means that the local air permeance was completely redundant to the local basis weight. The redundant  $r^2$  for local air permeance was 0.26 with the divergent data point and 0.39 without the divergent data point. Thus, regions with high air permeance had strong temperature increase due to the low basis weight in these regions - not because of low local density. The exclusive information about the local temperature increase provided by local basis weight was in turn  $r^2=0.17$  and  $r^2=0.32$  with and without the divergent data point, respectively. Finally, it needs to be taken into account that the lateral air leakage during the local air permeance measurement of extensible kraft paper had an effect on the above-described statistical analysis also.

## 4.5 Conclusions

This chapter offered comprehensive answers to the research questions defined in Section 2.4. These answers are concluded in the following description.

The first research question dealt with the possibility to compensate the reducing breaking strain of extensible kraft paper due to decreased solids content during MD compaction with increasing tensile index and/or form factor in order to keep the TEA index constant. The laboratory and industrial scale studies revealed that the MD compaction of paper becomes more efficient with higher solids content due to decreasing plastic Poisson's ratio, i.e. the paper network has higher resistance against shear and it compacts more instead. As a result, the prepared extensible kraft paper has more pronounced microcreped structure which in turn leads to the higher sigmoidal shape of the MD specific stress versus strain curve. This means lower form factor and tensile stiffness index as well as higher strain at break. The tensile index remains nearly unchanged or increases slightly. Consequently, the TEA index increases but not as much as the increasing breaking strain would suggest due to the decreasing form factor. Still, the strain clearly dominates over the form factor in the development of TEA index, and thus the prevention of TEA index loss with increasing form factor does not

seem to be possible, i.e. the trade-off between load carrying ability during stretching (tensile stiffness index, yield point and form factor) and TEA index is inevitable. On the other hand, the increase in breaking strain and TEA index of extensible kraft paper is clearly achievable without sacrificing the tensile index by increasing the solids content during MD compaction. Some indications also appeared that MD form factor increases with Clupak nip pressure - possibly through more even stress distribution caused by higher uniformity of microcreped structure.

The research questions of the second topic focused around the differences in time-dependent mechanical behavior of kraft paper and extensible kraft paper in MD. In this way, the practical mechanical performances of the two papers were estimated and compared. The performed DMA, creep and creep recovery analyses illustrated the more ductile/viscous nature of extensible kraft paper through lower storage modulus and higher  $\tan \delta$  as well as higher creep compliance and lower relaxation ability. For both papers, the ductile/viscous behavior became stronger when the dry atmosphere was replaced with the humid one due to the moisture induced softening of the amorphous fiber wall components and weakening of the interfiber bonds. The creep compliance of the extensible kraft paper increased and the relaxation ability decreased considerably, i.e. the risk for failure became very high, when the RH was increased dynamically during the cyclic creep-recovery testing. The applied creep stress together with the possible accelerated creep related stresses exceeded the yield point which was in turn reduced by the increased RH (increased ductility/viscosity) and the deformations induced during the previous creeps (loading history). Thus, the paper started to deform in an almost ideally plastic manner (strain hardening close to zero) through the pullout of the microcreped structure, and as a consequence, the creep rate and strain became very high. The effect of the same loading and climate history on the considerably stiffer and more brittle kraft paper with higher load carrying ability was essentially different, i.e. the increase in creep compliance and decrease in relaxation ability was much weaker along the test. This difference illustrates the significance of a sufficiently high yield point on the mechanical performance of extensible kraft paper. The influence of dry atmosphere with constant temperature as well as humid atmosphere with dynamically increasing temperature (similar effect on paper structure as dynamically increasing RH) in combination with loading history was considerably smaller on the deformation of kraft and extensible kraft paper during cyclic creep-recovery testing. In other words, majority of the plastic strain occurred during the first creep cycle after which the creep strain was almost entirely elastic and viscoelastic. During DMA, the dynamically increasing temperature together with the loading history seemed to have in turn a smaller influence on the viscoelastic behavior of extensible kraft paper, i.e. the storage modulus decreased less and the transient  $\tan \delta$  peak temperatures were higher.

The research questions of the third topic dealt in turn with the local structural properties of kraft paper which cause the high localization of tensile damage (high

local temperature) with the question how the microcreped structure of extensible kraft paper changes the distribution of tensile damage (distribution of temperature increase). In the study it was found that one of the following three conditions must be met for high local temperature to occur in the kraft paper strip: (1) low local basis weight, (2) low local density or (3) a combination of the two. Statistical modeling quantitatively revealed that basis weight and density are both contributing to locally increased temperature under tensile load. A combination of moderately low values for basis weight and density was found to create higher local temperature than extremely low values for one of the two. The induced microcreping effect led to a more even distribution of temperature just prior to rupture. The statistical modeling also quantitatively showed that the combined ability of local basis weight and local air permeance to explain the total variation in local temperature was weaker in comparison to the kraft paper due to the microcreped structure. Whether the influence of microcreped structure was considerable or minor, remained however unclear. It could be argued that the microcreped structure of extensible kraft paper reduced the relative differences between local tensile stiffnesses caused by variations in local basis weight and density - possibly through stronger microcreping effect in the strongest regions with high basis weight and density - and thus the distribution of tensile stress became more even. Furthermore, a major difference in the conditions of high local temperature to occur was that both local basis weight and local air permeance were low in the case of extensible kraft paper. The statistical modeling also quantitatively revealed that the local air permeance was completely redundant to the local basis weight, i.e. local density did not play a role in the development of high local temperature. However, the lateral leakage during the measurement of local air permeance due to the rough microcreped surface structure might have distorted the results. Finally it is interesting to mention that the extensible kraft paper strip with heaviest localization of tensile damage was the weakest - as in the case of kraft paper.

This thesis is concluded in the following Chapter 5 by giving an outlook on potential improvements as well as future research to further improve the production process and properties of extensible kraft paper.

## Conclusions and Outlook

This thesis has approached the structural and mechanical properties of extensible kraft paper from the following three perspectives: (1) relation between microcreped structure and specific stress versus strain curve (mechanical properties), (2) influence of microcreped structure on time-dependent mechanical properties when exposed to different combinations of atmospheres, temperatures and loading histories and (3) Influence of microcreped structure on distribution of tensile damage (distribution of temperature increase). This thesis is concluded here by giving an outlook on potential improvements as well as future research to further improve the production process and properties of extensible kraft paper.

It became quite clear that the decrease in solids content during MD compaction with the Clupak extensible unit inevitably leads to the trade-off between TEA index and form factor. In other words, it seems extremely unlikely that tensile stiffness index, yield point and load carrying ability during the pullout of the microcreped structure could be increased in this manner without simultaneously losing TEA index. Increasing breaking strain and TEA index without sacrificing tensile index is in turn clearly achievable by increasing the solids content during MD compaction. It was found that the higher solids content during MD compaction leads to more pronounced microcreped structure. The study also clearly illustrated that the induced microcreping effect leads to the more even distribution of tensile damage. Taking these facts into consideration, it would be plausible to assume that the more pronounced microcreped structure increases the evenness of tensile damage distribution. More precisely, it could be argued that the microcreping effect becomes increasingly stronger in the strongest regions with high basis weight and density, and thus the tensile stiffnesses in these regions decrease closer to the ones in the weak regions with low basis weight and density. This hypothesis should be tested in the upcoming studies by including a local surface topography measurement, e.g. infinite focus

## 5. Conclusions and Outlook

---

microscope or OptiTopo [INNVENTIA, 2012], to the procedure for investigating the relationship between local structural properties and local tensile damage.

Then what would be the ways to overcome this trade-off between TEA index and form factor of extensible kraft paper? One option could be the optimization of specific stress versus strain curve through increasing the solids content during Clupak compaction. As the outcome would be higher breaking strain and TEA index, the final compaction level has to be reduced by decreasing the speed difference between inlet and outlet of the Clupak nip in order to reach the same breaking strain and TEA index values with the paper produced with lower solids content during Clupak compaction. This would undoubtedly have a positive impact on tensile index. Also the production of paper would increase due to the higher speed after Clupak nip. The influence on tensile stiffness index, yield point and form factor should be in turn investigated by an industrial scale trial. However, the resulting more pronounced microcreped structure (higher roughness), which is harmful for printing quality, has so far prevented this kind of trials. The calender solutions installed in modern sack kraft paper machines, e.g. the shoe calender installed in PM7 in Mondi Steti [MONDI, 2014], could offer a possibility to test this approach by reducing the roughness back to an acceptable level.

Another approach could be to continue the development of paper web forming process technologies further in order to reach more homogeneous structure of fiber network - including better formation and more even local density values. The yield point could be increased in this manner due to the more even distribution of local strains in the elastic region of specific stress versus strain curve. The achieved improvement in tensile damage distribution would also lead to the higher tensile index and breaking strain. However as the average global tensile stiffness index is proportional to the average elastic energy in paper, the increased structural homogeneity (less variation in local tensile stiffnesses) would most probably affect only weakly on the stiffness index. Furthermore, the improved formation could lead to a decreased air permeance, although not seen in the results of this thesis, which would in turn be harmful for the air removal during bag filling, i.e. another trade-off situation is confronted.

Third way to overcome the trade-off problem between TEA index and form factor could be through proper design of fiber-based composite structures. In other words, a small amount of chemical which would increase the tensile stiffness index and yield point of extensible kraft paper could be added by coating in the drying section of a paper machine. One option could be to utilize the Clupak extensible unit as a coater by adding the chemical with the lubrication water sprayed onto the Clupak cylinder surface. Also spray coating technologies could offer a solution. However, the smearing tendency of the added chemical on the remaining drying section is a potential risk factor. A possible option for the added chemical is glyoxal [BASF, 2015] which would reinforce the microcreped structure by crosslinking fiber wall polymers.

## 5. Conclusions and Outlook

---

It should be further studied with the developed laboratory method whether glyoxal or some other chemical with similar effect could actually help in overcoming the trade-off between TEA index and form factor. The main disadvantages of this approach are the possible investment requirements for suitable coating technology and the heat required to cause the crosslinking reaction.

Fourth perspective to improve the mechanical performance and possibly also to overcome the trade-off problem between TEA index and form factor would be to optimize the properties of extensible kraft paper to the conditions where it is actually used. Paper properties are normally measured in a standard climate of 23°C and 50% RH. However, the climate in South-East Asia, which is one of the emerging market regions for extensible kraft paper, is often much more humid, i.e. close to 80%. Consequently, the extensible kraft paper behaves in a considerably more ductile/viscous manner in comparison to the behavior in the standard climate. By contrast, industrial bags have been also used to deliver cement to Antarctica where the average annual temperature is -47°C and RH close to zero [PACKAGING NEWS, 2013]. This in turn means much higher brittleness in comparison to the behavior in the standard climate. Thus, there might be potential to improve the mechanical performance of extensible kraft paper further through customization of the structure and chemistry to the prevailing end-use conditions. This could mean for example lower amount of Clupak compaction when used in hot and humid conditions and higher amount of Clupak compaction when used in cold and dry conditions. Potential problems for this approach are the changing conditions during the lifetime of the bags and strong weakening of interfiber bonds due to moisture. However, if the interfiber bonding could be kept strong enough while simultaneously compensating part of the Clupak compaction with moisture induced ductility, the possibilities to improve the mechanical performance, and thus also to overcome the trade-off between TEA index and form factor, would be high in the tropical conditions.

As the description above and the conclusions in Section 4.5 clearly illustrate, solving the conflict between TEA index and form factor is extremely challenging. However, by patiently continuing the in-depth research together with creative thinking, the ultimate means to overcome the conflict will be findable.

# Bibliography

- M. Alava and K. Niskanen. The physics of paper. *Reports on Progress in Physics*, 69(3): 669–723, 2006.
- M. Alava and K. Niskanen. *In-plane tensile properties*, volume 16 of *Papermaking Science and Technology*, chapter 5, pages 181–228. Paperi ja Puu, 2nd edition, 2008.
- B. Alince, A. Vanerek, M. H. de Oliveira, and T. G. M. van de Ven. The effect of polyelectrolytes on the wet-web strength of paper. *Nordic Pulp and Paper Research Journal*, 21(5):653–658, 2006.
- Anasys. Introduction to dynamic mechanical analysis, March 2015. URL <http://www.anasys.co.uk/library/dma1.htm>.
- O. Andersson and L. Sjöberg. Tensile studies of paper at different rates of elongation. *Svensk Papperstidning*, 56(16):615–624, 1953.
- BASF. Glyoxal from BASF - the sustainable solution, March 2015. URL [http://www.intermediates.basf.com/chemicals/web/en/function/conversions:/publish/content/news-and-publications/brochures/download/BASF\\_Glyoxal\\_basic\\_presentation.pdf](http://www.intermediates.basf.com/chemicals/web/en/function/conversions:/publish/content/news-and-publications/brochures/download/BASF_Glyoxal_basic_presentation.pdf).
- S. Borodulina, A. Kulachenko, S. Galland, and M. Nygård. Stress-strain curve of paper revisited. *Nordic Pulp and Paper Research Journal*, 27(2):318–328, 2012.
- J. P. Brezinski. The creep properties of paper. *Tappi Journal*, 39(2):116–128, 1956.
- E. M. Burrow. Extensible paper-its development, production, and use. *Paper Technology*, 6(5):423–430, 1965.
- S. L. Cluett. US patent 2,624,245: Modified paper and method for its manufacture, 1953.
- Clupak. Producing Clupak extensible paper with an extensible unit, January 2014. URL [http://www.clupak.ch/01\\_clupakmachine/clupakmachine\\_index.html](http://www.clupak.ch/01_clupakmachine/clupakmachine_index.html).
- D. W. Coffin and C. C. Habeger. The mechanics of sorption-induced transients in the loss tangent. *Journal of Pulp and Paper Science*, 27(11):385–390, 2001.
- J. M. Considine, D. E. Gunderson, P. Thelin, and C. Fellers. Compressive creep behavior of paperboard in a cyclic humidity environment-exploratory experiment. *Tappi Journal*, 72(11):131–136, 1989.

- J. M. Considine, C. T. Scott, R. Gleisner, and J. Y. Zhu. Use of digital image correlation to study the local deformation field of paper and paperboard. In *Proceedings of 13th Fundamental Research Symposium*, pages 613–630, Cambridge, UK, 2005.
- M. H. de Oliveira, M. Maric, and T. G. M. van de Ven. The role of fiber entanglement in the strength of wet papers. *Nordic Pulp and Paper Research Journal*, 23(4):426–431, 2008.
- D. P. Dumbleton. *Longitudinal compression of individual pulp fibers*. PhD thesis, Lawrence University, Appleton, WI, USA, 1971.
- D. P. Dumbleton. Longitudinal compression of individual pulp fibers. *Tappi Journal*, 55(1):127–135, 1972.
- D. P. Dumbleton, K. P. Kringstad, and C. Soremark. Temperature profiles in paper during straining. *Svensk Papperstidning*, 76(14):521–528, 1973.
- K. I. Ebeling. Distribution of energy consumption during the straining of paper. In F. Bolam, editor, *Proceedings of 5th Fundamental Research Symposium (Cambridge, UK, 1973)*, pages 304–335, London, UK, 1976. Technical Section of The British Paper and Board Industry Federation.
- C. Fellers. *Paper physics*, volume 4 of *Pulp and Paper Chemistry and Technology*, chapter 2, pages 25–67. de Gruyter, 2009a.
- C. Fellers. *The structure of paper and its modelling*, volume 4 of *Pulp and Paper Chemistry and Technology*, chapter 1, pages 1–24. de Gruyter, 2009b.
- M. Gimåker, M. Nygård, L. Wågberg, and S. Östlund. Shear strength development between couched paper sheets during drying. In U. Hirn, editor, *Progress in Paper Physics Seminar*, pages 191–193, Graz, Austria, 2011. Verlag der Technischen Universität Graz.
- G. N. Greaves, A. L. Greer, R. S. Lakes, and T. Rouxel. Poisson’s ratio and modern materials. *Nature Materials*, 10(11):823–837, 2011.
- A. Gregorova, J. Lahti, R. Schennach, and F. Stelzer. Humidity response of kraft papers determined by dynamic mechanical analysis. *Thermochimica Acta*, 570:33–40, 2013.
- C. C. Habeger and D. W. Coffin. The role of stress concentrations in accelerated creep and sorption-induced physical aging. *Journal of Pulp and Paper Science*, 26(4):145–157, 2000.
- A. Hagman and M. Nygård. Investigation of sample-size effects on in-plane tensile testing of paperboard. *Nordic Pulp and Paper Research Journal*, 27(2):295–304, 2012.

- U. Hirn and J. Lahti. A framework for linking IR thermography with full field structural material data using image registration. *Submitted to Composites Part B: Engineering*, 2015.
- U. Hirn and R. Schennach. A quantitative analysis of different fiber-fiber bonding mechanisms. In *Proceedings of Progress in Paper Physics Seminar*, Raleigh, NC, USA, 2014.
- U. Hirn, M. Lechthaler, and W. Bauer. Registration and point wise correlation of local paper properties. *Nordic Pulp and Paper Research Journal*, 23(4):374–381, 2008.
- D. T. Hristopulos and T. Uesaka. Structural disorder effects on the tensile strength distribution of heterogeneous brittle materials with emphasis on fiber networks. *Physical Review B*, 70(6):064108, 2004.
- C. Hyll. *Infrared emittance of paper - method development, measurement and application*. PhD thesis, The Royal Institute of Technology, Stockholm, Sweden, 2012.
- C. Hyll, H. Vomhoff, and L. Mattsson. A method for measurement of the directional emittance of paper in the infrared wavelength range. *Nordic Pulp and Paper Research Journal*, 27(5):958–967, 2012a.
- C. Hyll, H. Vomhoff, and M. Nygård. Analysis of the plastic and elastic energy during the deformation and rupture of a paper sample using thermography. *Nordic Pulp and Paper Research Journal*, 27(2):329–334, 2012b.
- C. B. Ihrman. Behaviour of paper under dynamic loading; part 3. A comparative study of extensible and ordinary kraft paper. *Svensk Papperstidning*, 67(16):626–630, 1964.
- C. B. Ihrman and O. E. Öhrn. Extensible paper by the double-roll compacting process. In F. Bolam, editor, *Proceedings of 3rd Fundamental Research Symposium (Cambridge, UK, 1965)*, pages 410–434, Manchester, UK, 2003. FRC.
- Innventia. OptiTopo - a unique method to correlate surface topography and print defects, November 2012. URL <http://www.innventia.com/Documents/Produktblad/Material%20processes/Pappersyta/OptiTopo%20-%20product%20sheet.pdf>.
- F. Johanson and J. Kubat. Measurements of stress relaxation in paper. *Svensk Papperstidning*, 67(20):822–832, 1964.
- R. A. L. Jones. *Soft condensed matter*, volume 6 of *Oxford Master Series in Condensed Matter Physics*. Oxford University Press, 2002.
- C. Josefsson. Global demand for sack kraft paper. In *44th Annual Prima Conference*, Vienna, Austria, May 2013. Prima.

- I. Kajanto, J. Laamanen, and M. Kainulainen. *Paper bulk and surface*, volume 16 of *Papermaking Science and Technology*, chapter 3, pages 88–113. Fapet Oy, 1998.
- J. Ketoja. *Rheology*, volume 16 of *Papermaking Science and Technology*, chapter 8, pages 295–318. Paperi ja Puu, 2nd edition, 2008.
- M. Kimura and H. Shimizu. Stress and strain behavior of low grammage spot in paper during elongation. *Japan Tappi Journal*, 39(8):55–62, 1985.
- M. Kimura, H. Shimizu, and K. Nakata. Effect of formation on load-elongation behavior of paper. *Japan Tappi Journal*, 39(9):47–57, 1985.
- P. Kolseth and A. de Ruvo. *The measurement of viscoelastic behavior for the characterization of time-, temperature-, and humidity-dependent properties*, volume 1 of *Handbook of physical and mechanical testing of paper and paperboard*, chapter 2, pages 255–322. Marcel Dekker, 1983.
- A. Komppa and K. Ebeling. Correlation between the areal mass and optical densities in paper. In J. Brander, editor, *Proceedings of 7th Fundamental Research Symposium (Cambridge, UK, 1981)*, pages 603–633, Manchester, UK, 2003. FRC.
- M. J. Korteoja, A. Lukkarinen, K. Kaski, D. E. Gunderson, J. L. Dahlke, and K. J. Niskanen. Local strain fields in paper. *Tappi Journal*, 79(4):217–224, 1996.
- M. J. Korteoja, A. Lukkarinen, K. Kaski, and K. J. Niskanen. Computational study of formation effects on paper strength. *Journal of Pulp and Paper Science*, 23(1):18–22, 1997.
- M. J. Korteoja, K. J. Niskanen, M. T. Kortschot, and K. K. Kaski. Progressive damage in paper. *Paperi ja Puu*, 80(5):364–372, 1998.
- K. Kulasinski, S. Keten, S. V. Churakov, D. Derome, and J. Carmeliet. A comparative molecular dynamics study of crystalline, paracrystalline and amorphous states of cellulose. *Cellulose*, 21(3):1103–1116, 2014.
- J. Lahti, F. Schmied, and W. Bauer. A method for preparing extensible paper on the laboratory scale. *Nordic Pulp and Paper Research Journal*, 29(2):317–321, 2014.
- M. Leskelä and S. Simula. *Rheology and moisture effects*, volume 16 of *Papermaking Science and Technology*, chapter 8, pages 260–283. Fapet Oy, 1998.
- Lorentzen & Wettre. *Autoline 300; operating instructions for following methods: Code 80-538, Code 80-545, Code 80-515, Code 80-516, and Code 80-510*. Kista, Sweden.
- Lorentzen & Wettre. *SE 062 Tensile tester*. Kista, Sweden, 2003.

- K. Maddern. Sack kraft; stretching paper to the limit. *Appita Journal*, 56(6):419–420, 2003.
- MathWorks. MATLAB R2014b Documentation; imresize function, March 2015. URL <http://se.mathworks.com/help/images/ref/imresize.html>.
- Mondi. Next-generation paper machine PM7 goes live at Mondi Steti, May 2014. URL [http://www.mondigroup.com/products/desktopdefault.aspx/tabid-1346/345\\_read-27080/](http://www.mondigroup.com/products/desktopdefault.aspx/tabid-1346/345_read-27080/).
- Mondi. Sack kraft paper, March 2015a. URL <http://www.mondigroup.com/products/de/desktopdefault.aspx/tabid-1807>.
- Mondi. 3D animation Mondi sack kraft paper production, March 2015b. URL <https://www.youtube.com/watch?v=qs8Ugfz28L0&list=PL68b5MZu2v6wyiwLjyTMJeW8d-WP3aBNw>.
- Mondi Bag Application Centre. Dropping of industrial bags. 2008.
- J. Neter, M. H. Kutner, C. J. Nachtsheim, and W. Wasserman. *Applied linear statistical models*. McGraw-Hill, 4 edition, 1996.
- K. Niskanen and P. Pakarinen. *Paper structure*, volume 16 of *Papermaking Science and Technology*, chapter 1, pages 11–58. Paperi ja Puu, 2nd edition, 2008.
- B. Norman. *Web forming*, volume 8 of *Papermaking Science and Technology*, chapter 6, pages 216–288. Paperi ja Puu, 2nd edition, 2007.
- B. Norman and D. Wahren. Mass distribution and sheet properties of paper. In F. Bolam, editor, *Proceedings of 5th Fundamental Research Symposium (Cambridge, UK, 1973)*, pages 7–70, London, UK, 1976. Technical Section of The British Paper and Board Industry Federation.
- R. J. Norman. Dependence of sheet properties on formation and forming variables. In F. Bolam, editor, *Proceedings of 3rd Fundamental Research Symposium (Cambridge, UK, 1965)*, pages 269–298, London, UK, 1966. Technical Section of The British Paper and Board Industry Federation.
- M. Ostoja-Starzewski and J. Castro. Random formation, inelastic response and scale effects in paper. *Philosophical Transactions A*, 361(1806):965–985, 2003.
- Packaging news. Cementing a place on the coldest continent, August 2013. URL <http://www.packagingnews.com.au/news/cementing-a-place-on-the-coldest-continent>.
- R. Paetow and L. Götsching. Querkontraktionszahl von Papier. *Das Papier*, 44(6): 229–237, 1990.

- D. H. Page, R. S. Seth, B. D. Jordan, and M. C. Barbe. Curl, crimps, kinks and microcompressions in pulp fibres: their origin, measurement and significance. In V. Puntton, editor, *Proceedings of 8th Fundamental Research Symposium (Oxford, UK, 1985)*, pages 183–227, Manchester, UK, 2003. FRC.
- P. Pakarinen, H. Kiiskinen, P. Kekko, and J. Paltakari. *Drying and paper quality*, volume 9 of *Papermaking Science and Technology*, chapter 7, pages 236–295. Paperi ja Puu, 2nd edition, 2010.
- E. Poppel. Paper-rheology - an applied science. *Applied Rheology*, 6(6):269–275, 1996.
- Pöyry. *Sack paper*, volume 1 of *World Paper Markets up to 2025*, chapter 10, pages 172–186. Pöyry Management Consulting Oy, Vantaa, Finland, 2011.
- K. Salminen. *The effects of some furnish and paper structure related factors on wet web tensile and relaxation characteristics*. PhD thesis, Lappeenranta University of Technology, Lappeenranta, Finland, 2010.
- C. Scott-Kerr. Manufacture of multiwall sack papers. *Pulp and Paper Canada*, 98(5):45–48, 1997.
- R. S. Seth. Understanding sheet extensibility. *Pulp and Paper Canada*, 106(2):33–40, 2005.
- C. A. Shoudy. The Clupak paper story. *Tappi Journal*, 42(1):108–110, 1959.
- A. Tejado and T. G. M. van de Ven. Why does paper get stronger as it dries? *Materials Today*, 13(9):42–49, 2010.
- J. L. Thorpe. Paper as an orthotropic thin plate. *Tappi Journal*, 64(3):119–121, 1981.
- A. Vainio. *Interfibre bonding and fibre segment activation in paper: observations on the phenomena and their influence on paper strength properties*. PhD thesis, Helsinki University of Technology, Espoo, Finland, 2007.
- A. Vishtal and E. Retulainen. Boosting the extensibility potential of fibre networks: a review. *BioResources*, 9(4):7951–8001, 2014.
- H. Vomhoff and M. Bouveng. Measurement of small-scale permeance variation. In *PaperCon*, Atlanta, USA, May 2010. Tappi.
- L. C. Walker. Dynamic mechanical spectroscopy of paper. *Thermochimica Acta*, 367:407–414, 2001.
- Wikipedia. Sanford Lockwood Cluett, March 2015a. URL [http://en.wikipedia.org/wiki/Sanford\\_Lockwood\\_Cluett](http://en.wikipedia.org/wiki/Sanford_Lockwood_Cluett).

- Wikipedia. Climate in Jakarta, Indonesia, March 2015b. URL <http://en.wikipedia.org/wiki/Jakarta>.
- L. Wong, M. T. Kortschot, and C. T. J. Dodson. Effect of formation on local strain fields and fracture of paper. *Journal of Pulp and Paper Science*, 22(6):213–219, 1996.
- T. Yamauchi. *Application of IR thermography for studying deformation and fracture of paper*, chapter 1, pages 3–26. Infrared Thermography. InTech, 2012.
- T. Yamauchi and K. Murakami. Observation of the deforming and fracturing processes of paper using thermography. In C. F. Baker, editor, *Proceedings of 10th Fundamental Research Symposium (Oxford, UK, 1993)*, pages 825–847, Leatherhead, UK, 1993. Pira International.
- T. Yamauchi and K. Murakami. Observation of deforming process of a poorly formed papersheet by thermography. *Sen-i Gakkaishi*, 50(9):424–425, 1994.
- K. C. Yeh, J. M. Considine, and J. C. Suhling. The influence of moisture content on the nonlinear constitutive behavior of cellulosic materials. In *Proceedings of the 1991 International Paper Physics Conference*, pages 695–711, Kona, HI, USA, 1991. Tappi.